UNIVERSITA' DEGLI STUDI DI PADOVA

Dipartimento di Ingegneria Industriale DII

Corso di Laurea Magistrale in Ingegneria Energetica

Modelling and optimization of a domestic hot water heat pump

Relatore: Prof. Davide Del Col

Correlatori: Prof. Wiebke Brix Markussen

Post-doc Erasmus Damgaard Rothuizen

Ing. Kasper Korsholm Østergaard

Laureando: Danese Matteo 1059163

Anno accademico 2014/2015

to my father
to thank him and to make him proud of me

It is good to have an end to journey toward;
but it is the journey that matters, in the end.

— Ursula K. Le Guin

Abstract

Nowadays, the figures describing the impact of the water heating as end use in the residential sector are alarming both in terms of energy consumption and carbon emissions. The domestic hot water heat pumps, even if they are already characterised by a large market, are expected to become even more attracting because of the incoming regulations about the ecodesign and energy labelling requirements for electric conventional water heaters and electric heat pump water heaters. This study analyses an air source heat pump water heater, considering a specific case-study in which the condenser is wrapped around the tank. The work was accomplished in cooperation with the company Metro Therm A/S, Rundinsvej 55, 3200 Helsinge, Denmark and it was prepared at the Section of Thermal Energy, Department of Mechanical Engineering, Technical University of Denmark (DTU).

The system is modelled both in steady-state and dynamic conditions. The dynamic model emerged to replicate the real temperature profiles in the tank with a maximum discrepancy lower than 15% with respect to the temperature lift of the water starting from 10°C. Specific investigations were performed on the condenser tube length and diameter, on the internal heat recovery unit and on possible alternative refrigerants to R134a. No significant improvements in terms of COP were observed, but the alternative geometries can enable a significantly reduction of the costs. Minichannel condensers emerged to be infeasible in the existing system configuration due to the excessive pressure drops.

According to the simulations, a reduction of the outer condenser tube diameter from 9.95 mm to 6 mm can enhance the COP of the heating up process by 2% and lower the expenditure for the condenser by 36%. Experimental investigations, proved that the system with the reduced diameter enabled a reduction of 1.5 hour of the duration of the heating up process. Finally, the height in the tank of the sensor controlling the operation of the compressor did not affect the system performances according to the predictions from the models, and the heat pump was proved to be able to efficiently heat up the domestic hot water up to 60°C.

Sommario

Al giorno d'oggi gli indicatori che riportano l'impatto, in termini di consumo energetico e di emissioni, derivante dal settore per il riscaldamento dell'acqua domestica sono allarmanti. Basta pensare che, secondo dati riportati in letteratura, il riscaldamento dell'acqua domestica è stato responsabile del 14% del consumo totale europeo di energia nel settore domestico nell'anno 2003 [6]. Inoltre, a testimonianza del suo notevole impatto in termini di emissioni, è stato certificato che tale settore ha causato il 13% delle emissioni di gas serra provenienti dal settore residenziale negli Stati Uniti nel 2007 [10].
Le pompe di calore per acqua sanitaria possono sensibilmente migliorare la situazione grazie alla loro elevata efficienza. Il loro mercato si è già dimostrato particolarmente interessante nel triennio 2010-2013, in cui le installazioni annuali in Europa ammontarono a 60000 [13]. E' lecito aspettarsi un successo ancora maggiore nei prossimi anni, in seguito all'iniziativa della Commissione Europea di introdurre a partire da Settembre del 2015 delle etichette energetiche e di ecodesign per i sistemi elettrici convenzionali e le pompe di calore per il riscaldamento dell'acqua.
Di conseguenza, questo lavoro, preparato alla sezione di Thermal Energy della Technical University of Denmark, è incentrato sulla modellazione e analisi di una pompa di calore per acqua calda sanitaria, con lo scopo di poterne migliorare le prestazioni in modo da rendere ancora più vantaggiosa la prossima diffusione di questo sistema nel mercato. In particolare, la pompa di calore prodotta dall'azienda Metro Therm, situata presso Rundinsvej 55, 3200 Helsinge, Denmark, è stata utilizzata come caso studio. Più nel dettaglio, sono stati presi in considerazione quattro aspetti. I primi due sono stati la geometria del condensatore e la possibile eliminazione dello scambiatore per recupero di calore interno al sistema. Poi si è valutata la possibilità di usare refrigeranti alternativi al R134a impiegato attualmente nella pompa di calore analizzata. Infine l'attenzione è stata focalizzata sulla strategia di controllo usata per azionare il rilascio di calore dal sistema.
Per eseguire le analisi precedemente elencate, è stata necessaria la creazione di un modello nell'ambiente EES (Engineering Equation Solver) per le simulazioni in condizioni stazionarie e uno in Dymola per la valutazione di situazioni dinamiche. La creazione e la verifica dell'attendibilità di tali modelli è stato un altro degli obiettivi principali della tesi. Infatti la politica aziendale attuale consiste nel valutare migliorie alla pompa di calore solamente tramite test sperimentali, soluazione sicuramente più costosa e meno flessibile rispetto a simulazioni analitiche. I modelli creati si propongono quindi l'ambizioso obiettivo di dare slancio all'attività di R&D dell'azienda.

Per quanto riguarda il primo modello in EES, è stato considerato il processo di riscaldamento dell'acqua da 19°C a 55°C usando come base dati sperimentali forniti dall'azienda. La natura concava del profilo di temperatura dell'acqua nel serbatoio con il tempo ha implicato la scelta di considerare quattro step nel modello, ciascuno dei quali usato per interpolare fasi successive del riscaldamento dell'acqua. Tale decisione è stata presa al fine di ottenere una riproduzione più fedele del fenomeno. Più nel dettaglio, è stato scelto di concentrare le analisi sul quarto step, cioè l'ultima porzione del processo di riscaldamento in cui l'acqua viene scaldata approssimativamente da 43°C a 55°C. Aspetto chiave nella creazione di tale modello è stata la scelta delle opportune correlazioni per i coefficienti di scambio termico nelle sezioni del condensatore. Gli output di questo modello in termini di calore scambiato nelle sezioni di desurriscaldamento, condensazione e sottoraffreddamento del condensatore, sono stati usati come input per il modello dinamico in Dymola, tramite funzioni interpolatrici correlanti la temperatura dell'acqua e il calore scambiato in ogni sezione. In questo secondo modello, sono stati riprodotti il più fedelmente possibili tutti i fenomeni di convezione e conduzione che accadono all'interno del serbatoio pieno d'acqua, tenendo conto della stratificazione interna. Il programma creato può considerarsi un buon compromesso tra sforzo computazionale e accuratezza delle previsioni. Infatti, il modello monodimensionale sviluppato ha mostrato una massima discrepanza con i dati sperimentali minore del 15%, rispetto all'incremento di temperatura dell'acqua partendo da 10°C.
Per quanto concerne i principali risultati ottenuti dalle analisi, è necessario precisare che, in seguito a simulazioni preliminari, si è deciso di focalizzarsi su due possibili configurazioni del condensatore alternative a quella impiegata nel sistema prodotto da Metro Therm. Il condensatore attualmente in uso ha un diametro esterno di 9.95 mm e una lungheza di 54 m. Le due alternative considerate presentano entrambe una lunghezza e un diametro rispettivamente di 6.95 mm e 70 m, e si differenziano per il fatto che una include lo scambiatore interno di calore nel sistema mentre l'altra non comprende tale componente. Inizialmente sono state valutati gli effetti delle due configurazioni sul coefficiente di scambio termico e sulle perdite di pressione. E' stato appurato come il coefficiente di scambio termico del flusso bifase aumenti notevolmente riducendo il diametro del tubo, in seguito all'istaurarsi del regime anulare. Tuttavia, le variazioni in termini di COP, calcolato per i quattro step del processo di riscaldamento dell'acqua modellati in EES, sono risultate molto limitate. Tale conclusione è stata confermata dal modello dinamico, provando la bontà dell'attuale condensatore utilizzato. E' stato tuttavia riscontrato che le configurazioni alternative considerate garantiscono una notevole riduazione dei costi del sistema, diventanto quindi molto interessanti. In particolare, si è osservato che l'applicazioni di minicanali non è fattibile a causa delle ingenti cadute di pressione introdotte dal diametro ridotto. Nel mercato esistono però degli arrangiamenti per limitare l'impatto delle perdite di pressione, cosa che renderebbe i minicanali molto vantaggiosi. Per quanto riguarda le analisi sulla strategia di controllo usata per la pompa di calore, è stato osservato che la temperatura di set point alla quale il funzinamento del sistema viene interrotto (on/off control strategy), può essere innalzata fino a 60°C con una riduzione in termini di COP del 10% rispetto a una temperatura di set point di 52°C. Infine, una insignificante influenza dell'altezza nel serbatoio del sensore usato per verificare la temperatura di set point è stata riscontrata in

termini di COP.
Come anticipato in precendenza, si è verificata anche la possibilità di rimpiazzare il refrigerante R134a con altri fluidi. In particolare, quattro fluidi alternativi sono stati applicati: R290, R600a, R1234ze e R1234yf. Le analisi sono state condotte considerando solo l'ultimo step del processo di riscaldamento dell'acqua nel modello EES, e assumendo un'efficienza isentropica di 0.7 per il compressore operante con tutti i 5 fuidi implementati. In queste condizioni, R600a è risultato il refrigerante migliore in termini di COP, mentre R290 si è dimostrato il più vantaggioso considerando la portata volumetrica e quindi le dimensioni e il costo del compressore.
Infine, è opportuno menzionare i risultati ottenuti dai test sperimentali condotti. E' stato scelto di testare un condensatore lungo 54 m e con un diametro esterno di 6 mm. Il processo di riscaldamento dell'acqua è stato ridotto di 1.5 ore rispetto alla configurazione attualemte impiegata. Non è stato possibile avere un riscontro in termini di COP dato che il lavoro del compressore non è stato misurato, ma le simulazioni hanno mostrato un incremento del COP del 2%.

Contents

Nomenclature

Abbreviations

ASHPWH	Air source heat pump water heater
COP	Coefficient of Performance
IHEX	Internal heat exchanger
in	Inlet
LMTD	Logarithmic mean temperature difference
out	Outlet
PI	Piping and Instrumentation

Greek letters

α	Heat transfer coefficient, W/m^{2}K
Δk	De-stratification conductivity, W/mK
Δp	Pressure drop, bar
ΔT	Temperature difference, K
Δt	Time step, s
ϵ	Effectiveness, -
η_{is}	Isentropic efficiency of the compressor, -
μ	Dynamic viscosity, kg/ms
ρ	Density, kg/m^3

Roman letters

$\dot{m}$	Mass flow rate, kg/s
$\dot{Q}$	Heat transfer rate , W

Nomenclature

$\dot{V}$	Volumetric flow rate, m^3/s
A	Area, m^2
C	Cost, €
Cp	Specific heat at constant pressure, J/kgK
E_{tapped}	Tapped energy, J
f	Friction factor, -
o	Constants for the refrigerant mass flow rate, -
r	Mass fraction of water recirculating in the tank, % /s
T	Temperature, °C
U	Overall heat transfer coefficient, W/m^2K
u	Bulk velocity, m/s
x	Thermodynamic vapour quality, -
X_{tt}	Martinelli parameter, -
z	Constants for the compressor isentropic efficiency, -
D	Diameter, mm
F	Froude number, -
H	Heigh of the tank, m
h	Specific enthalpy, J/kg
k	Thermal conductivity, W/mK
L	Length, m
n	Times the condenser is wrapped around the tank, -
Nu	Nusselt number, -
Pr	Prandtl number, -
Q	Heat, J
R	Wall thermal resistance, mK/W
Ra	Rayleigh number, -
s	Wall thickness, mm

V	Volume, m^3
W	Compressor energy, J
x	Thermodynamic vapor mass quality, -
y	Distance from the bottom of the tank, m

Subscripts

avg	Average
c	Condenser
cond	Condensing setion
desup	Desuperheating section
e	Evaporator
r	Refrigerant
sub	Subcooling section
suc	Compressor suction
sup	Superheating
tot	Total
w	Water

1 Introduction

1.1 Impact of water heating in the residential sector

One of the moving engine from this work comes from an alarming indicator provided by Eurostat concerning the European final energy consumption: the total consumption in EU (28 countries) during 2013 was 1104584.6 thousand tons of oil equivalent, and the residential consumption amounted to 295763.1 thousand tons of oil equivalent. This means that the share of consumption in residential sector on the overall final energy consumption was approximately 27% [1]. Figure 1.1 shows the residential energy consumption for the European countries. From the Figure it emerges that France, Germany, Italy, United Kingdom and Poland are the nations with the highest residential consumptions, which amount respectively to 28.5%, 27.5%, 28.8%, 29.5% and 32.2% of the national final energy consumptions. As mentioned by Vieira et al. [2], the future expansion of the residential sector is expected to further increase its impact on the overall energy consumption. This upward trend of the domestic energy consumptions is confirmed also by the Energy Information Administration [3] for the USA, which consider three possible projections for the residential energy consumptions in 2030. According to the "Reference case", the residential electricity consumption is expected to raise mainly because of the increasing water heating, home cooling and "other appliances" consumptions. The prediction hypothesizes a 24% growth in the residential electricity consumption from 2007 to 2030.

For these reasons, a better understanding of the characteristics of the residential final energy consumption is strongly required. Swan et al. [4] tried to accomplish this difficult task by reviewing modelling techniques used to estimate the end use energy consumption in the aforementioned sector. Two approaches were identified: top-down and bottom up. The former exploits historic energy data and regress the dwelling consumptions by means of macro-economical indicators, climate data and energy price. The latter is based on the extrapolation of estimated energy consumption for a few number of households to a national or regional scale.

Thanks to these modelling techniques it is possible to estimate the impact of the different end uses on the residential energy consumptions. It was observed by Min et al. [5], using a

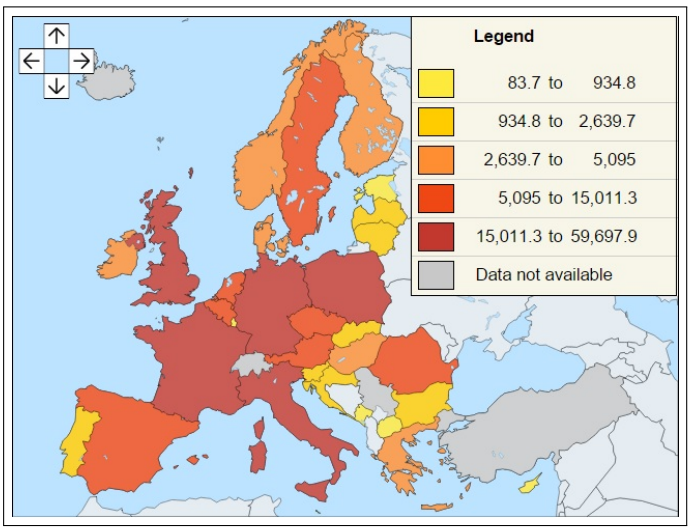

Figure 1.1: Final energy consumption in the residential sector for European countries [1 000 tonnes of oil equivalent] [1]

combination of the bottom-up and top-down approaches to quantify the residential energy end use contributions in United States, that the hot water supply plays a major role, being one of the biggest source of consumptions. This data are confirmed also for European countries by Lombard et al. [6], Singh et al. [7] and the Sustainable Energy Authority of Ireland [8]. Lombard et al. [6] report that in 2003 the share of domestic hot water consumption on the overall residential consumptions was 26% in Spain, 22% in UK and 14% for all Europe. Singh et al. [7] evaluate the feasibility of the goal proposed by the UK to reduce by 80% for 2050 the greenhouse gas emission compared to the level of 1990. The authors focused on the efficiencies of the space and water heating technologies because in 2006 they accounted for 83% of the total domestic consumptions in UK. Dividing the two contributions, the author reports that the contribution of the water heating was 25%, much higher than cooking and lighting plus appliances, respectively 2.8% and 14.7%. The Sustainable Energy Authority of Ireland [8] refers to the Irish energy use in the domestic sector and the most recent data presented in the report are for 2011. The authors report the residential sector electricity end use for 2011: the hot water resulted to give the greatest contribution, i.e. 25%, followed by small appliances and lighting respectively with a share of 19% and 16%.

The aforementioned figures clearly stress the importance of the water heating in the residential sector energy and electricity consumptions. Its key role is even more highlighted by considering environmental issues and more in details the green house gas emissions by end use for the domestic sector.
The Energy Information Administration [3] emphasized that natural gases and liquid fuels find applications in the domestic sector mainly for space and water heating. This statement is clearly reflected in Figure 1.2, in which the GHG emissions by end use in the domestic

sector in the United States for the year 2007 are reported. The impact of water heating on the overall emissions for the residential sector was 13%. According to the "Reference case" in the report *Annual Energy Outlook 2014 with projections to 2040* [9], in which predictions for the electricity use for the different end uses in 2040 are presented, this large use of fossil fuels for water heating is not expected to stop. It is stated that in 2040 natural gas is still expected to account for more than half the fuel exploited in dwellings for space heating, cooking and water heating.

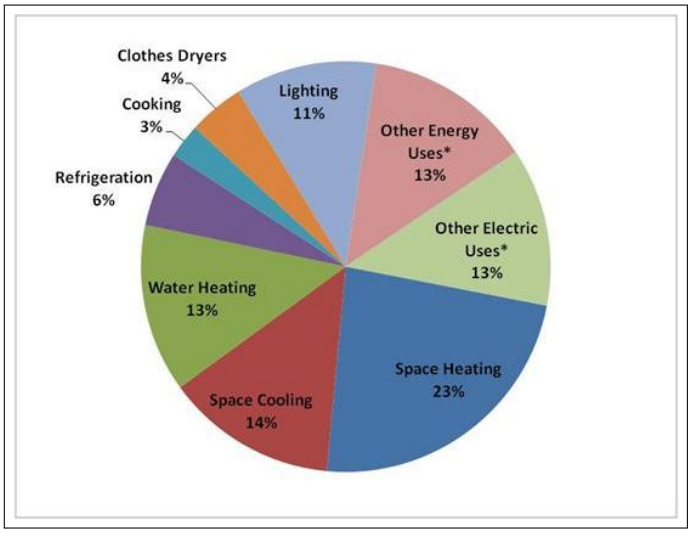

Figure 1.2: Greenhouse gas emissions by end use in the domestic sector for US during 2007 [3] [10]

1.2 Technologies for water heating

After mentioning the previous figures, it is worthy to list the main technologies used nowadays to heat up the water.
For what concerns the existing technologies for water heating in the dwellings, a first distinction needs to be done between storage water heater and demand water heaters. The former are characterised by the presence of an insulated tank containing the water which is heated up. The latter do not include any storage capacity, but the water is heated up only when necessary. The storage water heaters are the most common in the market. The application of demand water heater is not widespread mainly because of their limited output capacity. This solution is more suitable for low-use applications such as vacation houses [11].
Among the storage water heaters, the main technologies used to heat up the water consist on the application of fossil fuels, electricity, solar energy, district heating or heat pumps and they are briefly explained in the following. Fossil fuel water heaters are based on the presence of a burner in the bottom of the tank or on the ignition, generated by an electrical spark, of

a vaporizing mixture of air and the fossil fuel. Electric water heaters often include a double electric element, one placed in the bottom of the tank and one in the top. When the tank is plenty of cold water, the upper electric element is prioritized and it heats up the water in the top of the tank. After the water temperature reaches the desired set point temperature setted in the thermostat, the lower electric element is activated. The working principle of a solar collector water heater consists on the absorption of solar energy in a solar collector by means of an absorber transferring the heat to the opportune solar collector fluid. This fluid, thanks to a spiral or a mantle located in the tank, heats up the water in the tank. Finally, the heat pump water heaters are based on the application of a heat pump releasing heat to the water from the condenser. A more detailed explanation of the latter solution will be presented in Chapter 2.

1.3 Attractiveness of domestic hot water heat pump

The awareness of the alarming situation concerning the water heating in the domestic sector incited the European Commission to consider urgent measures. A key action in this sense will be the incoming regulation regarding the ecodesign and energy labelling requirements for electric conventional water heaters and electric heat pump water heaters. According to what published by the European Commission in the Official Journal 6th of September 2013, the labels, which are going to be mandatory since September 2015, are required to report "the water heater's energy class and the related load profile, annual electricity consumption (final) as well as sound power level" [12]. These actions are expected to be beneficial for a further development of the domestic hot water heat pumps (DHWHP), thanks to their much higher efficiencies if compared with the electric boilers and other storage water heaters. According to DELTA Energy & Environment [13], the market of the domestic hot water heat pump has already been very flourishing during the triennium 2010-2013: the yearly installations totaled to 60000 across Europe. The forecast for the DHWHP market predicts an even more shining future: the yearly installations are expected to duplicate by 2017, and the new incoming regulations are expected to play a major role in this sense. The reason for this success lays in the fact that heat pump water heaters are considered an attractive option to promote energy savings in households. Moreover, they are seen as an efficient way to reduce carbon emissions in hot-water heating and they are designed as renewable by the EU's Renewable Energy Directive of 2009 if they meet the minimum requirements of eco-labelling stated in Commission Decision 2007/742/EC [14].
Several investigations found in the literature focused on the application of air source heat pumps for water heating. For example, Liu et al. [15] optimized and analysed the performances of a multi-functional heat-pump system using as heat source ambient air and gray water in UK residential buildings. Four possible configurations were considered: air-source-only evaporator, water-source-only evaporator, parallel of air and water as heat sources, series of air and water as heat sources. Both the space and water heating were considered. Even if the system was observed to perform better in space heating plus hot water mode, the author stated that the COP in only water heating mode is much higher than conventional electrical

heaters. The system with parallel sources combination offered the best performances among the other three alternatives. However, the author also mentions that air source heat pumps are widely installed due to their low initial costs and the large availability of air. The heat transfer process is strongly simplified by the application of a fan circulating the air, while other systems require more complex processes, such as additional pipes and pumps, in order to store energy [2]. Their main disadvantage is due to the yearly ambient temperature variations which affect the thermal performances: they are reduced for cold weather conditions.
Finally, Imbrahim et al. [16] analysed the performances of an air source heat pump water heater (ASHPWH) in the Lebanese context, comparing them with the ones of an electric water heater, the most common alternative. From this comparison it emerged that the ASHPWH:

- guarantees electrical energy savings from 69% to 82%;
- halves the time elapsed to achieve one heating cycle;
- reduces the GHG emissions from 7.47 kg CO_{2-eq} to approximately 2 kg CO_{2-eq} per one heating cycle.

1.4 Purpose of the study

The goal of this study is to model and to evaluate possible improvements in terms of COP for an air-source domestic hot water heat pump focusing on the condenser. It is interesting to evaluate the precision in which the temperature profiles in the storage tank can be predicted by means of thermodynamic models. To achieve these goals, a specific case study will be considered: the analysed heat pump will be the METROAIR AQUA produced by the company Metro Therm A/S [17]. At the moment the company lacks of a model able to predict the performances of the heat pump and mainly bases its choices on experimental tests to evaluate improvements on the system. A thermodynamic model can represent a way more attractive and cheaper solution to identify enhancements of the heat pump. First of all a steady-state model is built up in the Engineering Equations Solver (EES) environment in order to replicate the heating up process of the domestic hot water in the tank. Secondly, the findings from this model are used to implement a dynamic model in the Dymola environment to enable the inclusion of the time variable in the study.
The models will be applied to conduct several sensitivity analysis in order to identify possible improvements in the performances of the cycle in terms of COP. Four issues will be considered: the condenser geometry, the possibility to use different refrigerants in the cycle, the position of the water temperature sensor on the cycle performances, the goodness of an internal heat exchanger in such a system. In the following sections, a brief explanation and background will be provided for each of the four aforementioned researches. Moreover, for each investigation, a question reporting the purpose of the different analysis will be addressed in order to clarify their goals.

1.4.1 Condenser geometry

The questions guiding the investigations on this topic are: how does the condenser diameter influence the system COP? Do minichannel condensers improve the COP? What is the impact of the condenser length on the heat pump COP?

METROAIR AQUA' s condenser is a tube heat exchanger. The length and the diameter of the heat exchanger will be varied in order to evaluate possible enhancement of the heat transfer coefficient and the effects on the system COP.
More in details, the heat transfer coefficient in the condenser will be calculated implementing in the model the opportune correlations: different diameters will be tested, with the consideration also of mini condenser geometries. In fact, Cavallini et al. [18] emphasize the importance of the application of minichannels for air conditioning and refrigeration. They enable the installation of compact heat exchangers, the reduction of the refrigerant charge and the possibility to boost the spreading of natural refrigerants. The authors also state that it is very important to pay particular attention when applying correlations for macrochannels to minichannel geometries without experimental validations, due to the changes in gravity, viscous share and surface tension force. For this reason, a cautious literature review will be performed before implementing the correlations for the heat transfer coefficient.
Imbrahim et al. [16] observed that micro-condensers lower the condensing pressure if compared to macro condenser, resulting in higher COP. For a better understanding of the trends of the heat transfer coefficient for different diameters, the flow regime of the condensing refrigerant for different diameters will be evaluated in this study. Then the attention will be focused on the tube length. According to Zhang et al. [19], in which an air source heat pump water heater was optimized, the COP shows an inverted U-trend with a maximum by varying the condenser pipe length. Ibrahim et al. [16] assesses an increasing-converging trend for the COP with the condenser length.
The effects of the different configurations on the pressure drops will also be evaluated in order to estimate their impact on the heat pump running costs.

1.4.2 Different refrigerants

The main question for this topic is: which is the most suitable refrigerant to replace R134a?

R134a, currently used as refrigerant in the analysed heat pump, is a partly halogenated hydrocarbon (HFC). The HFC refrigerants were partly banned in Denmark after 1/01/2007 and nowadays only small refrigeration system are built applying F-gases, i.e the refrigerant charge needs to be lower than 10kg [20]. For what concerns the market of the DHWHP, it is still legal to use HFC heat pumps in Denmark, but new regulations are expected to come soon. For this reason this study will also analyse some alternatives to R134a. Following the same procedure presented in the Section 1.4.1, the condenser geometry will be optimized looking at the system

COP for the cycles with the tested refrigerants. The aim of this investigation is to find the most suitable refrigerant to replace R134a both considering the system COP and the volumetric flow rate, which gives indications about the expenditures for the compressor.

1.4.3 Temperature control

The main questions to be answered for this topic are: how is the heating up process of the domestic hot water influenced by different system configurations? Which is the extent of the COP reduction when the heat pump is required to heat up the domestic hot water at 60°C? How does the position of the hot water temperature sensor in the bottom of the tank influence the system COP?

After the thermodynamic model will be validated, it will be used to estimate the performances of the heat pump in terms of COP for different system configurations.
This study aims also to investigate the performances of the DHWHP when it is required to heat up the domestic hot water to 60°C. The COP is expected to drop because of the higher condensing temperature, but the extent of this reduction needs to be evaluated. This analysis is relevant because several EU countries require particular actions in order to prevent the risk of Legionella growth. For example, Bernardo et al. [21] mentioned that the Swedish industry regulations recommend to perform a weekly thermal disinfestations at 60°C during 10 minutes in case of water stored at temperatures lower than 60°C.
Another analysis will concern the position of the water temperature sensor in the bottom of the tank. A higher position of the sensor is expected to increase the system COP, but on the other hand a lower position increases the amount of available hot water in the tank. The influence of the sensor height in the tank on the DHWHP performances will be investigated.

1.4.4 Internal heat recovery unit

The main question for this topic is: is the internal heat exchanger beneficial for a DHWHP?

The current refrigeration cycle of the studied application includes an internal heat recovery unit. However, this additional heat exchanger is not always beneficial for the cycle and it can result in lower COP. In fact the addition of an internal heat recovery unit affects the compressor work due to the shift of the thermodynamic state point at the suction of the compressor and the slope of the isentropic lines. This study will detect if the internal heat exchanger increases the COP for the considered application or if it would be beneficial to remove it.
In the literature, several investigations were found concerning the goodness of an internal heat exchanger in refrigeration systems. For example, Eleiwi [22] presents practical studies conducted on a car air conditioning system operating with R134a at two different compressor speeds, i.e 1450 rpm and 2900 rpm. The performances of the cycle with and without internal

heat exchanger are analysed. From the experiments it emerged that for both the compressor speeds, the COP was enhanced by including the heat recovery unit in the cycle. Moreover, the effectiveness of the internal heat exchanger was also reported: it was between 0.61 and 0.75 for a compressor speed of 1450 rpm and between 0.60 and 0.73 for a compressor speed of 2900 rpm. Pottker et al. [23] conducted experimental investigations about the effect of condenser subcooling on an air conditioning system using R134a and R1234yf. It was observed that for both refrigerants the COP faces a maximum due to the trade-off between the beneficial effect of the increased refrigerating effect and the detriment of the higher compressor work. For R134a the maximum extent of the increase of the COP was 9%.
For what concerns the application of the performances of a heat pump with a liquid-suction heat exchanger, Payne et al. [24] investigated the performances of flammable refrigerants in water-to-water heat pumps for dwellings both in cooling and heating mode. Looking at the heating mode, which is interesting for this study, the authors found that the internal heat recovery unit in the cycle operating with R290 worsens the COP of 5% if compared with the cycle without internal heat exchanger. On the other hand, the cycle using as refrigerant a mixture of R32/290 faced an increase of the COP greater then 8% thanks to the addition of the liquid-section heat exchanger.
Due to the previous inconsistent indications, it is worthy to mention the findings deriving from the analysis of Domaski et al. [25]. The authors stated that the benefits caused by an internal heat exchangers in the cycle depend on both the operating conditions and fluid properties, with the heat capacity resulting as the most influential property. Systems showing good performances in terms of COP in the basic configuration are only marginally affected by the liquid-suction heat exchanger, which can have a positive or negative impact. On the other hand, cycles with poor COP are improved by the introduction of the heat exchanger.
For these reasons, it is interesting to evaluate the influence of the heat recovery unit on the system.

1.5 Thesis outline

In this section the structure of the thesis is explained in order to facilitate its reading.

- **Chapter 1** aims to highlight the attractiveness of the domestic hot water heat pump to reduce consumptions and emissions in the water heating end use and explains the goals of the present study.
- **Chapter 2** explains the configuration of the analysed domestic hot water heat pump and lists some other system arrangements present in the market.
- **Chapter 3** presents the main equations and assumptions applied to model the air source heat pump water heater both in steady-state and dynamic conditions.
- **Chapter 4** shows the strategy adopted to simulate the heating up process in the steady-state model and provides some more explanations concerning the application of the

models.

- **Chapter 5** contains the result from the steady-state simulations. Different system configurations and alternative refrigerants are evaluated. The influence of the main assumptions required to build the model is verified.
- **Chapter 6** presents the findings from the dynamic model. Initially a validation of the model and some explanations concerning the temperature profiles are given. Then the model is applied to investigate the performances of three system configurations
- **Chapter 7** shows the findings from the experimental tests conducted on an alternative system arrangement.
- **Chapter 8** summarizes the main findings from the analysis and also the main limitations of the model. Some ideas for further investigations are suggested.
- **Chapter 9** concludes the study by recalling the logical path followed and by mentioning the most important numerical results from the investigations.

2 Heat pump water heaters

At the beginning of this chapter, the technology state of art for the air source heat pump water heater is investigated. Initially, the system configuration used in the METROAIR AQUA is presented. Then possible alternative system arrangements found in the literature are described. Finally, a brief explanation of the technology applied for ground source heat pump water heaters is presented.

2.1 Air source heat pump water heaters

The Piping and Instrumentation diagram (PI diagram) for the considered application is depicted in Figure 2.1. It consists of a single stage electrically driven vapour compression cycle inclusive of an internal heat recovery unit which applies as working principle the Reverse Carnot Cycle. The energy carrier is the refrigerant R134a. The evaporator is an air cooler which applies forced convection, by means of a variable speed fan, to transfer heat from the air to the refrigerant. At the outlet of the evaporator, the refrigerant in gaseous form enters at first the internal heat recovery unit and then the rotary compressor where it reaches higher temperature and pressure levels before being transported to the condenser. In the condenser, which is wrapped around the domestic hot water tank, the R134a condenses and heat is released to the hot water embedded in the tank. At the outlet of the condenser the refrigerant flows again in the internal heat recovery unit, preheating the working fluid exiting the evaporator before the compressor suction. The cycle ends with the expansion process performed by a thermostatic expansion valve, in which the refrigerant is throttled until the evaporation pressure.
During peak hours, extra heat can be supplied to the domestic hot water thanks to the backup integrated electrical immersion heater, which has a capacity of 1.5 kW. The electric heater is placed in the upper part of tank and consequently it heats up the upper portion of water. Its activation is controlled by means of an operating thermostat measuring the temperature at point 9 in Figure 2.1 and of a set point temperature. The electric heater starts when the water temperature T_9 is lower than the set point temperature minus 5°C and it stops when T_9 equals the set point. It must be specified that this backup heat source should be used only when

it is strictly necessary, due to its much higher energy consumptions compared to the heat pump. More in details, in the user manual of the METROAIR AQUA [17] it is suggested that the starting of the immersed heater may be beneficial for the system at ambient temperature lower than 0°C.

For a better understanding of the cycle operation, some informations regarding the compres-

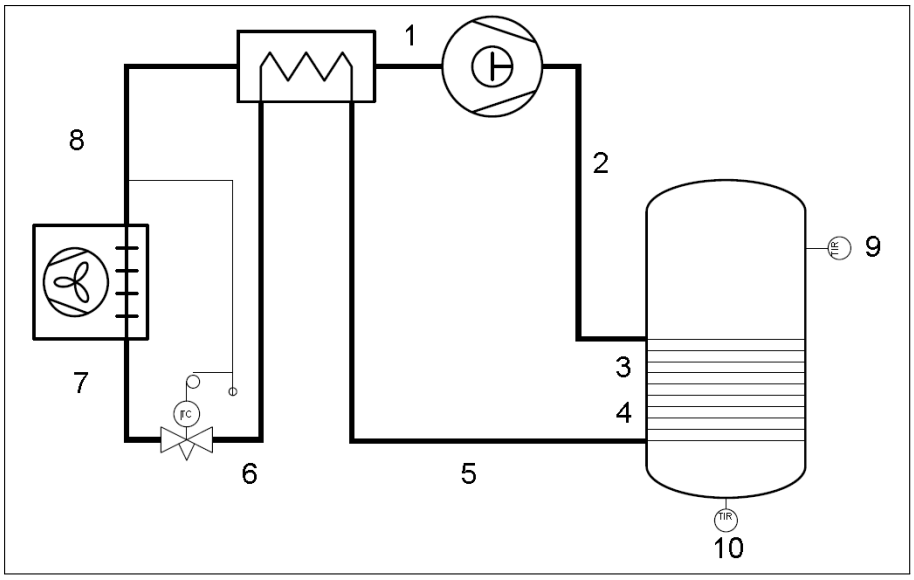

Figure 2.1: PI diagram of the METROAIR AQUA.

sor control strategy need to be provided. The control system on the compressor is an on/off control and its operation is regulated by means of a sensor measuring the temperature at the bottom of the tank (T_{10} in Figure 2.1) and of a set point temperature. Similarly to what happens for the electric heater, when the measured temperature T_{10} is lower than the set point minus 5°C the compressor is switched on. It is shut down when the water temperature at the bottom of the tank (T_{10}) and the set point temperature are equalized. According to the terminology suggested by Guo et al. [26], the aforementioned strategy is a thermostatic control pattern because it is based on a setting water temperature to control the water temperature inside the tank. Another possible solution presented by the author is the timing control pattern in which the start-up time is determined. The optimal start-up time should correspond to the daily hours with the warmest ambient temperature, due to the better performances offered by the system.

Other system configurations for air source water heater found in the literature mainly concern and differ from the one analysed in this work because of the condenser. For instance, Guo et al. [26] and Zhang et al, [19] analysed ASHPWH with immersed condenser, while Morrison et al. [27] considered also systems based on integrated package with external condenser, as shown in Figure 2.2.

Both immersed and wrapped around the outside of the tank condenser coils can be found in the market, with a small preponderance of the latter solution. For example, the company

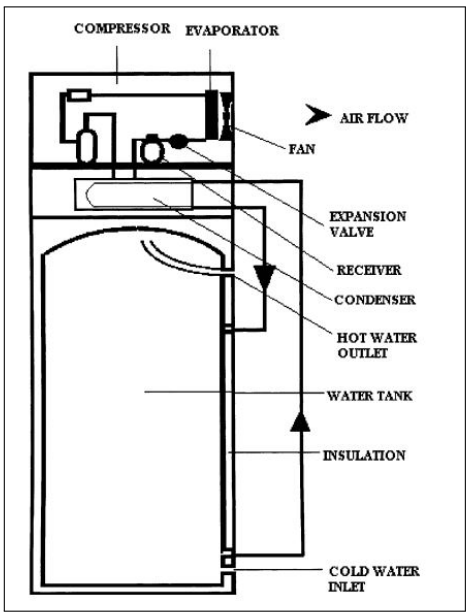

Figure 2.2: Integrated package with external condenser considered by Morrison et al [27].

Kingspan [28] proposes an immersed condenser tube and reports yearly savings of 530£ on the heating bill compared to electric water heaters. Diplex [29] and Stiebel [30] adopt wrapped around solutions. The former reports that the water heater design is able to satisfy alone the 90% of the hot water demand, while the latter advertises a percentage of 70% of hot water needs met by the domestic water heater. The COP for the different systems are not mentioned because they all refer to different standards and consequently test conditions, and, as a consequence, their comparison would result unfair.

The company PHNIX [31] includes in its product portfolio microchannel heating coils

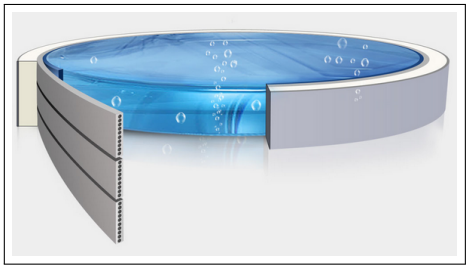

Figure 2.3: Micro-channel heating coil [31].

wrapped outside the hot water tank, as shown in Figure 2.3. In the manufacturer catalogue, it is stated that this solution enables a higher contact area between the water inside the tank and the condenser reaching a COP of 3.2 based on standard DS/EN 16147 [32], which will be considered also in this study.

Finally, another system configuration present in the market (Danfoss [33]) consists on the

application of a micro plate heat exchanger as depicted in Figure 2.4. According to what described in the manual, this solution enhances the heat transfer and consequently the heat pump efficiency and due to its compactness reduces the refrigerant charge. This system is also characterised by the "TWS (Tap Water Stratification) technology", patented by the company. It consists on a technique according to which the water at the outlet of the micro plate heat exchanger flows in a coil immersed in the tank in order to heat up the domestic water, promoting the thermal stratification. The water inside the heater is split in different layers to reduce the time required for the hot water to reach the desired temperature.
Despite the secure interest of this innovative solution, its is not considered in this work. The reason for this choice is based on the willingness to firstly model the water heater implementing different condenser geometries, and then test the optimal solution at Metro Therm in-house laboratory. It would be impossible to test different condenser arrangements due to the different manufacturing process required. Moreover, the condenser coil wrapped outside the tank is considered to be still a good solution also because of the possibility to ensure a longer operating life for the unit due to absence of direct contact between the water and the condenser coil [31].

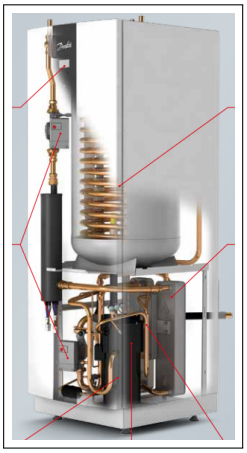

Figure 2.4: Micro plate condenser and TWS technology [33].

2.2 Ground source heat pump water heaters

Another possible configuration for heat pump water heater consists on the extraction of heat from the ground to evaporate the refrigerant. This system arrangement is called ground source heat pump water heater and it requires an additional heat exchanger buried in the ground. According to Shan et al. [34], who analysed a ground source heat pump, the soil temperature below 5 m under ground is stable and subjected to minor variations during the year. This fact enhances the COP compared to the other heat pumps and results in more stable performances throughout the year. However, the application of ground source heat pumps is limited because of the large area required by the ground heat exchanger. Both vertical and horizontal solutions

are adopted for the heat exchanger buried in the ground. Vertical solutions can require to drill holes deeper than 100 m.
In this study only air source heat pump water heaters are considered due to willingness to focus on the previously mentioned case study.

3 Model implementation

In this chapter, the models implemented to simulate the domestic hot water heat pump are presented.
At the first place, the model was built-up in the Engineering Equation Solver (EES) environment. It is an equation solving program able to solve non linear equations systems and to detect the fluids properties [35]. The heating up process of the domestic water in the tank performed by the heat pump is simulated in EES. During this process all the volume of domestic hot water inside the tank is heated.
Secondly, a model of the tank, inclusive of the heat transferred to the hot water from the wrapped around condenser, was built in the Dymola environment [36]. Dymola, based on the Modelica open standard, allows the implementation of dynamic simulations increasing the reliability of the model [37]. The goal of this second model is to simulate the temperature distribution along the tank and to replicate its heating phenomena.

3.1 Steady-state model

The equations required to model all the components depicted in Figure 2.1 are described in the following. The numbers indicating the thermodynamic state points in this section and for the rest of the report correspond to the ones of Figure 2.1. It must be specified that in the aforementioned figure, thermodynamic state points 3 and 4 represent respectively the outlet from the desuperheating section and the inlet to the subcooling section in the condenser. In other words, they detect where the condensing process intersect the Andrews thermodynamic diagram in the pressure-enthalpy diagram: the dew point curve characterised by saturated vapour and the bubble point curve in which saturated liquid condition occurs. These two additional thermodynamic state points are relevant for a better understanding of the pressure drops in the condenser, which will be introduced in the following.

3.1.1 Evaporator

Due to focus of the report on the condenser geometry, the evaporator was built-up in a simplified way, without considering correlations for the heat transfer coefficients in the two-phase and superheated sections.

The inlet and outlet temperatures air side were both fixed. Their values are presented in

Table 3.1: Assumptions for air temperatures at the evaporator

$T_{in,air}$ [°C]	7
$T_{out,air}$ [°C]	4

Table 3.1. These assumptions are due to the willingness to emulates as accurately as possible the heating up process of the domestic hot water in the tank following the indications of the Standard DS/EN 16147 [32], in which the temperature of the air supplied to the evaporator is fixed to 7°C. In this way the temperature difference air side was fixed and, as a consequence, the air mass flow rate was a free variable in order to satisfy the energy balance.
For what concerns the refrigerant side, the required assumptions are shown in Table 3.2. The UA value in the evaporator was assumed considering the indications from similar applications in the literature [16]. The heat transfer rate at the evaporator was calculated applying the logarithmic mean temperature difference (LMTD) expressed in Equation 3.1.

$$\dot{Q}_e = UA_e \Delta T_{ml,e} \tag{3.1}$$

in which, assuming a constant overall heat transfer coefficient along the evaporator [38],

$$\Delta T_{ml,e} = \frac{(T_{in,air} - T_e) - (T_{out,air} - T_e)}{ln\frac{(T_{in,air} - T_e)}{(T_{out,air} - T_e)}} \tag{3.2}$$

It must be mentioned that in Equation 3.2 the superheating is not considered and the temperature at the outlet of the evaporator refrigerant side was considered equal to the evaporation temperature. This is common practice in refrigeration field due to the fact that the ΔT_{ml} including the superheat is not representative and it would require to divide the heat exchangers in two sections in the model: the evaporation section and the superheating one.

Table 3.2: Assumptions refrigerant side at the evaporator

$UA_e \left[\frac{W}{m^2K}\right]$	130
ΔT_{sup} [K]	3

3.1.2 Internal heat exchanger

For what regards the internal heat recovery unit, commonly named liquid-suction heat exchanger, the only necessary assumption was the value of its effectiveness, set to 0.3. This low effectiveness was assumed due to the fact that the internal heat exchanger consists on the welding of the tubes at the liquid and vapour lines. The impact on the system of this assumption will the investigated in the report. The effectiveness was then expressed as

$$\epsilon = \frac{T_1 - T_8}{T_5 - T_8} \tag{3.3}$$

3.1.3 Compressor

The model of the applied rotary compressor, manufactured by *Shanghai Hitachi Electrical*, is WHP01900BSV-uxywz. The manufacturer catalogue was provided by the company and some of its details useful for this work and mentioned in the following are presented in Appendix A. The polynomials for calculating the volumetric and isentropic efficiency were not given in the catalogue. Consequently a function for the isentropic efficiency was derived applying an interpolating procedure in the Matlab environment [39]. The interpolating function is presented in Equation 3.4. Further explanation regarding the calculation and the values for the constants z_i can be found in Appendix A.

$$\eta_{is} = z_1 + z_2 T_c + z_3 T_e + z_4 T_c^2 + z_5 T_c T_e + z_6 T_e^2 + z_7 T_c^3 + z_8 T_c^2 T_e + z_9 T_c T_e^2 + z_{10} T_c^3 \tag{3.4}$$

For the calculation of the refrigerant mass flow rate, fixed by the compressor, the compressor displacement rate would be required. However, the manufacturer catalogue gives information only about the compressor volume, equal to 12.2ml/rev, but its velocity is not mentioned. As a consequence, a possible solution was to assume this velocity in order to detect the displacement volume. Following this path, a further assumption would have concerned the volumetric efficiency of the compressor. This rout would have implied an unacceptable uncertainty on the refrigerant mass flow rate. Consequently it was preferred to implement this parameter in the model by considering another interpolating procedure described in Appendix A. It is obtained by a graph presented in the manufacturer catalogue (Figure A.1), depicting the evolution of the mass flow rate as a function of the condensing and evaporation temperatures. The derived expression for the refrigerant mass flow rate is reported in 3.5 and the required constants are presented in Appendix A.

$$\dot{m}_r = o_1 + o_2 T_c + o_3 T_e + o_4 T_c^2 + o_5 T_c T_e + o_6 T_e^2 \tag{3.5}$$

3.1.4 Condenser

First of all the actual condenser geometry needs to be specified (Table 3.3). The outer diameter D_{out} was found from the condenser manufacturer catalogue. The condenser total length $L_{tot,cond}$ was found as shown in Equation 3.6 considering the fact that the condenser tube, made by aluminium, is wrapped around the tank.

$$L_{tot,c} = n\pi D_{out,tank} \tag{3.6}$$

where n is the number of times the condenser is wrapped around the tank.
Before analysing the implemented equations it is also necessary to specify that considering

Table 3.3: Condenser geometry specifications

D_{out} [mm]	9.95
s [mm]	1.4
$L_{tot,cond}$ [m]	54
n [-]	26

the route of the refrigerant inside the condenser, three heat transfer phenomena can be identified [38]:

- **Desuperheating**: the refrigerant vapour is cooled until it reaches saturated vapour conditions;
- **Condensation**: the saturated vapour is cooled to saturated liquid;
- **Subcooling**: the saturated liquid refrigerant is further cooled to a lower temperature.

The three aforementioned processes are considered separately in this work. Consequently, three different sections are considered, each of them with a constant UA value and mean logarithmic temperature difference. The three heat exchangers are imagined to be connected in series. One reason for this choice lays in the fact that the specific heat can largely differ between liquid and vapour conditions. Moreover, in case of an unique ΔT_{ml} for the overall condensing process, the desuperheating would take too much weight compared to condensation and subcooling due to the high temperature at the compressor discharge.
As these differences clearly empathised, different models and correlations for the heat transfer coefficients are required for the three heat exchange processes. They are described in the following for each of the three sections.
The last consideration before going through the different equations concerns the temperature drop in the subcooler, i.e. ΔT_{sub}, which was set to 5K. The impact of this assumption will be detected performing a sensitivity analysis.

Desuperheating section

The heat exchanged in the desuperheating section was calculated from the energy balance refrigerant side. The heat transferred in this section was also expressed considering the LMTD:

$$\dot{Q}_{desup} = U_{desup} A_{desup} \Delta T_{ml,desup} \tag{3.7}$$

The heat exchange area of the desuperheater was found applying Equation 3.8.

$$A_{desup} = \pi D_{in} L_{desup} \tag{3.8}$$

The logarithmic mean temperature difference in this section was expressed as

$$\Delta T_{ml,desup} = \frac{(T_c - T_{in,w,desup}) - (T_2 - T_{out,w})}{ln\frac{(T_c - T_{in,w,desup})}{(T_2 - T_{out,w})}} \tag{3.9}$$

where $T_{in,w,desup}$ is the water temperature at the inlet of the desuperheater and $T_{out,w}$ is the water temperature at the outlet of the desuperheater. $T_{in,w,desup}$ was calculated from the energy balance water side at the desuperheater.
The overall heat transfer coefficient U_{desup} was calculated by using Equation 3.10. In the equation $D_{out,c}$ needs to be expressed in [m].

$$U_{desup} = \left(\frac{1}{\alpha_{r,desup}} + \frac{1}{\alpha_{w,desup}} + R_{wall,desup} \pi D_{out,c} \right)^{-1} \tag{3.10}$$

In Equation 3.10 $R_{wall,desup}$ stands for the heat transfer coefficient for conduction through the tube's wall, which can be quantified applying Equation 3.11.

$$R_{wall,desup} = \frac{ln(D_{out,c}/D_{in,c})}{2\pi k} \tag{3.11}$$

The conductivity of aluminium included in Equation 3.10 was calculated at the wall temperature which was found by applying simultaneously with Equation 3.10 the Newton's law of cooling refrigerant side.
The correlations implemented to calculate the heat transfer coefficients refrigerant and water sides have to be specified. The heat transfer coefficient for the refrigerant flowing inside the condenser tube was calculated applying the Dittus-Boelter correlation reported in Equation 3.12 [40].

$$Nu = 0.026 Re^{0.8} Pr^{0.3} \tag{3.12}$$

The heat transfer coefficient refrigerant side was derived from the Nusselt number using the tube inner diameter as characteristic length. The range of applicability of the considered correlation is reported in Equation 3.13. The correlation was derived by the authors analysing

the heat transfer from water to the atmosphere in tubular automotive radiators [40].

$$0.7 < Pr < 120 \qquad 10000 < Re < 160000 \tag{3.14}$$

The decision concerning the most suitable correlation for the heat transfer coefficient water side was quite complicated. Some correlations for external free convection flows, free convection within parallel plate vertical channels and laminar flow in circular tubes [41] were firstly considered. However, it was preferred to apply Equation 3.15 presented in the work of Knudsen [42]. The correlation was derived by the author from empirical observations on the heat transfer from tank wall to domestic water in case of solar domestic hot water systems. This choice was due to the similarity with the application considered in this study: the solar domestic hot water system consisted on a mantle wrapped outside the hot water tank, in the same way of the condenser shown in Figure 2.1.

$$Nu = (0.186(H/D_{out,tank}) + 2.285)(Ra_y(D_{out,tank}/H)^4)^{0.26} \tag{3.15}$$

valid for

$$2.0 \leq H/D_{out,tank} \leq 3.7 \tag{3.16}$$

In the analysed case the $H/D_{out,tank}$ ratio is 2.12. Ra_y is the local Rayleigh number calculated at characteristic length y corresponding to the distance from the bottom of the tank. For the calculation of the Rayleigh number the difference between the wall temperature derived from the Newton's law of cooling refrigerant side and the average water temperature at the desuperheater was used as temperature difference. The conductance in the wall was neglected for the sake of simplicity. For this section of the condenser y equals 0.43 m: it is the distance between the bottom of the tank and the beginning of the condenser tube wrapped outside the water tank. y was used also as characteristic length to calculate the heat transfer coefficient water side from the Nusselt number.
For what concerns the calculation of the pressure drops refrigerant side in the desuperheater, Equation 3.17 was applied [38].

$$\Delta p_{desup} = f_{desup}\rho_{desup}u^2_{desup}\frac{L_{desup}}{D_{in,c}}10^{-5} \tag{3.17}$$

where the friction factor f_{desup} was found considering the Blasius correlation [38]:

$$f_{desup} = \frac{0.158}{Re^{0.25}_{desup}} \tag{3.18}$$

valid for $3000 \leq Re \leq 100000$.

Condensing section

Initially the heat exchanged in the condensing section was calculated by expressing the energy balance refrigerant side, similarly to what presented for the desuperheater. This value of the heat transfer rate was then applied in the energy balance water side in order to detect the inlet water temperature in this section, i.e. $T_{in,w,cond}$. Later, the heat transferred was expressed by means of the LMTD similarly to what presented in the desuperheating section. The the overall heat transfer coefficient was calculated as:

$$U_{cond} = \left(\frac{1}{\alpha_{r,cond}} + \frac{1}{\alpha_{w,cond}} + R_{wall,cond} \pi D_{out,c} \right)^{-1} \tag{3.19}$$

In Equation 3.19 the wall resistance was calculated similarly to Equation 3.11, but considering instead the wall temperature at the condensing section to calculate the thermal conductivity. The aforementioned temperature was found by applying the Newton's law of cooling refrigerant side in this portion of the overall condenser.
The heat transfer coefficient water side was derived in the same way described for the desuperheating section, i.e. applying Equation 3.15. The only differences lay in the calculations of the Rayleigh and Nusselt numbers:

- the temperature difference was expressed as the difference between the average water temperature and the wall temperature in the condensing section
- the characteristic length in the condensing section needed to be evaluated. The starting point for this computation was the knowledge of the desuperheater length. From its value it was possible to calculate the number of times the desuperheater wraps around the water tank. By multiplying this value for the outer diameter of the condensing tube it was possible to derive the distance from the bottom of the tank at which the condensing section begins, i.e. y_{cond}. The aforementioned procedure is summarized in Equation 3.20.

  $$y_{cond} = y_{desup} - \frac{L_{desup}}{\pi D_{out,tank}} D_{out,c} \tag{3.20}$$

  where, as stated in the previous section, y_{desup} equals 0.43 m.

For what concerns the calculation of the heat transfer coefficient refrigerant side, a distinction needs to be made between macrochannel geometries and minichannel ones. As aforementioned in the *Introduction*, Matkovic et al. [43] and Cavallini et al. [18] emphasizes that the phase change process for miniscale channels may be different than the one for macrochannels because of the variations of the impacts of gravity, surface tension and shear stress. As a consequence, the validity of the correlations for the heat transfer coefficient derived by analysis on macro-geometries needs to be verified in case of minichannels. More in details, Matkovic et al. [43] evaluated the heat transfer coefficients of R134a and R32 flowing inside a minichannel having a single circular diameter of 0.96 mm by measuring the local heat flux

and the saturation and wall temperatures occurring during condensation. Then, these values were compared with the ones derived from some models found in the literature. From this investigation it emerged that the model presented by Cavallini et al. [44] is the heat transfer model which gave the most accurate prediction of the heat transfer coefficients. For this reason, this correlation was applied for microgeometries. For macroscale channels the Shah's correlation was introduced into the model [45]. It was chosen to mention in the main body of the report only the two main equations for minichannel and macrochannel condenser, reported respectively in Equation 3.21 and 3.22. A more detailed explanations of the two correlations and the meaning of the parameters included in the two mentioned equations can be found in Appendix B. This choice was made to avoid to weigh the reading down.

$$\alpha_A = h_{LO}\left[1 + 1.128x^{0.8170}\left(\frac{\rho_L}{\rho_G}\right)^{0.3685}\left(\frac{\mu_L}{\mu_G}\right)^{0.2363}\left(1-\frac{\mu_L}{\mu_G}\right)^{2.144} Pr_L^{-0.100}\right] \tag{3.21}$$

$$\alpha_{TP} = h_L\left[(1-x)^{0.8} + \frac{3.8x^{0.76}(1-x)^{0.04}}{p_r^{0.38}}\right] \tag{3.22}$$

The same distinction is required also for the computation of the pressure drop. For macrogeometries the built-in EES function DELTAP-2phase-horiz was applied. It evaluates the pressure losses by summing the momentum and frictional pressure drops, due to the fact that the static pressure drop in a horizontal tube is nil. The former are found applying a void fraction derived from drift flux model [35], as suggested by Didi et al. [46]. The computation of the pressure gradient is performed by applying the Muller-Steinhagen and Heck correlation [46], which is reported in Appendix B.1.2. Then it is integrated in order to calculate the pressure drop from the tube inlet to its outlet. A constant heat flux is considered for all the length of the tube in order to have constant dL/dx [35]. On the other hand, for minichannel tubes it was decided to consider the interpolation described by Cavallini et al. [47] to estimate the pressure gradient in the condensing section. This was proved by Cavallini et al. [48] to be in good agreement with experimental results performed on minitube condensers. Again it was preferred to present only the main equation used to estimate the frictional pressure drop in minichannels (Equation 3.23). A linear dependence between the pressure and the condenser tube length was assumed for applying Equation 3.23. A more complex explanation will be provided in Appendix B.

$$\left(\frac{dp}{dz}\right) = \frac{\Phi_{LO}^2 2 f_{LO} G^2}{D_{hydraulic}\rho_L} \tag{3.23}$$

Subcooling section

Again the heat exchanged in the subcooler was expressed implementing the energy balances water and refrigerant side, as well as the LMTD. The same principle described for the condensing section was used to estimate the wall resistance. The length of the subcooler was

found by subtracting the lengths of the condensing and desuperheating sections to the overall condenser length. Moreover, the same equation was applied to calculate the heat transfer coefficient water side, i.e. Equation 3.15. Its characteristic length for the subcooler, i.e. y_{sub} was calculated in the same way as in Equation 3.20, detecting the number of times the condensing section wraps around the tank.
For the calculation of the heat transfer coefficient refrigerant side, it was decided to apply the Gnielinski correlation due to the low Reynolds number caused by the limited velocities typical of the refrigerant in its liquid form. The correlation is reported in 3.24: the tube inner diameter was used as characteristic length.

$$Nu = \frac{(f/8(Re-100)Pr)}{1+12.7(f/8)^{1/2}(Pr^{2/3}-1)} \tag{3.24}$$

where

$$f = (0.790ln(Re)-1.64)^{-2} \tag{3.25}$$

The previous equation is applicable in the range:

$$0.5 < Pr < 2000 \qquad 3000 < Re < 5 \cdot 10^6 \tag{3.27}$$

The pressure drops in the subcooler were calculated using 3.17.

3.1.5 Expansion valve

The expansion process is assumed to be isenthalpic, meaning that the heat losses in the expansion valve are neglected. This assumption can by justified by the small size of the valve.

3.2 Dynamic model

As aforementioned, the dynamic model of the tank in the Dymola environment was created in order to understand the distribution of the water temperature inside the tank.
The starting point for the creation of the model was the work accomplished by Cruickshank [49]. Her work consisted on the experimental and numerical evaluation of a novel multi-tank thermal energy storage, based on the connection of standard hot water tanks applying a single charge flow loop. The charge of each single tank was performed by applying both a natural convection heat exchanger and a thermosyphon loop. The application for the multi-tank thermal energy storage was a solar domestic hot water system. In order to predict the performances of the mentioned system, a numerical model was built in the TRNSYS simulation environment. It was then validated through laboratory tests.
The model of the stratified thermal storage is based on the split of the tank into N constant volume sections or nodes, which are assumed to be characterized by a full mixing and an uniform temperature, as presented in Figure 3.1. For the present study, it was chosen to divide

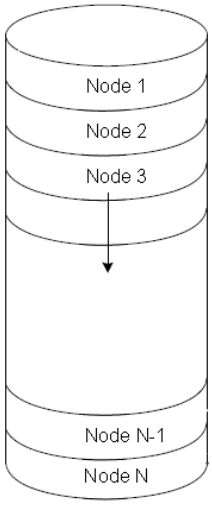

Figure 3.1: Hot water tank divided in different nodes in order to enable the modelling of thermal stratification [49].

the tank in 20 nodes. As suggested by Newton [50] and confirmed by Celador [51], the split of the water tank in 15 layers is sufficient to successfully represent the thermal stratification.
The prediction of the temperature in each node can be done by applying an energy balance to each section, taking into account both the influence of the adjacent nodes and the thermal losses to the surrounding ambient. To account for the impact of the adjacent nodes, it is necessary to include in the model mass and energy flows, considering both the energy transfer through vertical conduction from the tank walls and conduction between the layers. Moreover, in the specific case considered in the present study, also the heat transferred to the domestic hot water from the condenser wrapped around the tank needs to be included. The ordinary differential Equation 3.28 summarizes all the considered contribution representing the energy balance for node i-th: its understanding can be facilitated by looking at the control volume shown Figure 3.2. Figure 3.2 was taken from Cruickshank's report and then adjusted in order to take into account the relevant energy contributions in the present work.

$$\begin{aligned} M_i C_p \frac{dT_i}{dt} = & \frac{(k+\Delta k)A_{c,i}}{\Delta L_{i+1\rightarrow i}}(T_{i+1}-T_i) + \frac{(k+\Delta k)A_{c,i}}{\Delta L_{i-1\rightarrow i}}(T_{i-1}-T_i) + U_{amb,i}A_{s,i}(T_{amb}-T_i) \\ & - \dot{m}_{up}C_pT_i + \dot{m}_{up}C_pT_{i+1} + \dot{Q}_{cond,i} - rM_iC_pT_i - rM_iC_pT_i \\ & + rM_{i+1}C_pT_{i+1} + rM_{i-1}C_pT_{i-1} \end{aligned} \tag{3.28}$$

The initial values for each node temperature correspond to the ones at the beginning of the time step. An uniform temperature of 10°C is considered for the water in the tank before starting the heating up process. In order to detect the temperature distribution in the storage tank, Equation 3.28 needs to be applied to all the N nodes of the tank. In this way a set of N first-order differential equations is created. Due to the fact that the temperature of each node is affected by the temperature of the adjacent nodes, the aforementioned system of differential

equations needs to be solved simultaneously.
In Equation 3.28:

- $\dot{m}_{up}$ is the water flow rate up the tank. Only an upward flow rate is included due to the fact that the draw-off occurs from the top of the tank in the considered application.
- $A_{c,i}$ and $A_{s,i}$ represents respectively the cross-sectional area and the surface area of each node.
- ΔL corresponds to the center-to-center distance between two nodes;
- k is the water thermal conductivity which was assumed to be 0.58 W/mK.
- Δk is defined as the de-stratification conductivity. De-stratification occurs because of the mixing of node interfaces and conduction along the hot water tank wall. Shyu [52] observed that stratification faces a more rapid decay compared to one theoretically estimated when the conductivity of water is used. This happen because of the higher conductivity of the wall material which promotes convection motion along the hot water tank wall and de-stratification inside it. This additional thermal conductivity is calculated as:

$$\Delta k = k_{wall} \frac{A_{c,wall}}{A_{c,fluid}} \tag{3.29}$$

  where k_{wall} is the thermal conductivity of the tank material, i.e. steel in the specific case, and is set to 16 W/mK. According to Newton [50], Equation 3.29 represents a good approximation to estimate the "real" conduction between adjacent nodes. However, a value derived from experiments for this conductivity factor is preferable because in the equation the additional convection motion in the tank is not included, underestimating the stratification decay.

- $\dot{Q}_{cond,i}$ corresponds to the heat transferred to the hot water by the condenser wrapped around the tank. This heat is different for the desuperheating, condensing and subcooling section, as it will be further explained and analysed later on in the report.
- r represents the mass fraction of water which is assumed to be recirculated in the tank and it is expressed in $\frac{\%}{s}$. This additional parameter, not included in Cruickshank's work, is an attempt to include in the model the mixing phenomena between the layers inside the tank. According to Dwivedi [53], the inclusion of mixing phenomena and their validation through experiments is a further step to raise the reliability of dynamic models of hot water tanks.
  To keep the model as realistic as possible, an if-statement were introduced in the model to control the last four terms on the right side of the equal sign in Equation 3.28. These terms are the ones introducing in the model the mixing between the different layers, occurring because of gravity and buoyant effect. This phenomena cause the deposit

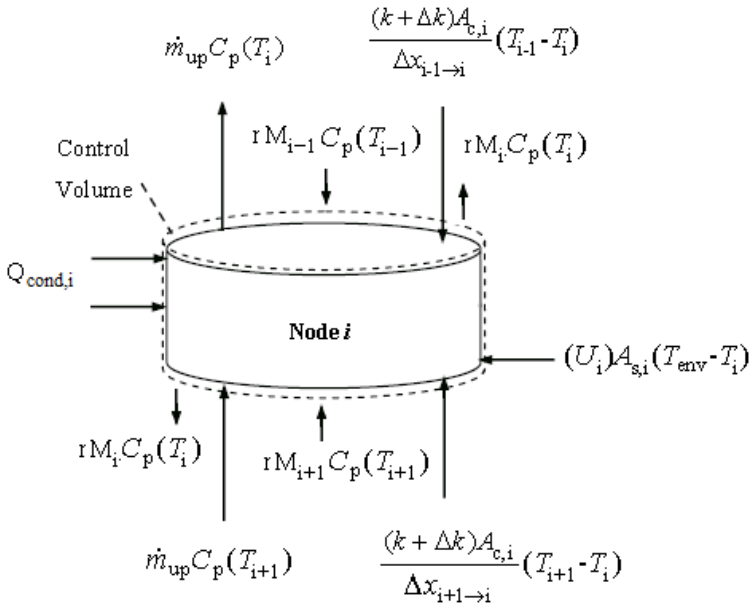

Figure 3.2: Control volume used for node i.

of water with different temperature to a certain height in the tank according to the the density difference: light density brings hot water to the above layers while cold water is transported to the bottom layers because of its heavy density [54]. The implementation of this behaviour in the model required the aforementioned if-statement. The mixing between the node i and the node above (i-1) was allowed only if the temperature in node i was higher than the one in node i-1. If this condition was not fulfilled, no mixing was occurring between the nodes. On the other hand, the mixing between node i and the node below (i+1) was permitted only if the temperature in the layer i+1 was higher than the one in node i. If T_i was higher than T_{i+1} the mixing was not allowed and set to zero. This concept in graphically shown and clarified in Figure 3.3.

For what concerns the heat released to the hot water from the condenser, some constraints needed to be applied. First of all, the thermostatic control strategy described in Chapter 2 was introduced in the tank. A sensor measuring the water temperature was imagined to be placed in each layer of the tank. One of this layer, initially at the bottom of the tank, and a certain set point temperature, initially 52°C, needed to be selected in order to emulate the on/off control strategy of the heat pump. The heat from the condenser was transferred to the hot water when the temperature at the chosen layer was equal to the set point temperature minus 5 K. The heat transfer was then stopped again when the set point temperature was reached in the chosen layer. It was possible to implement the control in the model by introducing an integer variable fluctuating according to the temperature at the chosen layer.
The second constraint required for $\dot{Q}_{cond,i}$ regarded the nodes to which the heat was applied.

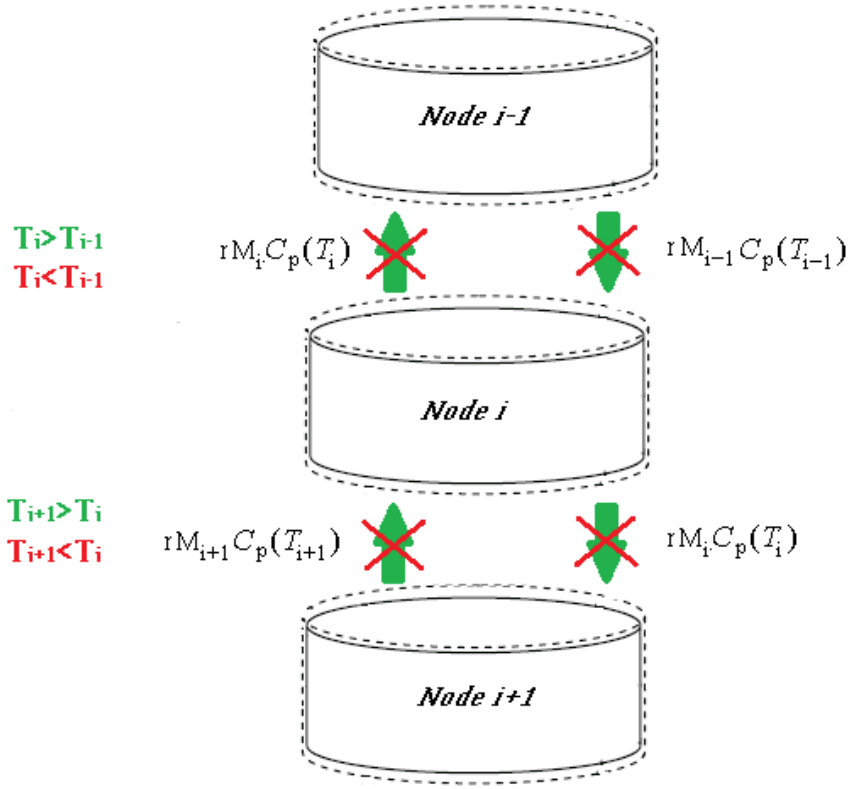

Figure 3.3: Regulation of the mixing between three adjacent layers.

It was possible to identify these nodes by considering the values for y, i.e. the distance from the bottom of the tank at which each section of the condenser starts, from the steady-state simulations. Three if-statements were introduced in the model to indicate the locations of the desuperheating, condensing and subcooling section.
For the calculation of the compressor work, some functions relating the work of the compressor to the average water temperature along the overall condenser were derived for each analysed condenser geometry. The calculation of the instantaneous COP, i.e. for each second, was performed applying Equation 3.30, considering all the heat transferred from the condenser and the compressor work of the second under investigation.

$$COP = \frac{\dot{Q}}{\dot{W}} \tag{3.30}$$

It was decided to calculate also the average COP (COP_{avg}) considering all the cumulative energies in the considered time step.

In order to evaluate the discrepancy between the predictions from the model and the experimental results, Equation 3.31 was used. The initial temperature ($T_{initial}$) of 10°C was used as

benchmark in order to calculate all the discrepancies.

$$Discrepancy = \frac{T_{experiments} - T_{predictions}}{T_{experiments} - T_{initial}} \tag{3.31}$$

4 Simulation strategy

In Chapter 3 the equations implemented in the EES and Dymola environments to build the models were presented. In this chapter, the way in which these models were applied and some further required assumptions are described.
Initially, the strategy adopted to replicate through the EES model the hot water heating up process is presented. Then the adjustments required to the model to enable the comparison of the performances of the system working with different refrigerants are explained. Moreover, the correlations used to derive the costs of different system configuration are described. Lastly, the assumptions necessary to enable the implementation in the Dymola model of tapping profiles from the tank according to the indication given in the Standard DS/EN 16147 are summarised.

4.1 Other assumptions

Some other assumptions considered are:

- the pressure drops in the pipes connecting the different components are not considered. This choice is due to their limited length caused by the compactness of the analysed application.
- the pressure drop in the evaporator and in the internal heat recovery unit are disregarded.
- defrosting issues are not considered in the report even for low values of the air temperature supplied to the evaporator.
- the fan power is disregarded in this analysis.
- it is assumed that the contact surface between the tube and the tank corresponds to the overall vertical section of the tube.

4.2 Heating up process in the steady-state model

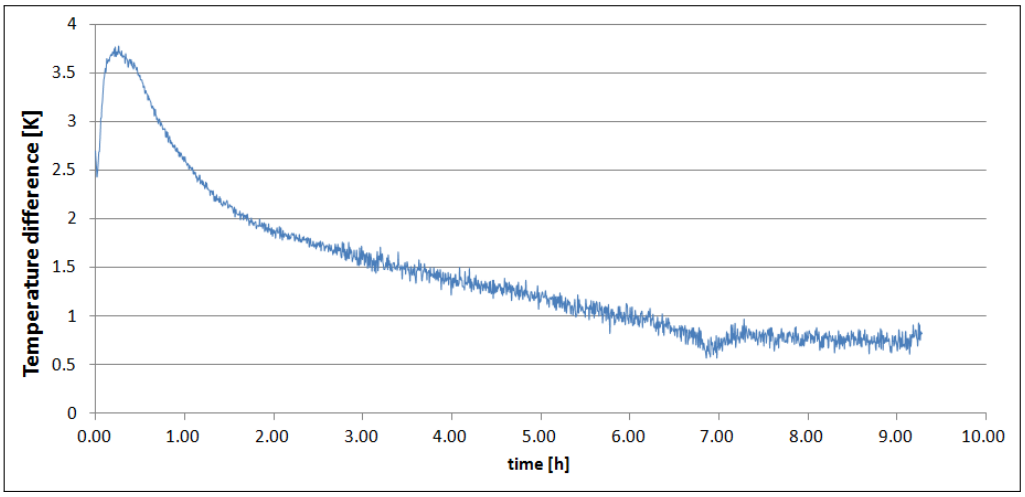

(a) Variation with the time of the temperature difference between T_9 and T_10.

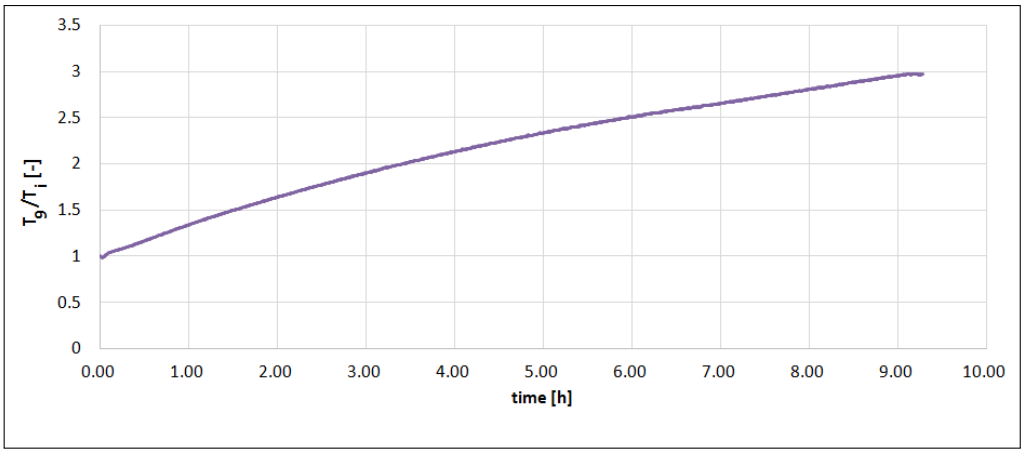

(b) Evolution of the temperature T_9 during the heating up process.

Figure 4.1

The heating up process was simulated in EES based on experimental results provided by Metro Therm. The experiments were conducted in a insulated chamber in which the ambient temperature was kept to 20°C and the air was supplied to the evaporator at 7°C, as stated in the Standard EN 16147. The hot water temperature was measured at the middle of the tank and at its bottom, as depicted in Figure 2.1 by the locations of the sensors at points 9 and 10. Several experimental data were given and at this stage of the analysis it was decided to take into account the one characterised by the highest temperature difference between T_9 and T_{10}. The temperature at point 9 was higher than the one in point 10 during all the process due to the thermal convection and the water recirculation inside the tank. The trend over time of the temperature difference between T_9 and T_{10} is shown in Figure 4.1a. From the figure, it can

be observed that this ΔT reaches a peak after 22 minutes, then it shows a downward trend. A choice needed to be done about the water temperature profile to implement in the model. The worst possible case corresponds to the highest hot water temperature and consequently it was chosen to consider the temperature at point 9. Its evolution during the heating up process is depicted in Figure 4.1b, even though the numerical values of the y-axis are dimensionless. More in details the temperature at each time step is expressed as the ratio of its nominal value and the temperature at the time 0 (i.e. T_i). This choice is due to the confidentiality agreement with the company. From the figure it emerges that its trend is not linear, but it is steeper for low water temperatures. Consequently, the idea to divide the heating up process in four runs was considered a better approximation than considering a linear evolution of the temperature profile through the overall process. The inlet water temperature of each run was an input for the model, while the outlet water temperature for the different run was not fixed in the model, but it was an output from the program. Consequently, it was not possible to follow precisely the evolution of the water temperature depicted in Figure 4.1b. However, it was still considered more realistic to follow this route instead of approximating the heating up process with an unique linear temperature lift. The water mass flow rate for the four runs was derived from the water density, the overall water volume inside the tank and the duration of the different time steps. The water temperatures, time steps and water mass flow rates for each run are summarized in Table 4.1. It is necessary to highlight that some temperature lifts are overlapping in Table 4.1: for example the final water temperature for run 1 is 31.2°C and the initial water temperature for run 2 is 27°C. This means that the temperature raise from 27°C to 31.2°C is accomplished in both the two runs. As aforementioned, the reason for these discrepancies lay in the fact that the outlet water temperature is an output from the program. However, all the choices for the intervals summarized in the table were made considering worse cases compared to the experimental data. Consequently, improvements on the cycle for the considered runs are expected to be even more beneficial in the real process. To verify the validity of this statement, a more realistic model of the heating up process was built in the Dymola environment and experimental tests were performed on the improved condenser geometries: the aim of the steady-state simulations was to accomplish a first selection on the possible condenser configurations.
Table 4.1 shows the hot water temperature intervals for each run for the actual system configuration. When different configurations are simulated, the initial water temperature, the starting and ending time as well as the water mass flow rate are implemented in the model as shown in the table. On the other hand, the outlet water temperature is subjected to variations compared to the values depicted in the table due to the fact that it is an output from the model.

To avoid the repetition of the same analysis four times, one for each run, initially it was decided to conduct the investigations only on the forth run. Due to its highest water temperatures which are expected to result in greater condensing pressure, this run is expected to offer the worst performances. This assumption will be verified later on in the project by investigating the behaviour of runs 1, 2 and 3.

Table 4.1: Water temperatures, time steps and water mass flow rate for the four interpolating runs.

	Initial T_w [°C]	Final T_w [°C]	Starting time [h]	Ending time [h]	$\dot{m}_w$ [kg/s]
Run 1	19	31.2	0	2.82	0.028
Run 2	27	37.6	2.82	5.29	0.032
Run 3	37.6	46.7	5.29	7.48	0.036
Run 4	43	55.7	7.48	10.6	0.025

4.3 Alternative refrigerants

The performances of the forth run using some alternative refrigerants to replace R134a were also evaluated. To enable a fair comparison between the different refrigerants, some adjustments of the model were required.
First of all the outlet water temperature was fixed to 52°C, and the inlet water temperature and its mass flow rate were kept constant at the values shown in Table 4.1. In this way the heating capacity was an input for the program and the performances of the different refrigerants could be evaluated with the same required heat to the condenser.
Secondly, the correlations previously used to calculate the refrigerant mass flow rate and the compressor isentropic efficiency were removed. This choice was due to the fact that the correlations were derived for a real compressor using R134a as refrigerant, but they are expected to be different for other energy carriers. Consequently, it was chosen to set the isentropic efficiency to 0.7 and the refrigerant mass flow rate was calculated through an energy balance at the evaporator.
Finally, Equation 4.1 was added to the model in order to evaluate the volumetric flow rate at compressor suction.

$$\dot{V}_{suc} = \frac{\dot{m}_r}{\rho_{suc}} \tag{4.1}$$

The same parameter was used also by Mota-Babiloni et al. [55] to compare the adaptability of different refrigerants to existing compressors.
It was decided to present the results as a relative difference (%COP and $\%\dot{V}_{suc}$) of the system working with the alternative fluid taking as benchmark the system working with R134a, as shown in Equations 4.2 and 4.3.

$$\%COP = \left(\frac{COP_{alternative} - COP_{R134a}}{COP_{R134a}}\right)100 \tag{4.2}$$

$$\%\dot{V}_{suc} = \left(\frac{dotV_{suc,alternative} - dotV_{suc,R134a}}{dotV_{suc,R134a}}\right)100 \tag{4.3}$$

4.4 Economical evaluation

For a more realistic analysis of the system, it was decided to roughly take into account also the economical point of view. More in details, first of all a cost function was derived in order to estimate the expenditure per meter for the condenser coil for different diameters. It is presented in equation 4.4.

$$C_c = (0.1374 D_{out,c} + 0.2189)0.71 \tag{4.4}$$

The last term in equation 4.4, i.e. 0.71, corresponds to the coefficient required to convert the currency from Australian $ to €[56]. This conversion was required due to fact that the prices in the manufacturer catalogue, i.e. the company *Rapid Fab*, were provided in Austrlian Dollars [57]. The prices presented in the catalogue are not inclusive of the Australian Good and Service Tax.
Another required cost estimation concerned the expenditure for the suction/liquid heat exchanger. It was not possible to obtain a direct price from the company due to the fact that this component is not bought. It consists of the connection through welding, performed in the Metro Therm's production line, of the vapour and liquid lines. A possibility was to apply the correlation presented by Aprea et al. [58]. In this analysis the authors evaluated the advantages from a thermodynamic point of view offered by an internal heat recovery unit in refrigeration systems. Their investigation ends mentioning a simple cost estimation of the IHEX examined as a function of the cooling capacity of the plant, which is reported in Equation 4.5.

$$C_{IHEX} = Q_c^{0.75} \tag{4.5}$$

However this correlation would result in too high costs, i.e. approximately 200 €, due to the fact that, as aforementioned, the considered system does not include a proper heat exchanger for IHEX but it consists on two tubes welded together. Consequently, it was chosen to consider the costs reported in the price list for the suction line heat exchangers of the American company Doucette Industries Inc [59]. The aforementioned heat exchanger, shown in Figure 4.2, is characterized by four pipe connections: two for the liquid line and two for the vapour line which exchange heat inside the component. Its dimensions are relatively small and comparable with the ones of the pipes of the studied system. Consequently, it was decided to estimate the cost of the IHEX by considering the cost of the smallest suction line heat exchanger presented in the company price list. Its price amounts to 50 $, corresponding to 45 € applying the currency conversion [56].

4.5 Tapping cycle L in the dynamic model

Beyond the heating up process, it was also decided to use the Dymola model to simulate in a simplified way the tapping cycle L described in the Standard DS/EN 16147 [32]. Some main assumptions were required to enable the implementation of the aforementioned draw off

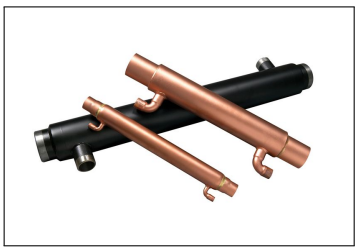

Figure 4.2: Suction line heat exchanger [56].

patter in a simplified way:

- for each tapping a certain energy requirement to be met is specified. These energy requirements are considered in this analysis only to detect the corresponding water mass flow rate, as it will be specified in the following lines. The fulfilment of these requirements is not checked.

- in the Standard, different kinds of tappings are specified: some of them requires to achieve an average temperature of the water tapped (considering a minimum useful temperature increase of 0 K), while for other tappings the energy starts to be useful only when a certain temperature is reached (the minimum useful temperature increase varies from 15 K to 30 K). This distinction was not considered in the model and no minimum useful temperature increase is considered for all the cases.

- in case of dish washing tapping a temperature difference of 45 K is required between the cold water entering in the tank and the tapped water. Because of the difficulties in reaching this ΔT with the only heat pump, the eventually missing temperature difference can be covered applying an electrical resistance heater. However, its presence is disregarded in the model.

- the power absorbed by the fan in the evaporator is not considered.

For the calculation of the tapping mass flow rate, firstly the equivalent volume of hot water ($V_{equivalent}$) at a certain temperature was evaluated for every time step. This was done performing an energy balance (Equation 4.6) for the domestic hot water including the energy required for each tapping as indicated in the Standard. The tapped energy (E_{tapped}) was expressed in J. The inlet water was considered at 10°C as specified in the Standard, while the temperature for the tapped water was set to 52°C. The resulting ΔT specified in Equation 4.6 is 42 K. Constant values of 4200 J/kgK and 1000 kg/m^3 were assumed respectively for the specific heat at constant pressure of the water and the water density.

$$V_{equivalent} = \frac{E_{tapped}}{Cp_w \rho_w \Delta T} \tag{4.6}$$

The goodness of the calculation shown in Equation 4.6 is confirmed by a note in the Standard. For the tapping cycle L, it is mentioned that the volume of equivalent hot water at 60°C is supposed to be 0.1998 m^3. If the temperature of the tapped water is set to 60°C instead of 52°C and the equivalent volumes for each time step are summed, the result is precisely 0.1998 m^3. Finally, the water mass flow rate was calculated from the equivalent volume of hot water for each time step considering the duration of each time interval. Basically the aforementioned calculation assumes that during the tapping cycle the water inside the tank is always at 52°C. Certainly this assumption is not realistic, but the tapping cycle was only used to compare different system configurations. The numerical results deriving from the investigation cannot be realistic, but they can be used to compare different system designs. The water mass flow rates are shown in Table 4.2 together with the duration of each time interval implemented in Dymola. Moreover it was decided to include for every time step in the table also the minimum ΔT at which the useful energy can be counted or the ΔT desired to be achieved, depending on the type of tapping. This parameter will be considered later on in the report.

Table 4.2: Duration of each time interval, corresponding water mass flow rates and minimum ΔT at which the useful energy can be counted for tapping cycle L [32].

Time step [s]	Tapping flow rate [kg/s]	$\Delta T_{minimum}$ or $\Delta T_{desired}$ [K]
0	0	0
300	0.0071	15
1500	0.0190	30
900	0.0024	15
1200	0.0018	15
1200	0.0613	30
300	0.0071	15
900	0.0024	15
900	0.0024	15
1800	0.0012	15
3600	0.0006	15
3600	0.0006	30
900	0.0024	15
3600	0.0006	15
2700	0.0024	45
3600	0.0006	15
3600	0.0006	15
5400	0.0004	15
900	0.0024	15
900	0.0024	30
1800	0.0012	30
5400	0.0004	15
1800	0.0083	45
1800	0.0409	30

5 Results from steady-state simulations

In this chapter the findings from the steady-state simulations conducted in the EES environment are presented.

5.1 Macrochannel condenser

In this section the results deriving from the investigations on the length and diameter of macro-scale condenser tubes are presented. Initially, the performances of the system with its actual configuration are shown for different tube diameters keeping a constant condenser length or a constant condenser heat exchange area. Secondly the effects on the cycle caused by the removal of the internal heat recovery unit are presented. The results presented will concern the forth run for the heat pump heating up process. Some considerations regarding the other runs will be introduced later on.

The system COP for the forth run of the actual system configuration was found to be 3.2.
Figure 5.1 depicts the system COP as a function of the condenser tube diameter keeping either the condenser length or the condenser heat exchange area equal to the one of the actual system configuration. From the graph it emerges that an increase of the diameter slightly worsens the system COP. Consequently, it was chosen to focus the further investigations on smaller tube dimensions. In fact, the COP faces a slightly upward trend if the condenser diameters is reduced. However, as indicated by the scale of the y-axis, the magnitude of the COP variations is very limited.
As easily predictable, the reduction of the tube diameter keeping a constant condenser heat exchange area results to be more beneficial than the case with constant length. This is simply due to the fact that in order to maintain a constant heat exchange area for a reduced diameter the condenser length needs to increase with respect to the 54 m of the actual system configuration. More in details, approximately 83 meters of condenser tube are required to keep a constant heat exchange area, i.e. 1.44 m^2, if the diameters is reduced to 6.95 mm. In this case, the system COP is increased by 1.3%, while in case of constant length and a diameter of 6.95

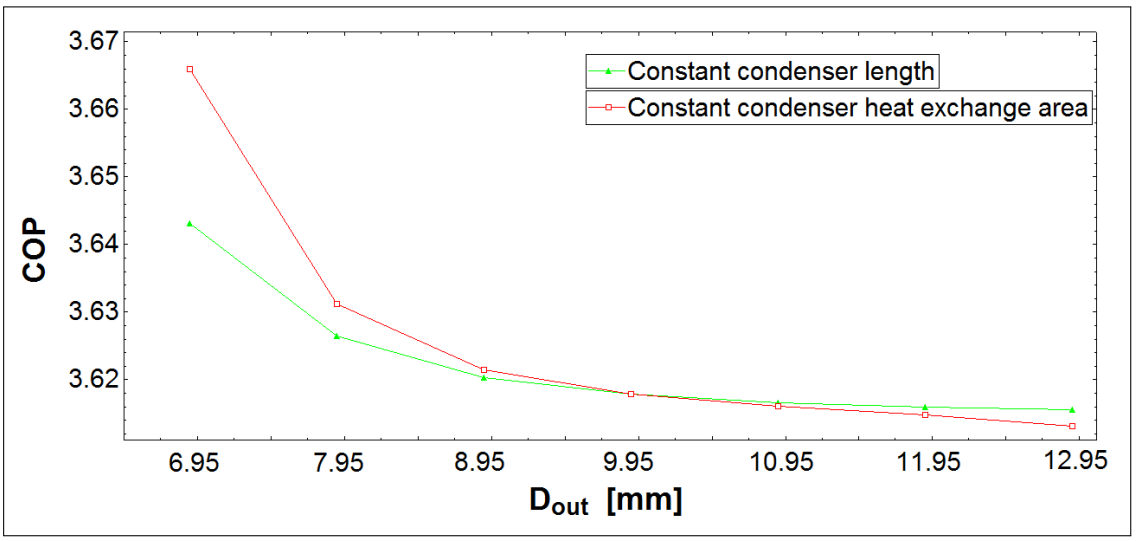

Figure 5.1: System COP as a function of the condenser tube outer diameter.

mm its raise amounts to 0.7 %.

Due to the similarity between the considerations about the two trends depicted in Figure 5.1, it was decided to analyse only the case with reduced diameters and constant condenser heat exchange area, and only point out the differences with the other case. This choice is due to the higher COP enhancement guaranteed by this case.

The first cycle parameter considered when reducing the tube diameter is the heat transfer coefficient refrigerant side in the condensing section. Its evolution as a function of the refrigerant quality is depicted in Figure 5.2 for different diameters. The lower considered limit for the refrigerant quality was fixed to 0.1 instead of 0 to avoid convergence issues in the program. It can be observed that smaller diameters imply an increase of the aforementioned parameter. The reason for these trends needs to be found in the flow patterns inside the condenser tubes, because of their strong impact on the heat and momentum transfer processes [18]. The evolution of the flow regimes of the refrigerant in the channel is shown in Figure 5.3 for different diameters. They are reported in the Taitel and Dukler flow regimes map, which was developed by the two authors in order to enable a prediction of the relation between "properties of the fluid, pipe diameter, gas and liquid mass flow rates and angle of inclination to the horizontal" at which the flow regime variations occur [60]. The Froude number and the Martinelli parameter are considered to draw the map in Figure 5.3. As it emerges from the Figure, three flow regimes can be observed during the condensing process :

- *annular-dispersed flow*: it is characterized by a continuous annular liquid film, thicker in the bottom than in the top, surrounding the perimeter of the tube. The core region inside the horizontal tube is constituted by gas and it is often disturbed by liquid droplets. The entrainment fraction can vary from zero, i.e. completely annular flow, to a value close to

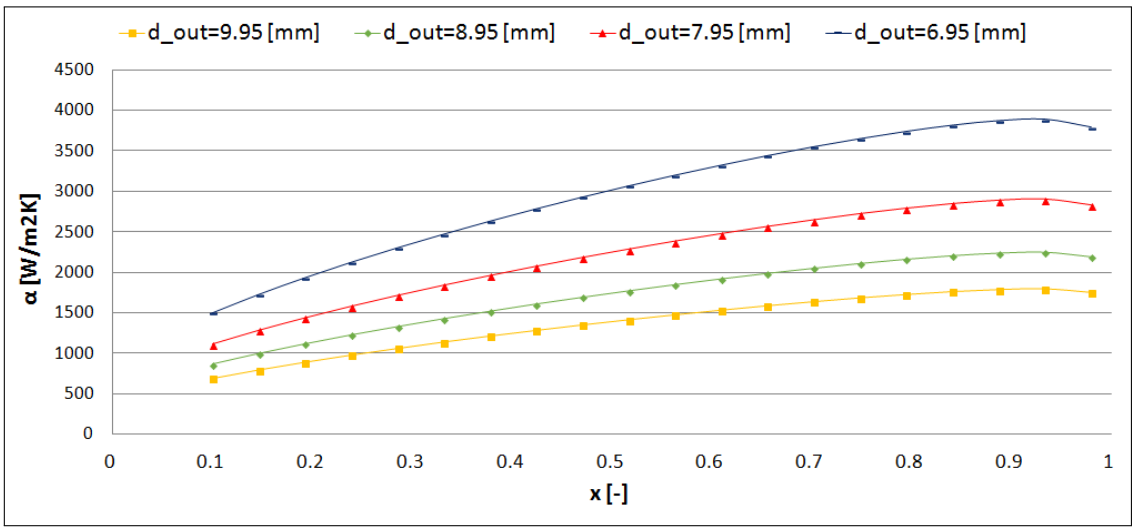

Figure 5.2: Heat transfer coefficient as a function of the refrigerant quality in the condenser for different diameters.

one, i.e. completely dispersed flow.

- *stratified wavy flow*: differently than the stratified flow in which the two phases are completely separated, in the stratified wavy flow, occurring at higher gas velocities, some waves are created in the interface between the phases, even though their crests do not reach the upper part of the tube.

- *intermittent flow*: it occurs for high gas velocities and it is characterized by large amplitude liquid waves formed at the interface between the two phases and reaching the top of the tube which is nearly continuously wetted.

Comparing Figure 5.2 and Figure 5.3, it clearly emerges that a reduction of the condenser tube diameter implies a shift of the flow regime from stratified flow to annular-dispersed flow, enhancing the refrigerant heat transfer coefficient in the condensing section. This is due to the fact that the velocity of the two-phase fluid is enhanced for smaller diameters because of the reduction of the cross sectional area of the tube. The increase of the heat transfer coefficient is caused by the better thermal properties of the refrigerant in its liquid form compared to the refrigerant in gaseous phase. In fact, the perimeter of the tube, through which the heat exchange with the hot water in the tank occurs, is completed wetted by liquid in case of annular flow. On the other hand, in case of stratified flow almost half of the pipe perimeter is in contact with gas.
This first investigation emphasizes that an advantage of a reduced condenser tube diameter lays in the increase of the heat transfer coefficient refrigerant side in the condensing section. This implies a greater U value in the condensing region, which raise its UA value. More in details, reducing the outer diameter from 9.95 mm to 6.95 mm, the U_{cond} varies from 677

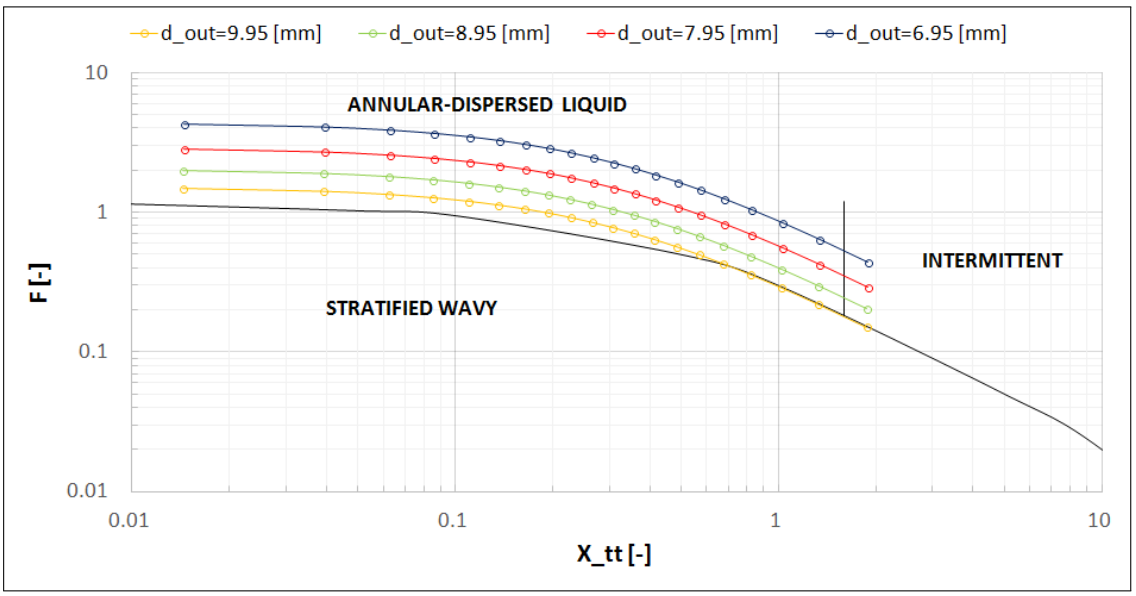

Figure 5.3: Evolution of the flow patterns during condensation in the Taitel and Dukler map for different diameters.

W/m^2K to 957 W/m^2K. Another positive contribution to the UA value in the condensing section for smaller diameters is the increasing heat exchange area of this section to the detriment of the desuperheating area. The heat exchange areas of the two sections for the aforementioned condenser diameters are summarized in Table 5.1. The variations of the heat exchange area of the subcooling section are negligible. This shift between the areas is beneficial for the system due to the higher heat transfer guaranteed by two phase flow compared to the single phase. Moving from a diameter of 9.95 mm until a diameter of 6.95 mm the UA_{cond} is increased from 798 W/K to 1225 W/K.

Table 5.1: Desuperheating and condensing heat exchange areas for condenser diameters of 9.95 mm and 6.95 mm.

	D_{out} = 9.95[mm]	D_{out} = 6.95[mm]
A_{desup} [m^2]	0.24	0.14
A_{cond} [m^2]	1.18	1.28

The same considerations about the U value in the condenser can be applied to the case with reduced diameter and constant condenser length. In fact the evolution of the flow regimes and of the heat transfer coefficient refrigerant side in the condensing section are almost the same as what presented in Figure 5.2 and Figure 5.3. However, due to the reduced overall condenser heat transfer area caused by the shorter length, the overall heat transfer coefficient in the condensing section, i.e. UA_{cond}, is reduced. More in details, moving from a tube diameter

of 9.95 mm to a diameter of 6.95 mm in case of constant length, A_{cond} and UA_{cond} decrease respectively from 1.18 m^2 and 798 W/K to 0.8 m^2 and 764 W/K.

Table 5.2: Variation of Δp for condenser diameters of 9.95 mm and 6.95 mm.

	D_{out} = 9.95[mm]	D_{out} = 6.95[mm]
Δp_{desup} $[bar]$	0.022	0.150
Δp_{cond} $[bar]$	0.085	1.160
Δp_{sub} $[bar]$	-	0.003

Other parameters investigated and influenced by the variations of the condenser length and diameter are the pressure drops in the desuperheater, the condenser and the subcooler. Their variation reducing the diameter from 9.95 mm until 6.95 mm keeping a constant heat exchange area is summarized in Table 5.2. As shown in the table, the increased condenser length and smaller diameter considerably affect the pressure drops in all the three sections of the condenser. The higher pressure drops have two main effects on the system: an increase of the condensing pressure and a greater enthalpy difference in the condenser, mainly in the condensing section. These two effects are visible from the comparison of the pressure-enthalpy diagrams for the cases, shown in Figure 5.4. Lowering the diameter, the condensing pressure increases from 14.2 bar to 14.4 bar. On the other hand, as aforementioned, the increased pressure drop cause a higher enthalpy difference across the condenser resulting in a greater heating capacity: from 1332 W to 1349 W. The evaporation pressure is subjected to minor variations as well as the water temperature at the outlet of the condenser, i.e. respectively 0.01 bar and 0.2°C. Moreover, it can be observed that the isentropic efficiency efficiency of the compressor is slightly enhanced with the smaller diameter, resulting in a constant compressor work.
The same behaviour was observed for the investigation performed with lower diameters and constant condenser length. This justifies the increase of COP for lower diameters despite the reduction of the overall heat transfer coefficients.

5.1.1 Analysis on the internal heat recovery unit

As aforementioned in the preamble of this section, another investigation performed concerned the analysis of the effects caused on the system by the removal of the internal heat recovery unit for different condenser lengths and diameters. The results are summarized in Figure 5.5. As it can be seen, the removal of the heat exchanger is not beneficial for diameters of 8.95 mm and 9.95 mm.
As representative for the two aforementioned cases, it was decided to compare the systems with and without IHEX having a condenser length of 54 m and an outer diameter of 9.95 mm. It was observed that all the heat transfer coefficients refrigerant sides were subjected

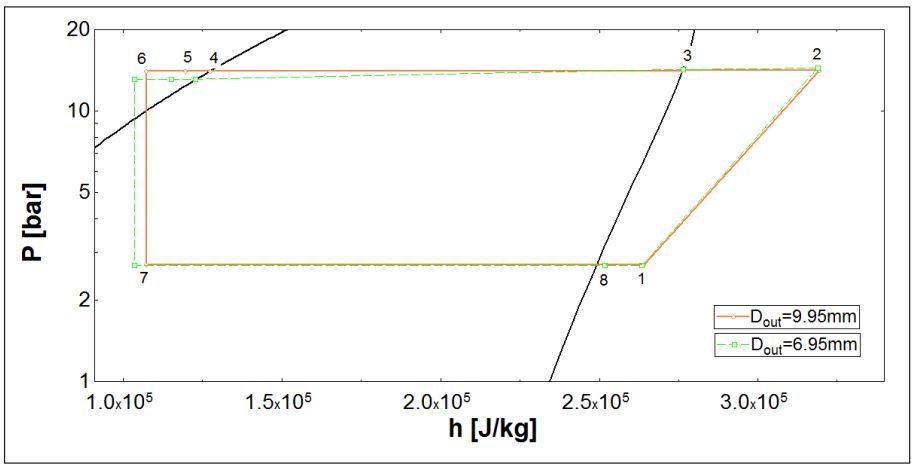

Figure 5.4: Pressure-enthalpy diagrams for condenser diameters of 9.95 mm and 6.95 mm.

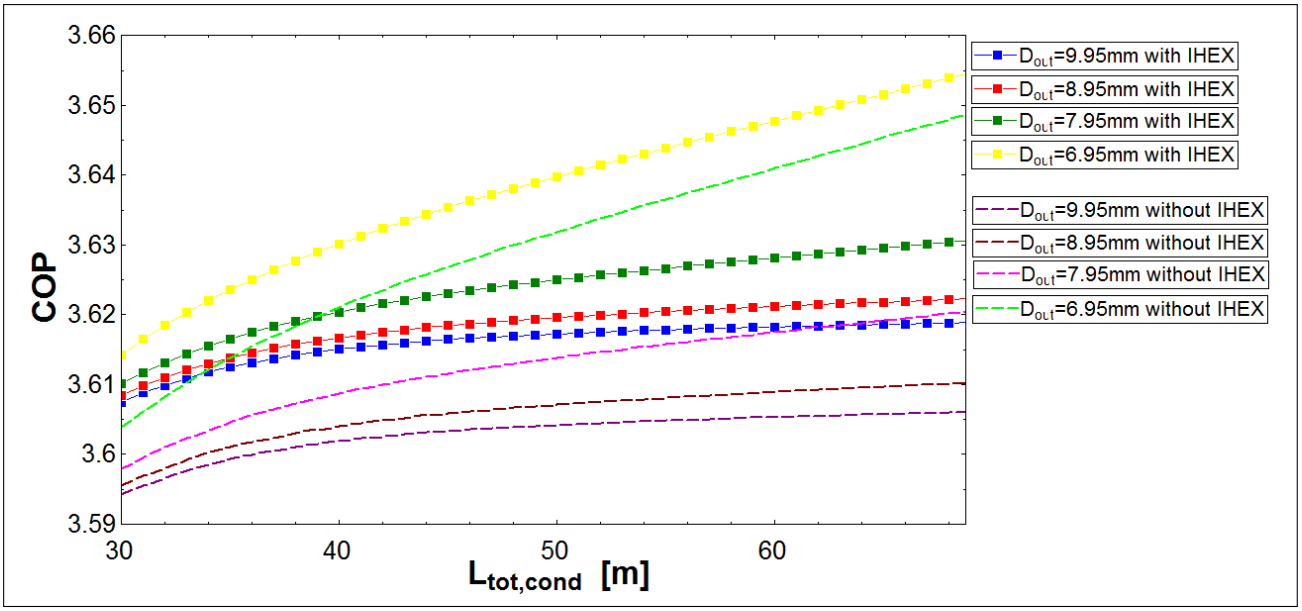

Figure 5.5: COP as a function of the condenser length for different diameters with/without IHEX.

to minor variations. The same happens for the heat transfer coefficient water side in the desuperheating and condensing sections and for the heat exchange areas of the three sections. These observations justify the similarity of the UA values in the condenser and subcooler. For what concerns the heat transfer coefficient water side in the desuperheater, a reduction from 1903 W/m^2K to 1660 W/m^2K was caused by the removal of the internal heat recovery unit. This decrease is caused by the reduction of 6K of the wall temperature in the desuperheater caused by the reduction of the heat transferred in this section for the case without IHEX (Figure 5.6). The lower wall temperature significantly reduces the Rayleigh number lowering also the

Nusselt number, as shown in Equation 3.15. However, despite this difference, also the UA values in the desuperheater are very similar for the two cases: the dominant resistance for the heat exchange is represented by the refrigerant side, in which the heat transfer coefficient is around 350 W/m^2K for the both the desuperheating sections. The similarity between the UA values in all the sections of the condenser for the two considered cases explains the almost coincidence of the condensing pressures. Consequently, the reason for the higher COP of the case with IHEX lays in the significantly higher amount of heat exchanged in the desuperheatig section, as highlighted by the two pressure-enthalpy diagrams shown in Figure 5.6. The higher heat transferred justifies the difference between the two outlet water temperatures: from 55.6°C to 54.8°C respectively for the case with and without heat exchange. This increase of the heating capacity overcomes the slightly lower compressor work of the case without IHEX caused by its higher isentropic efficiency.
The evolution of the COP in both the two cases previously analysed, shows a flat trend after a certain condenser length. This trend is caused by the absence of variations in many influential parameters of the system, such as the U values and the condensing and evaporating pressures.

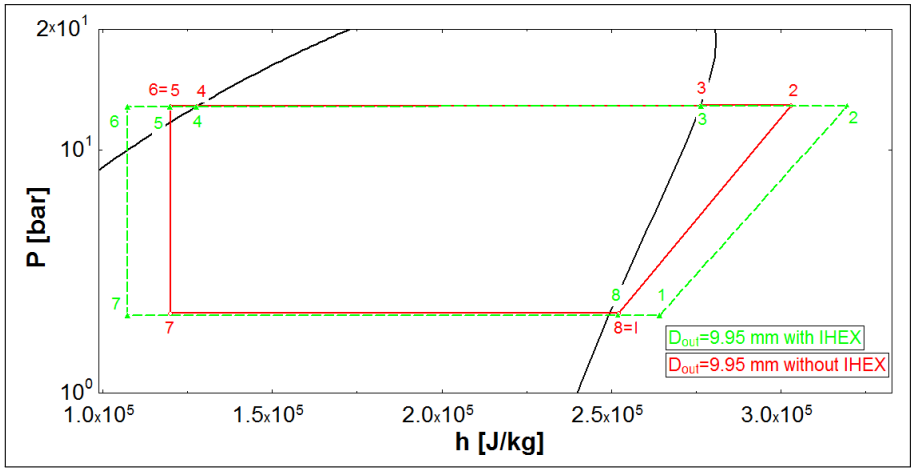

Figure 5.6: Pressure-enthalpy diagrams for a condenser length of 54 m and a diameter of 9.95 mm with and without IHEX.

It is worthy to compare in the same way the case with $D_{out} = 6.95mm$ without IHEX and the one with $D_{out} = 9.95mm$ with IHEX, in order to understand the reason why the removal of the heat recovery unit becomes beneficial. As for the previous comparison, a condenser length of 54 m is considered for both cases. This choice implies different condenser heat exchange areas for the two cases: 1.44 m^2 for the largest diameter and 0.93 m^2 for the other case. Despite the smaller heat transfer area which results in smaller UA values for all the sections in the condenser, the latter shows a higher COP. As in the previous example, the heat transferred in the desuperheater is higher if the system is comprehensive of the heat recovery unit. However, this time, the significantly higher pressure drops introduced by a diameter of 6.95 mm raises

mainly the enthalpy difference in the condensing section resulting in a greater heat exchanged, even though they also contribute to the higher condensing pressure. This fact is graphically visible in Figure 5.7.

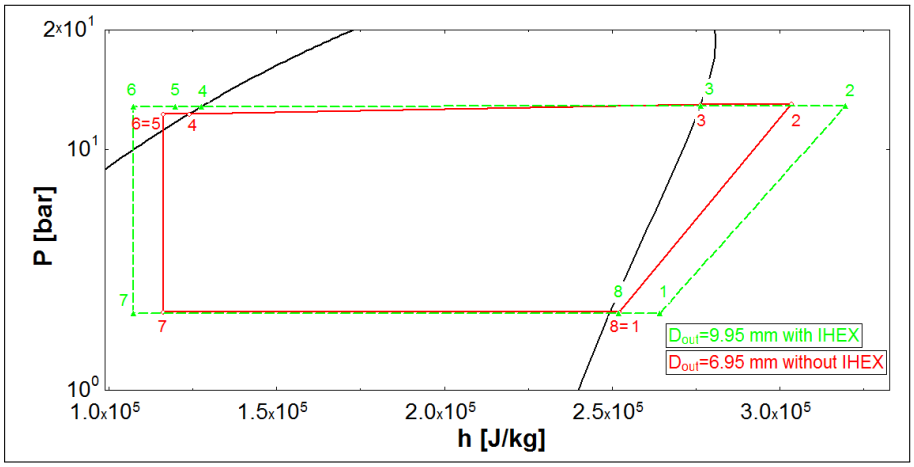

Figure 5.7: Comparison between pressure-enthalpy diagrams for a diameter of 9.95 mm with IHEX and a diameter of 6.95 mm without IHEX both having a condenser length of 54 m.

It must be mentioned that the extent of the COP enhancement for the cases presented is quite limited. Taking as benchmark the COP of the system with the actual configuration, the two most valid solutions shown in Figure 5.5 are both characterized by a reduced diameter of 6.95 mm and a condenser length of 70 m. One is comprehensive of the internal heat exchanger, while the other one does not include this component in the system. The former increases the COP by 1.2 % while the second raise it by 0.8 %. However, it must be mentioned that these improvements concern only the last portion of the heating up process of the water, i.e. Run 4. The effects on the other runs will be presented later on during the report. Moreover, the attractiveness of these alternative system arrangements is increased if the economical perspective is taken into account. In fact, a reduction of the condenser tube diameter from 9.95 mm to 6.65 mm significantly reduces the expenditure for the condenser coil. Applying Equation 4.4, the cost per meter drops respectively from 1.13 €/m to 0.83 €/m. If the actual condenser length of 54 m is maintained for both cases, the expenditure for the condenser coil decreases from 61 €to 44.8 €, implying a reduction of 16%. A comparison between the overall costs of the condenser coils and IHEX for the actual system configuration and the ones considering a diameter of 6.95 mm and a condenser length of 70 m, are presented in Figure 5.8. The cost for the IHEX was assumed to be 45 €, as specified previously in the report. From the figure it clearly emerges that the configuration without IHEX implies a noticeable reduction of the cost: it is almost halved. Also for the other system arrangement with a reduced diameter of 6.95 mm the cost is slightly reduced. Its cost is similar to the one of the actual configuration due to the fact that the advantage of the smaller diameter, is almost nullified by the greater

condenser length.
Consequently, from the economical point of view the solution with a condenser diameter of 6.95 mm, a length of 70 m and without IHEX seems particularly attractive. It must be mentioned that the numerical values presented in Figure 5.8 result from assumptions on the costs for the condenser and the IHEX and the real prices can differ from the assumed ones. However, the general trend of the costs varying the diameters and removing the internal heat recovery unit is expected to be the same also in reality.

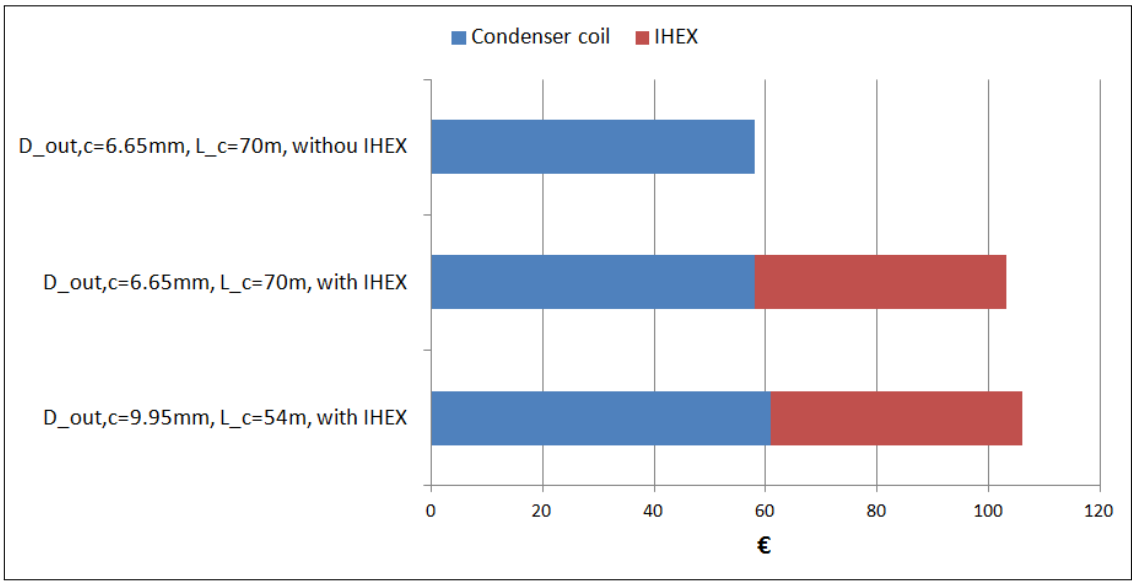

Figure 5.8: Costs comparison.

5.2 Sensitivity analysis

In this section, some sensitivity analysis on the input parameters of the system are shown. Firstly, the effects on the system COP for Run 4 of the assumed parameters required to build up the model are quantified. The extent of their impact on the COP is shown in a spider diagram. In this diagram, depicted in Figure 5.9, the percentage variation of the system COP is compared with the percentage variation of each of the assumed values. The analysis was conducted on the original cycle configuration: with a condenser diameter of 9.95 mm, a length of 54 m and inclusive of internal heat recovery unit. As shown in the figure, the considered parameters are:

- the overall heat transfer coefficient of the evaporator: UA_{evap}. Its value was originally assumed to be 130 W/K. It was varied from 100 W/K to 160 W/K.
- the superheating in the evaporator: ΔT_{sup}. It was assumed to be 3 K. Its value was varied from 1 K to 10 K.

- the effectiveness of the internal heat recovery unit: ε. It was initially set to 0.3. In this investigation the effectiveness of the heat exchanger was varied from 0.2 to 0.5.
- the thickness of the condenser tube: s. Its value was measured to be 1.4 mm with a laser range finder. However, due the uncertainty of the instrument, it was chosen to vary this thickness from 1 mm to 2 mm.
- the outlet air temperature: $T_{air,out}$. It was initially fixed to 4°C in the program. The considered range of variation is from 1 °C to 6 °C.
- the subcooling in the condenser: ΔT_{sub}. It was assumed to be 5 K. This value was varied from 4 k to 10 K.

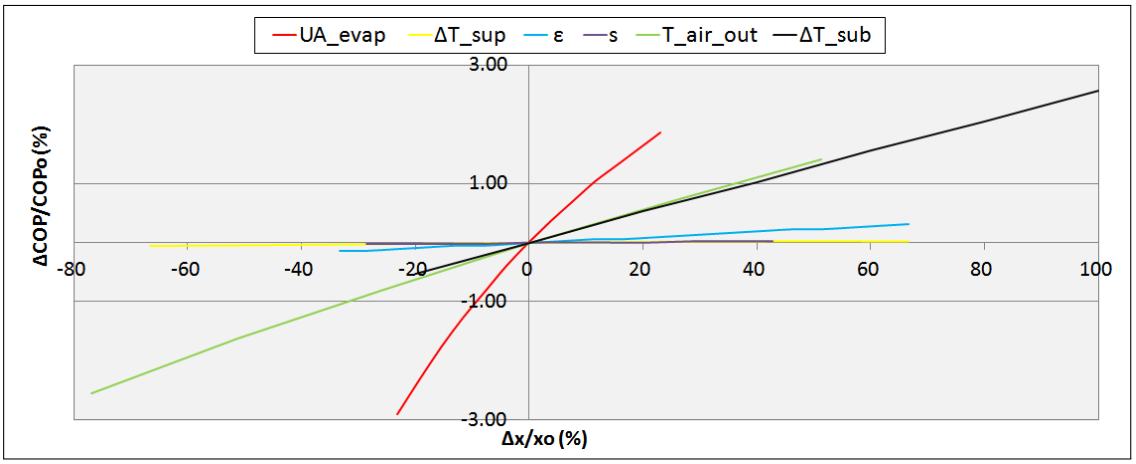

Figure 5.9: Percentage variation of system COP as a function of the percentage variation of the assumed parameters

From Figure 5.9 it emerges that the assumed value which affect the results the most is the overall heat transfer coefficient of the evaporator, due to its steepest trend. This parameter has a strong influence on the evaporating pressure, which is increasing for higher values of the UA_{evap}. From an UA_{evap} of 100 W/K to a value of 160 W/K the evaporation pressure increases of approximately 12%. This fact considerably affect the pressure ratio: it shows a decreasing trend when the overall heat transfer in the evaporator is increased, which is beneficial for the system. On the other hand, also the refrigerant mass flow rate and the isentropic efficiency of the compressor, which are expressed as a function of T_c and T_e, are influenced by the analysed parameter: both of them are increased for greater values of the overall heat transfer coefficient in the evaporator. The variation of the pressure ratio, of $\dot{m}_r$ and of η_{is} affect the compressor work and the heating capacity of the condenser. Both of them are decreased for lower values of the UA_{evap} but with a different extent. If the analysed parameter is reduced from its reference value, i.e. 130 W/K, to 100 W/K the compressor work is reduced of approximately 2%, while the heating capacity decreases of 5%. The detriment caused by the lower heating capacity prevails justifying the reduction of the system COP when

the overall heat transfer in the evaporator is reduced.
Figure 5.9 reveals that other two parameters having similar and considerable effects on the system COP are the assumed outlet air temperature and the subcooling. The influence of $T_{air,out}$ is investigated at first. The behaviour of the system when this temperature is raised from 1 °C to 6 °C reflects the one observed for the overall heat transfer coefficient of the evaporator. Again both the condensing and the evaporation pressures face an increase affecting the compressor work, the condenser heating capacity, the refrigerant mass flow rate and the isentropic efficiency of the compressor. These variations result in noticeable fluctuations of the COP amounting to 4% from the lowest to the highest extreme of the analysed interval.
For what concerns the explanation for the influence of the subcooler on the condenser COP, Figure 5.10 helps the understanding of how the share of the overall condenser heat exchange area varies between its three sections. As predictable, when the subcooling is increased the heat exchange area of the subcooler section becomes larger, mainly at the expense of the condensing section. Consequently, due to the fact that the U values are almost constants for the three portions of the condenser, the UA value of the subcooler is enhanced when the ΔT_{sub} increases, while the overall heat transfer coefficient in the other two sections is worsened. In the system, both higher values for the heat transferred in the subcooler and a lower amount of heat exchanged in the condensing and desuperheating sections can be observed. However, the extent of the the increase of the former overcomes the reduction of $\dot{Q}_{cond}$ and $\dot{Q}_{desup}$ resulting in a overall greater heat transferred in the condenser. This prevailing contribution of $\dot{Q}_{sub}$ combined with the observation of minor variations of the compressor work explains the raise of the COP for higher soobcoolings.
Finally, Figure 5.9 suggests that the impacts of the assumptions concerning the effectiveness

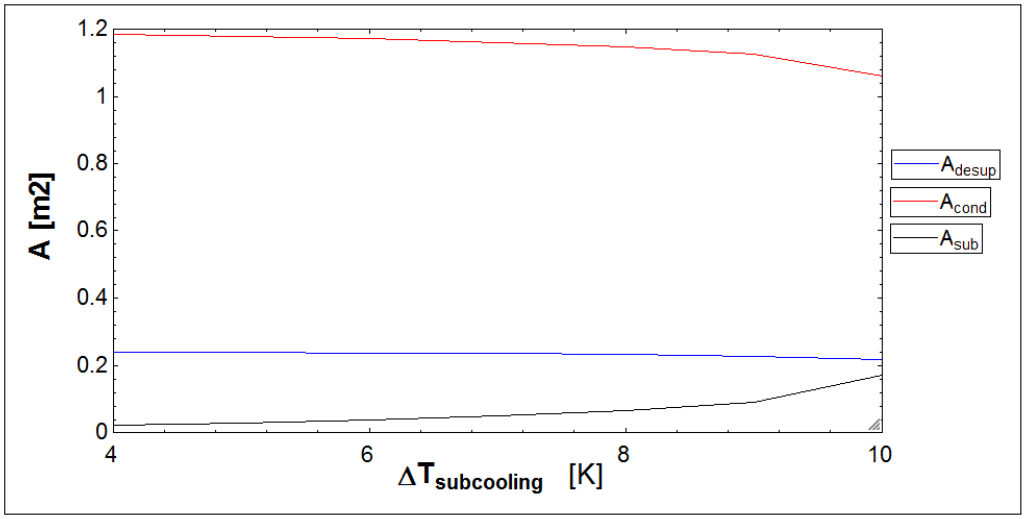

Figure 5.10: Variations of the heat exchange areas for the three sections in the condenser as a function of the subcooling.

of the IHEX, the thickness of the condenser tube and the superheating on the system COP is almost negligible. In fact, even for noticeable fluctuations of the aforementioned parameters,

the percentage of variation of the COP shows a flat trend.

Table 5.3: Heat transfer coefficient water side for the three condensing sections.

$\alpha_{w,desup}$ $[W/m^2K]$	1903
$\alpha_{w,cond}$ $[W/m^2K]$	1383
$\alpha_{w,sub}$ $[W/m^2K]$	1271

As mentioned in Chapter 3, the refrigerant mass flow rate and the compressor isentropic efficiency are found in the model by means of some correlations derived from data provided in the manufacturer catalogue. Both of them are characterised by a certain degree of uncertainty due to the fact that the correlations were found applying an interpolating procedure. Consequently, it is worthy to evaluate their impact on the system COP. The reference values for the compressor isentropic efficiency and the compressor mass flow rate are respectively 0.68 and 0.00667 kg/s. Both of them were varied of ± 20%. Their impact on the system COP is depicted in Figure 5.11. The figure highlights that the isentropic efficiency is a crucial parameter for the model, due to its sharp impact on the compressor work. The system COP is increased by almost 14% if η_{is} is raised by 20%, while it is reduced by 15% if the isentropic efficiency drops by 20%. Also the refrigerant mass flow rate has a considerable impact on the system COP which fluctuates of ± 6% for the considered range of variation for $\dot{m}_r$.

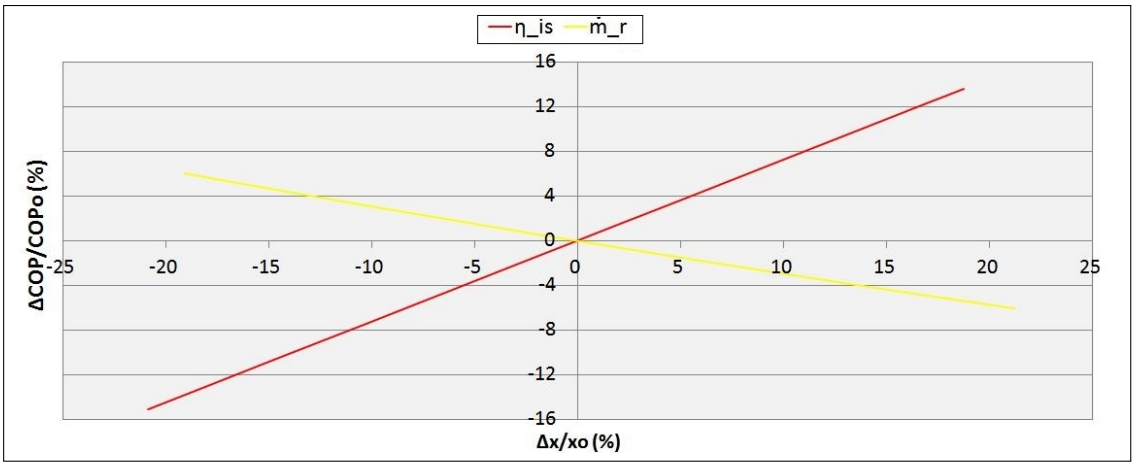

Figure 5.11: Sensitivity analysis on the compressor work and refrigerant mass flow rate.

Another sensitivity analysis performed on Run 4 for the original system configuration focuses on the heat transfer coefficients water side. As mentioned in previous chapters, several

correlation were considered before choosing the one presented by Knudsen [42]. The results derived from the implemented correlation for the α_w in the three condensing sections are presented in Table 5.3. The values follow the expected trend: they decrease moving from the desuperheater to the subcooler. Three factors were observed to justify this trend. Firstly, one reason is expected to lay in the decreasing water temperatures from the desuperheating to the subcooling: the water properties are all calculated at the average water temperatures. Secondly, the wall temperature, which is directly proportional to the Rayleigh number, drops moving from the desuperheater to the subcooler. Thirdly, the contribution of the characteristic length at which the Rayleigh and the Nusselt numbers are calculated needs to be taken into account. This characteristic length, i.e. y, corresponds to the distance from the bottom of tank at which each section of the condenser begins. For the desuperheating section this value was set to 0.43 m, while for the condensing and subcooling section it was calculated as explained in Equation 3.20. Its value is respectively 0.39 m and 0.18 m for the two aforementioned sections. Higher values of this parameter result in higher Rayleigh numbers due to its proportionality with the third power of y, increasing the heat transfer coefficient.
A parameter analysis was performed on the three heat transfer coefficient water sides to detect their impact on the system COP. The results are plotted in Figure 5.12. The figure was drawn varying individually each parameter and considering as reference values the ones shown in Table 5.3. When the heat transfer coefficient water side in one section of the condenser was varied, the α_w of the remaining two sections was kept fixed to the values presented in the table. From the graph it emerges that the impact of the water heat transfer coefficients on the COP can be considered nil even for huge variations of these parameters. This is due to the fact that for Run 4 of the original system configuration the refrigerant is the dominant resistance to the heat transfer. The aforementioned results are expected to be different for system configurations with lower condenser tube diameters due to the enhanced values of the heat transfer coefficients refrigerant side.

The final investigation concerns the inlet air temperature, which corresponds to the temperature of the air supplied to the evaporator. Its value was set to 7°C according to what stated in the standard EN 16147. In this section, disregarding the indication from the standard, it was decided to vary this value in order to evaluate the trend of the system COP for Run 4 throughout all the year. Two locations were chosen as representative for different weather conditions: Copenhagen and Paris. The implemented values for the average monthly ambient temperatures, taken from an online database [61], are shown in Table 5.4. The aforementioned source provides two values for the average monthly ambient temperatures named respectively as “average high temperature” and “average low temperature”. For each month it was preferred to implement in the model the latter in order to evaluate the system performances in the most adverse weather condition. It was decided to use the values presented in Table 5.4 as temperatures for the air to be supplied to the evaporator. This simulation can represent the case in which the domestic heat pump is positioned in the basement of the house and the air is supplied to the evaporator through a duct sucking air from the outdoor ambient. The temperature difference between the inlet and the outlet air temperatures in the evaporator

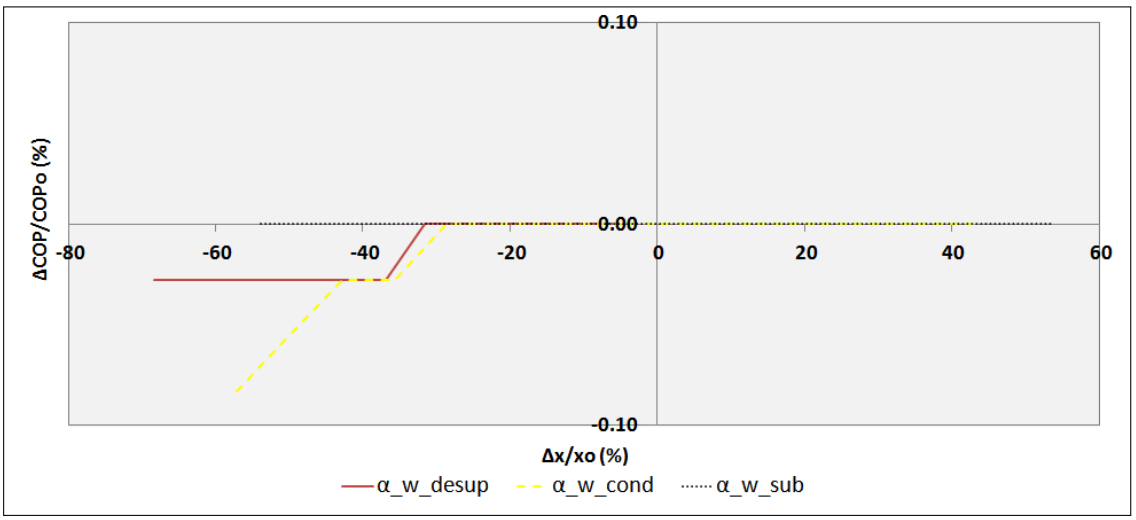

Figure 5.12: Percentage variation of system COP as a function of the percentage variation of the water heat transfer coefficients.

was fixed to 3 K.

The evolution of the COP with the ambient temperature in Copenhagen is reported for three

Table 5.4: Average monthly ambient temperatures for Copenhagen and Paris.

	T_{amb} Copenhagen [°C]	T_{amb} Paris [°C]
January	-1	3
February	-1	2
March	0	4
April	3	6
May	7	10
June	11	13
July	13	15
August	13	15
September	10	11
October	6	9
November	3	5
December	0	3

system configurations in Figure 5.13. The chosen configurations are:

- *Case 1*: condenser diameter 9.95 mm, condenser length 54 m , with IHEX.
- *Case 2*: condenser diameter 6.95 mm, condenser length 70 m , with IHEX.
- *Case 3*: condenser diameter 6.95 mm, condenser length 70 m , without IHEX.

These epithets for the three condenser configurations will be applied for the rest of the report. All the considered configurations show the same trend: the COP is higher during warm months. This can be justified taking into account the yearly trend of the pressure ratio, i.e. the ratio between the condensing temperature and the evaporation temperature. It is characterized by an U-shaped trend during the year, with approximate variations from 6.4 in January to 4.6 in July for the three considered cases. The heat transferred in the overall condenser has an inverted U-shaped trend, similarly to Figure 5.13, resulting in greater outer water temperature for summer months. The percentage COP variation from January to July amounts for all the cases to values around 22%. Finally, from the figure it emerges that Case 2 offers the best performances throughout all the year compared to the other cases, and Case 3 shows COP very close to Case 2. Both the aforementioned cases represents a slight improvement with respect to Case 1, which is the actual system configuration.
As aforementioned, a graph identical to the one presented in Figure 5.13 was drawn also implementing the ambient temperatures for Paris summarized in Table 5.4. However it is not reported due to its similarity with Figure 5.13. All the considerations mentioned before are valid also for this case. The only difference lays in the fact that the COP for all the months are higher for a system located in Paris due to the higher outdoor temperatures. For August and July the COP reaches a value of 4.

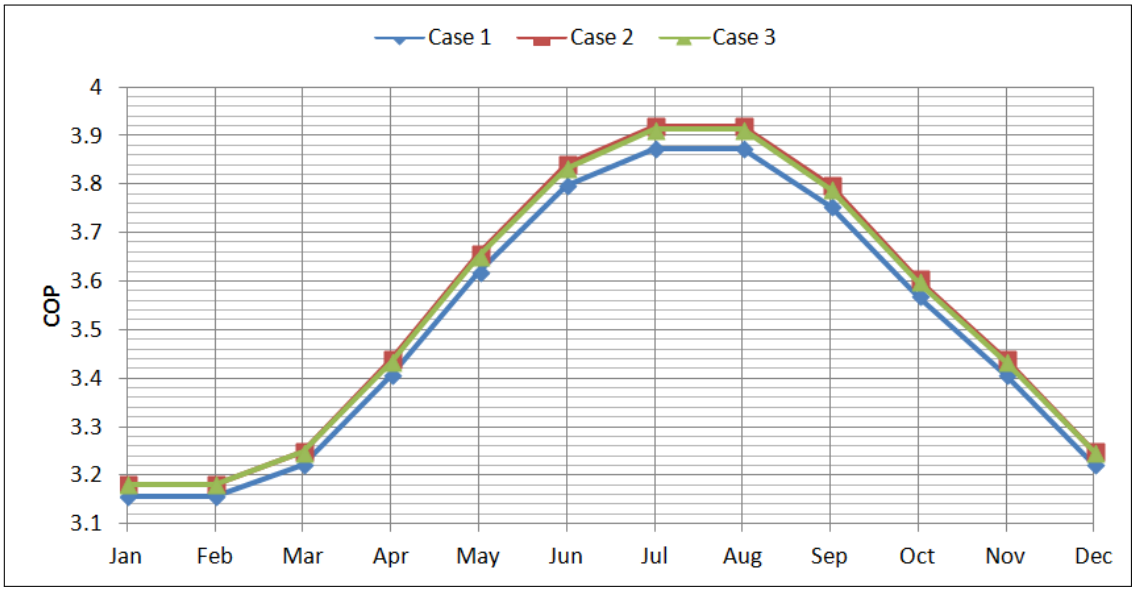

Figure 5.13: Yearly evolution of the system COP in Copenhagen for three system configurations.

5.3 Minichannel condenser

After the previous investigation concerning the condenser tube length and diameter, it was decided to further reduce its size. Before introducing the minichannel condenser, it is relevant

to estimate until which value of the outer macrocondenser tube diameter, the system COP shows an increase. Due to the fact that the pressure drops are directly proportional to the condenser length and indirectly proportional to the condenser diameter, it was chosen to maintain a value of 54 m for the length while reducing the diameter. This choice was due to the willingness to limit the detrimental effect of the pressure drop. The system COP as a function of the condenser diameter keeping a constant condenser length of 54 m is shown in Figure 5.14. Figure 5.14 shows that a reduction of the condenser diameter to values lower

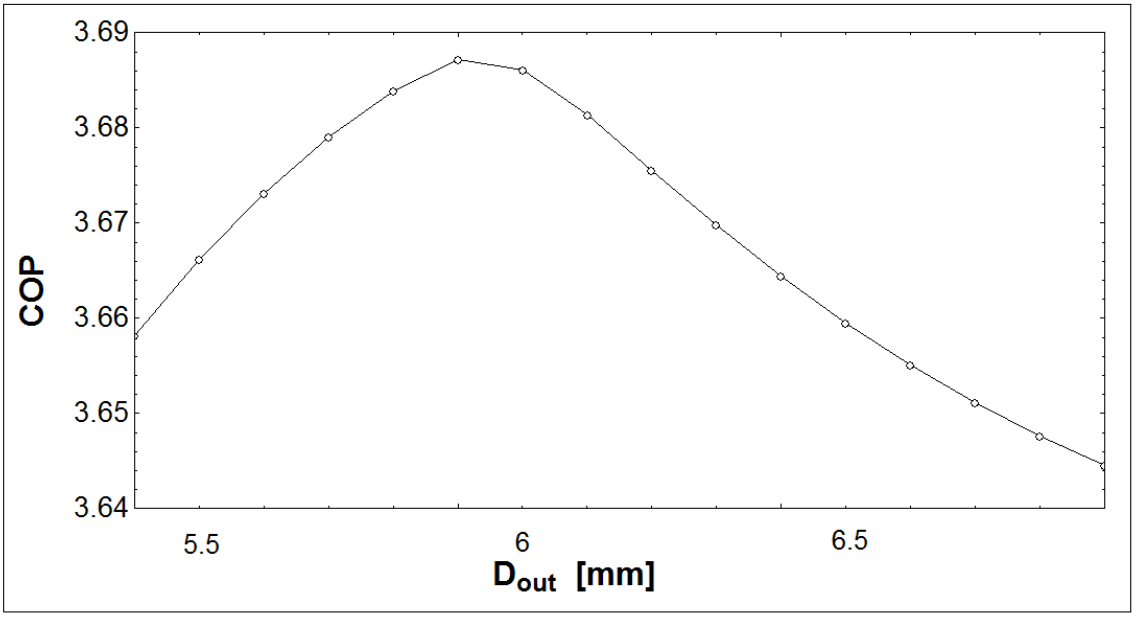

Figure 5.14: Trend of the COP varying the condenser tube diameter and keeping a constant length of 54m.

than 5.9 mm cause a reduction of the system COP. This is partly due to fact that the increasing pressure drops imply too high value for the condensing pressure, affecting the compressor work. Moreover, the overall heat exchange area in the condenser is excessively reduced and the subcooling section occupies a big portion of the condenser, reducing the area of the condensing section. Some numerical values of the aforementioned parameters for the system with a diameter of 5.9 mm and 5.4 mm are provided in Table 5.5.

Despite the awareness of the detrimental effect of the pressure drops on the system COP for very small outer condenser diameters, it was decided to analyse the performances of the forth run of the heating up process in case of minichannels. In this analysis, it was chosen to adopt the classification introduced by Kandlikar and Grande [62] to define the geometry of the minichannel. According to the authors, minichannels are single tubes or multiport extructed aluminium tubes characterised by an inner hydraulic diameter between 0.2 mm and 3 mm. The considered minichannel has an outer diameter of 3.4 mm, resulting in an inner diameter of 2 mm due to the fact that the tube thickness was kept constant. To reach reasonable values

Table 5.5: Numerical values of some key parameters for condenser diameters of 5.9 mm and 5.4 mm.

	$D_{out,c} = 5.9$ [mm]	$D_{out,c} = 5.4$ [mm]
$\alpha_{r,cond}$ $[W/m^2K]$	4209	5178
p_c $[bar]$	14.58	14.91
Δp_{desup} $[bar]$	0.19	0.25
Δp_{cond} $[bar]$	1.9	2.2
Δp_{sub} $[bar]$	0.034	0.2
$A_{tot,cond}$ $[m^2]$	0.760	0.671
A_{desup} $[m^2]$	0.054	0.035
A_{cond} $[m^2]$	0.612	0.3654
A_{sub} $[m^2]$	0.090	0.2713
UA_{desup} $[W/K]$	38.83	28.33
UA_{cond} $[W/K]$	658.3	423.5
UA_{sub} $[W/K]$	52.09	174.3

for the pressure drop, the condenser length was set to 16 m. Consequently, the heat exchange area in the condenser was 0.1 m^2.

The evolution of the flow regime inside the microchannel is presented according to the

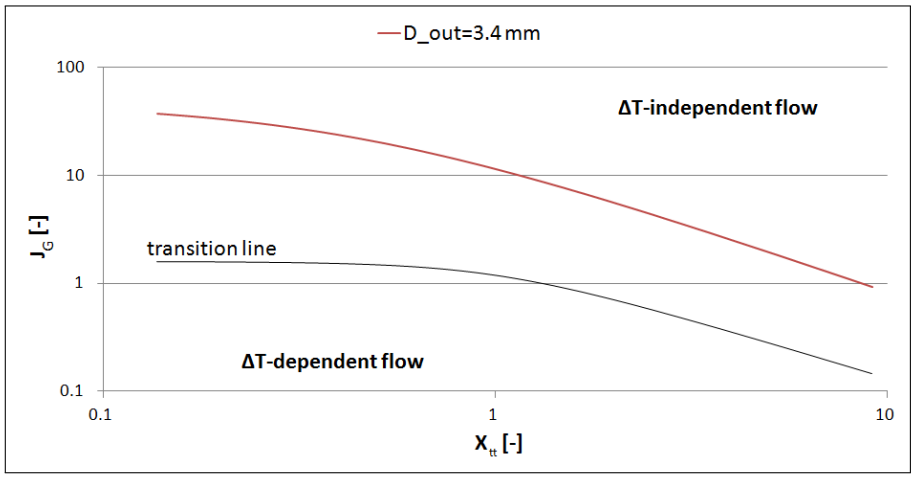

Figure 5.15: Evolution of the flow regime for microchannel condenser ($D_{out,c} = 3.4mm$).

indication of Cavallini et al. [44]. The authors considered only a ΔT-dependent and a ΔT-independent flow regime, requiring a single transition criterion. In fact, in previous investigations, the authors detected that for horizontal tubes dependence on ΔT is evident only if gravity is the dominant force. The evolution of the flow regime is depicted in Figure 5.15. The transition line was found applying Equation B.17 described in Appendix B. As it emerges from the figure, the evolution of the flow regime occurs entirely in the ΔT-independent region. According to what stated to the authors, this corresponds to annular flow. The evolution of

the refrigerant side heat transfer coefficient and pressure drop in the condensing section, calculated applying Equations B.18 and B.22 from Appendix B, with the refrigerant quality are shown in Figure 5.16. Moreover, it was decided to include in Figure 5.16a also the evolution of the refrigerant side heat transfer coefficient calculated applying the Shah's correlation (Equation B.7 in Appendix B).

From Figure 5.16a it emerges that the Shah's correlation predicts higher values for the heat

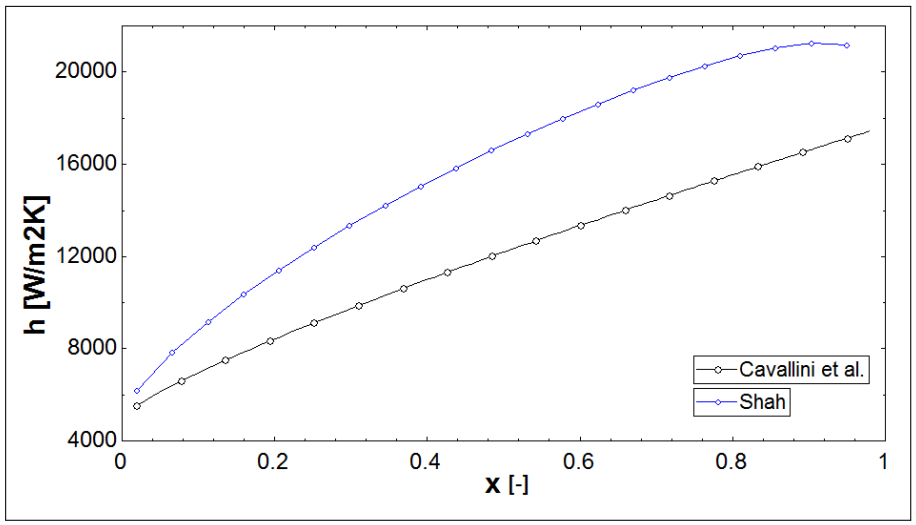

(a) Heat transfer coefficient as a function of the thermodynamic vapor mass quality calculated according to the Shah's correlation [45] and the Cavallini et al heat transfer model [44].

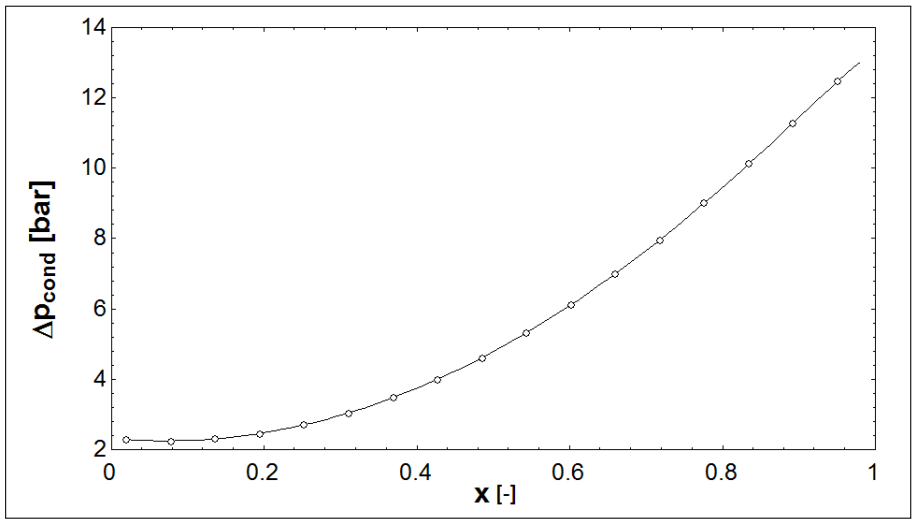

(b) Pressure drop as a function of the thermodynamic vapor mass quality.

Figure 5.16

transfer coefficient refrigerant side. However, for the reasons explained in Chapter 3, it was

decided to apply the Cavallini et al. heat transfer model to estimate the system performances. In fact, it was decided to roughly quantify the system COP using as refrigerant heat transfer coefficient and pressure drop in the condensing section the average values from the trends shown in Figure 5.16. A more precise estimation of the two aforementioned parameters would have been possible by implementing a discretization procedure. In other words, the consideration of intervals with constant heat flux or constant refrigerant quality variation and the calculation of the two parameters as the average over these intervals would enable more precise results. However, the awareness of the poor performances of the system with its actual configuration if a minichannel condenser is applied, discouraged a precise analysis.

The refrigerant heat transfer coefficient and pressure drop in the condensing section used in the simulation, as well as some relevant results from the model are summarised in Table 5.6. From the table it emerges that the condensing pressure dramatically raises above 21 bar and that the subcooling section occupies a relevant portion of the condenser: 33%. Moreover, the pressure drops in all the sections of the condenser are very high resulting in a COP of 3 for the forth run of the heating up process.
In order to graphically show the impact of the pressure drop on the system, it was decided to

Table 5.6: Numerical values of some key parameters for minichannel condenser with an outer diameter of 3.4 mm.

$\alpha_{r,cond}$ $[W/m^2K]$	9117
p_c $[bar]$	21.58
Δp_{desup} $[bar]$	1.68
Δp_{cond} $[bar]$	7
Δp_{sub} [bar]	1.21
$A_{tot,cond}$ $[m^2]$	0.1
A_{desup} $[m^2]$	0.007
A_{cond} $[m^2]$	0.06
A_{sub} $[m^2]$	0.033
UA_{desup} $[W/K]$	10.79
UA_{cond} $[W/K]$	101.1
UA_{sub} $[W/K]$	30.95
COP $[W/K]$	3
$T_{out,w}$ $[°C]$	55.9

compare in a pressure-enthalpy diagram the cycle with and without pressure drop using as condenser a tube of 3.4 mm with a length of 16 m. In order to estimate the refrigerant heat transfer coefficient of the case without pressure drop, a diagram similar to Figure 5.16a using the Cavallini et al. heat transfer model was created and the average values were used in the model. The result is shown in Figure 5.17. The figure empathizes that the condensing pressure is significantly reduced to 15.5 bar without taking into account the pressure drop. Moreover, the condensing section occupies the 83% of the overall condenser area, while the area of the

subcooling section amounts only to 4%. The resulting COP is 3.4, meaning that the pressure drops are responsible for a reduction of the COP of approximately 13%. Consequently, this

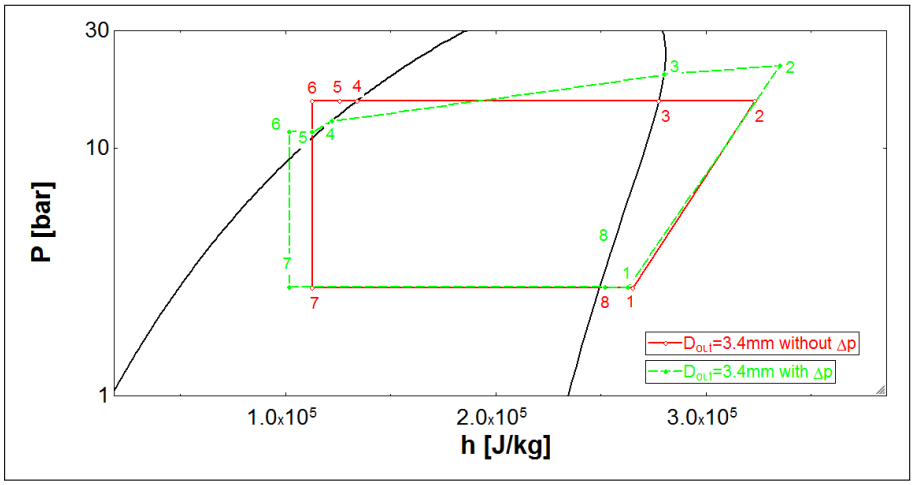

Figure 5.17: Comparison of the pressure-enthalpy diagram with and without pressure drop in case of minichannel condenser.

investigation suggests that the minichannels are not applicable to the system with the actual configuration, mainly due to the excessive pressure drop. However, some interventions to limit the pressure drop would considerably raise the attractiveness of the micro-geometries. More in details, the introduction of some manifolds in microchannel heat exchangers can considerably reduce the pressure drop. In fact, by means of the manifolds several microchannels can be connected in parallel. In this way the length travelled by the fluid in each minichannel would correspond to few rotations around the hot water tank. This arrangement can considerably reduce the pressure drop due to its direct proportionality with the heat exchanger length.
This innovative solution is proposed for the example by the manufacturer Sanhua [63]. An image of the micro-channel heat exchanger with manifolds manufactured by the company is given in Figure 5.18. As it can be seen from the vertical section of the manifold presented in the figure, the route of the refrigerant in the manifold is blocked in three points by means of some flaps. Consequently, the pressure drop needs to be found considering a mix of serial and parallel runs of the minichannels around the hot water tank. According to the company this solution:

- reduce the refrigerant charge up to 70%;
- help the different manufacturers to meet high Seasonal Efficiency Ratio and Heating Seasonal Performance Factor requirements;
- reduce the weight and volume up to 50% compared to macrogeometries;
- improve the efficiency of the heat transfer up to more than 30%;

- ensure a very limited performance reduction of the heat exchange with lifetime.

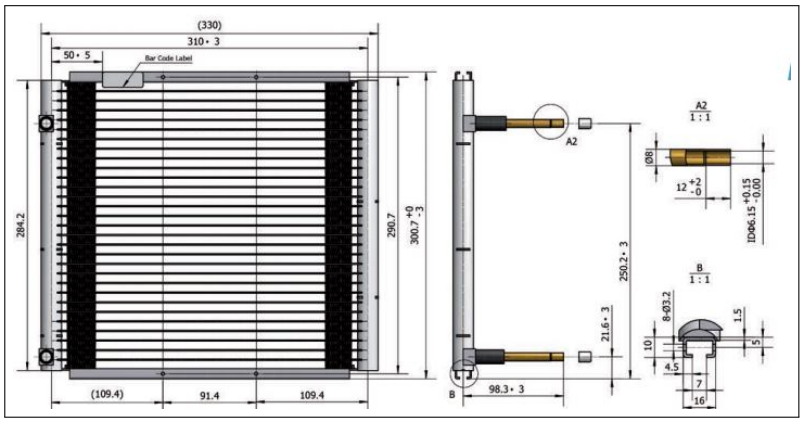

Figure 5.18: Micro-channel heat exchanger with manifolds manufactured by Sanhua [63].

Finally, to roughly quantify the economical savings for the acquisition of the condenser, Equation 4.4 can be applied. The cost of the condenser per unit of length is reduced from the 1.13 €/m of the actual diameter of 9.95 mm to 0.49 €/m for reduced diameter of 3.4 mm.

5.4 Alternative refrigerants

In this section, the performances of the system using alternative refrigerants as energy carrier are presented. The possible chosen alternatives are R290, R600a, R1234yf and R1234ze(E).
The refrigerants trans-1,3,3,3-tetrafluoropropene (R1234ze(E)) and 2,3,3,3-tetrafluoroprop-1-ene (R1234yf) are unsaturated fluorinated compounds which are also known as hydrofluoro-olefins (HFOs) refrigerants. They are considered promising alternatives to the commonly used refrigerants because of their particularly low atmospheric lifetime caused by their reactivity with atmospheric hydroxyl radicals [64]. More in details, according to Fukuda et al.[65] and Leck [66], R1234ze(E) and R1234yf are characterized by a GWP_{100} of respectively 6 and 4, while the GWP_{100} of R134a is 1430.
Leck [66] compared the refrigeration properties of R134a and R1234yf concluding that they are similar and that the HFO refrigerant is suitable to replace R134a in a wide range of applications. Fukuda et al. [65] tested from both a numerical and experimental point of the view the feasibility of R1234ze(E) for high-temperature heat pumps used for industrial purposes. The authors demonstrated that this low-GWP refrigerant is suitable also for these applications, rather than traditional refrigeration systems. A comparison between the local heat transfer coefficients of R134a and R1234yf during condensation at 40°C in a tube having a diameter of 0.96 mm is presented by Del Col et al. [67] for mass velocities varied from 200 to 1000 $kgm^{-2}s^{-1}$. It was observed that, in case of equal mass velocity, R1234yf is characterised by lower heat transfer coefficients: a reduction of 15% emerged at 200 $kgm^{-2}s^{-1}$ and a vapour quality of 0.4. Moreover, Navarro-Esbrì et al. [68] experimentally evaluated the possibility to

use R1234yf as a drop-in replacement of R134a in a refrigeration system. The results showed that the system COP and cooling capacity were reduced respectively by 19% and 9% when the HFO refrigerant was used. However, it was also observed that the application of an internal heat exchanger reduces the gap in energy performances between the two refrigerants.

R290 and R600a are natural refrigerants and are particularly attractive because of their nil ODP and low GWP, around 3. They are characterised by acceptable toxicity levels but both of them are flammable. The performances of R600a in a domestic refrigerator originally manufactured to work with R134a were analysed by Joybary et al. [69]. An exergy analysis was conducted on the original system, and it was observed that the compressor was characterized by the highest exergy destruction. Then it was decided to replace R134a with R600a and the Tagauchi method was applied in order to reduce the exergy destruction in the system with the natural refrigerant. The authors found that at optimal conditions the R600a charge amount was 55% lower than the one in the original system. This result, combined with the fact that R134a is two times more expensive than R600a, increases the economical attractiveness of the natural refrigerant. No considerations were reported concerning the system COP. Navarro et al. [70] analysed the feasibility of the application of R290 as a drop-in replacement of R134a in an open piston compressor. More in details, the authors conducted a comparative experimental study considering R1234yf and R290 as alternatives to R134a. It was concluded that both refrigerants are valid alternatives. R290 showed better performances from the efficiency point of the view in all the tested conditions: the volumetric and isentropic efficiency were enhanced by respectively 30% and 15%. Moreover, Danfoss [71] confirmed that R290 has been used in domestic heat pumps in Germany during last years, even though different level of success were encountered. However, it was concluded that propane is a possible refrigerant for domestic application with good performances in terms of energy efficiency, even though particular attention needs to be addressed to its flammability.

Before analysing the results, it is worthy to estimate how the performances of the system working with R134a are altered by the assumptions presented in Section 4.3. It was decided to replicate Figure 5.5 for three condenser geometries and system configurations, as depicted in Figure 5.19. The condenser length was set to 70 m for the condenser diameters of 6.65 mm, while it was 54 m for the condenser outer diameter of 9.95 mm. The label “real” in the Figure refers to the case in which the isentropic efficiency of the compressor and the refrigerant mass flow rate were found from the correlations derived from the real compressor. The label “fake” identifies the system implemented applying the assumptions described in Section 4.3.

From Figure 5.19 it emerges that the performances of the system are overestimated if the fake compressor is applied. In the following, it was decided to report some numerical results regarding the system with a condenser outer diameter of 9.95 mm with IHEX. The first reason for the different performances lays in the difference between the isentropic efficiencies: for the fake compressor it is set to 0.7 while for the real compressor it slightly fluctuates around the value of 0.68. Secondly, the two models are characterised by different refrigerant mass

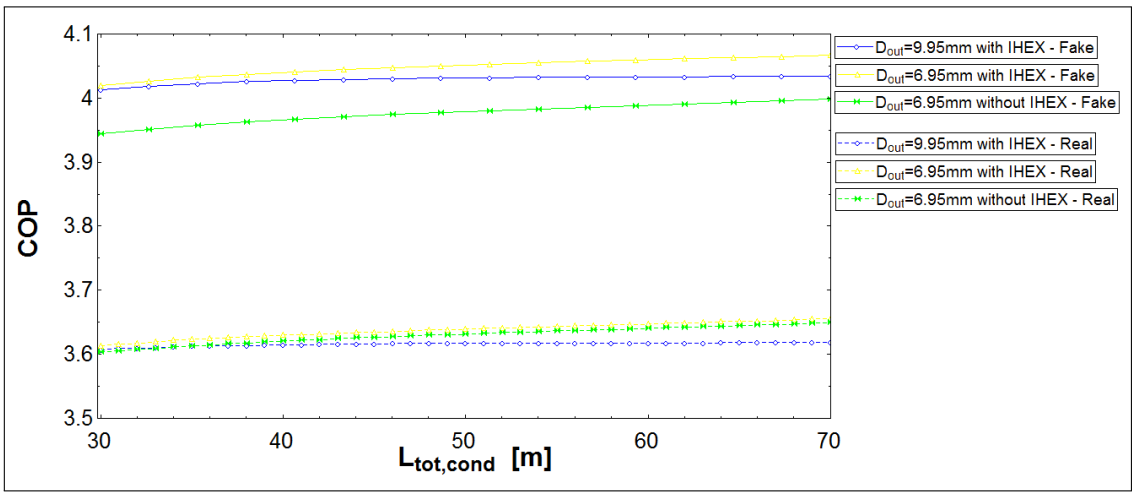

Figure 5.19: COP as a function of the condenser length for the system with the real compressor and with the fake compressor.

flow rates: for the real compressor its value is around 0.0067 kg/s while it is reduced to approximately 0.0047 kg/s by applying the fake compressor. This implies higher values for both the compressor work and the heating capacity for the real case. Thirdly, the heating capacity of the condenser differs for the two cases due to the fact that in the model with the real compressor the outlet water temperature was a free parameter. Its value was always approximately 3-4 K higher than the 52°C set for the case with fake compressor, resulting in a greater heating capacity for the model with real compressor. Fourthly, the pressure ratio was always bigger for the case with real compressor, resulting in an enhancement of the compressor work. Approximate value for the pressure ratios are 4.6 with the fake compressor and 5.3 in case of real compressor.
The detriment of the greater compressor work prevails over the benefit of the higher heating capacity, resulting in poorer performances of the system when the correlations derived from the real compressor are used.
From the figure, it can be also observed that for both cases the configuration with IHEX and $D_{out,c} = 6.95mm$ is the best one. However, the results for the system without IHEX and $D_{out} = 6.95mm$ are reversed for the two compressor models: its performances are worse than the actual system configuration, i.e. $D_{out,c} = 6.95mm$ with IHEX, in case of fake compressor. Finally, from the figure it emerges that for both the compressor models, the system COP are close for the three chosen system configurations.

It is also relevant to compare the pressure-enthalpy diagrams for the considered refrigerants. They are all shown in Figure 5.20, in which the liquid lines start from a pressure of 0 bar and a specific enthalpy of 0 kJ/kg to facilitate the graphical comparison of the curves. Figure 5.20 gives an indication about the latent heat of vaporization of each refrigerant. Higher latent heats require a lower refrigerant mass flow rate to provide the same heat at the condenser.

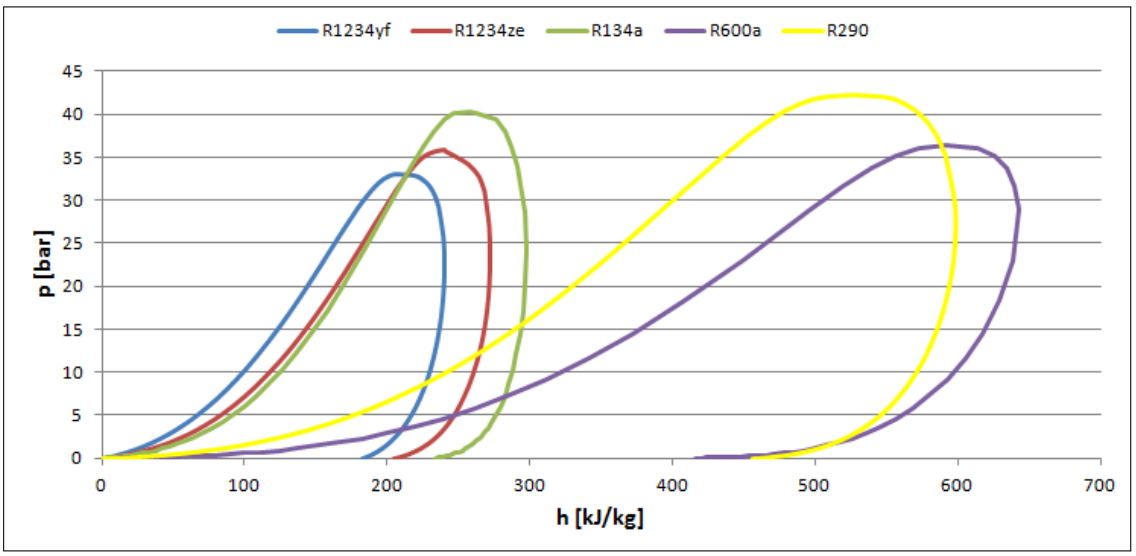

Figure 5.20: Comparison of the pressure-enthalpy diagrams for the alternative refrigerants.

Moreover, the figure confirms that all the considered fluids are suitable for the analysed application because they are characterised by similar operational ranges.

Initially, it was decided to analyse the performances in terms of COP and volumetric flow rates of the system working with different refrigerants considering its actual configuration, i.e a condenser outer diameter of 9.95 mm, an overall condenser length of 54 m and including the internal heat recovery unit. The COP and $\dot{V}_{suc}$ relative differences compared to R134a are shown in Figure 5.21. Figure 5.21 gives conflicting indications. From Figure 5.21a it emerges that the system working with R600a improves its performances by 1.6%. On the other hand, the same refrigerant is the one facing the highest enhancement of the volumetric flow rate, as shown in Figure 5.21b. A higher volumetric flow rate implies a bigger compressor and consequently raises the expenditure for this component. As a consequence, R600a does not seem attractive from the economical point of view, despite the slight improvement of the COP. Moreover, the figure highlights that the use of R1234yf as energy carrier lower the system COP by 2.5%, but implies a very limited increase of the volumetric flow rate compared to R134a, i.e. approximately 3%. The findings about the COP for the refrigerant R1234yf are aligned with what emerged from the literature. As aforementioned, according to Navarro-Esbrì et al. [68], the system without IHEX working with R1234yf showed significantly lower performances compared to the same system configuration working with R134a. In the current analysis, it was observed that if the heat recovery unit is removed and the condenser outer diameter and length are kept constant, the COP of system with R1234a is approximately 5% lower than the system working with R134a. Moreover, Navarro-Esbrì et al. [68] also empathized that the inclusion of the IHEX reduces the differences in energy performances. This is confirmed by Figure 5.21a, in which the COP differs by 2.5 %, halving the gap in energy performances compared

to the systems without IHEX. However, differently than what stated by Del Col et al. [67], the average heat transfer coefficient refrigerant side during the condensing process calculated using Equation B.11 presented in Appendix B is 2.5 % higher for R1234yf compared to R134a. However, this difference can be explained with the discrepancy in mass velocities between the two refrigerants. In fact, while Del Col et al. conducted experiments considering the same mass velocities for the two refrigerants, in the present study, due to the difference in refrigerant mass flow rate, the mass velocity for R1234yf is 106 $kgm^{-2}s^{-1}$, while its value is 84 $kgm^{-2}s^{-1}$ for R134a. Del Col et al. compared the saturation properties of the two refrigerant at 40°C and the authors stated that the difference between the liquid thermal conductivities of 18.3 % in favour of R134a is a key factor for explaining the higher heat transfer coefficient with equal mass velocity. In fact the aforementioned parameter influences the thermal resistance in the liquid film. In the current study, the condensing temperatures are very close to 50°C for both cases and the liquid thermal conductivity of R134a is 23.5 % higher than the one of R1234yf. However, the lower thermal resistance in the liquid film for the the system working R134a cannot overcame the advantage caused by the greater mass velocity for R1234yf resulting in a lower heat transfer coefficient.

From Figure 5.21 it also emerges that despite the slight reduction in COP, i.e. 1.3% , R290 is the only refrigerant with a lower volumetric flow rate with respect to R134a, with a $\%\dot{V}_{suc}$ of -26%. Consequently, this refrigerant can significantly lower the expenditure for the compressor. Finally, R1234ze shows almost the same performances as R134a in therms of COP, but it requires an increase of 33% of the volumetric flow rate.

The trend of refrigerant mass flow rates could be easily predicted considering Figure 5.20. The system working with R1234ze requires the highest mass flow rate (0.0060 kgs^{-1}) due to the smallest heat of vaporization. The system using R290 as energy carrier shows the smallest mass flow rate (0.0025 kgs^{-1}), even though its value was very close to the one required by the system working with R600a (0.0026 kgs^{-1}).

The pressure drops are not reported due to their limited values caused by the big size of the condenser considered in this investigation.

It was then decided to evaluate the performances of the system in terms of COP varying the condenser tube and diameter. The same system configurations presented in Figure 5.19 were considered for each refrigerant. It was chosen to present and compare only the configuration giving the best COP for each refrigerant. For all the analysed fluids the configuration with an outer condenser diameter of 6.65 mm, with IHEX and with a condenser length of 70 m showed the best COP. The trend of the COP with the condenser length is depicted in Figure 5.22. The trend of the volumetric flow rate was not presented because it was subjected to minor variations with the condenser length.

The indications deriving from Figure 5.21a are confirmed in Figure 5.22 also for the optimal system configuration among the considered ones. The only difference is the fact that for condenser length higher than 62 m the system working with R1234yf shows a higher COP that the system with R290. For condenser length higher than 62 m it can also be observed that

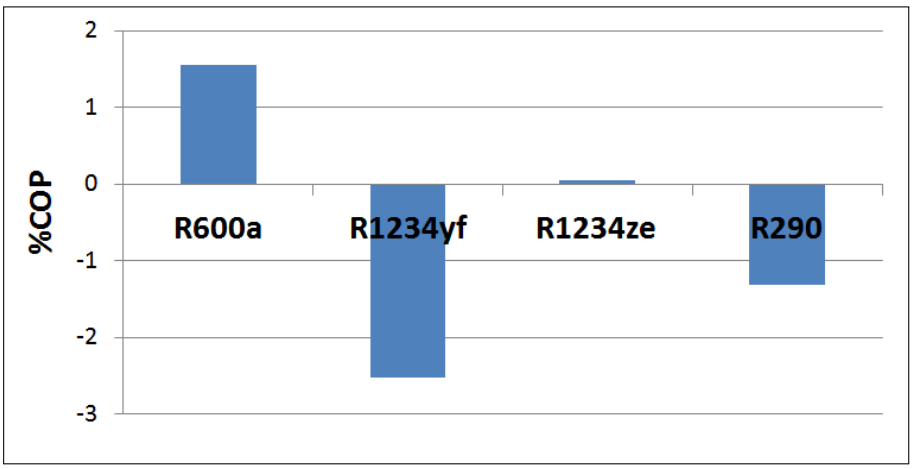

(a) COP relative difference for alternative refrigerants compared to R134a.

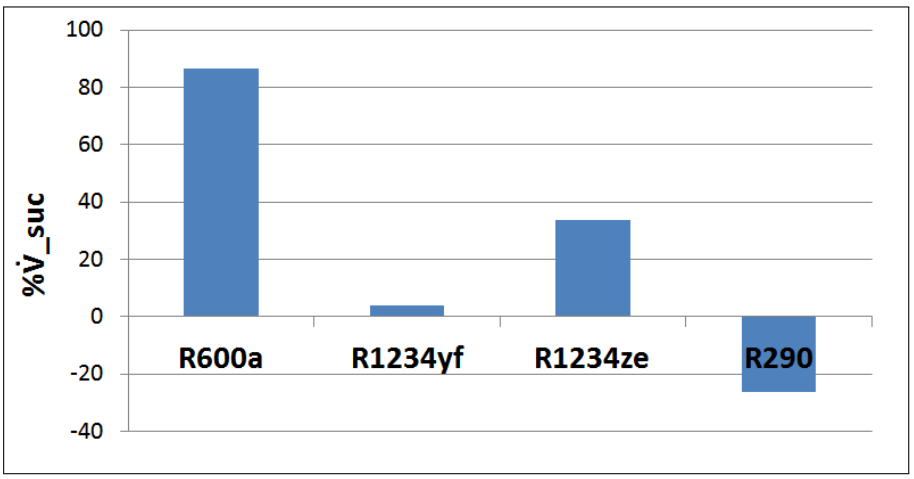

(b) $\dot{V}_{suc}$ relative difference for alternative refrigerants compared to R134a.

Figure 5.21

the trend of the system COP with R1234ze becomes flat. This is due to the fact that after this length the overall heat transfer coefficient in the condensing section and the refrigerant mass flow rate keep constant values.
The gap between the trend of the COP with R600a and the one of R1234yf is almost constant around a value of 5%. Finally, it can be concluded that for all the refrigerants, the COP is only marginally affected by the condenser length if its value is varied from 30 m to 70 m.

It is also relevant to show for the different refrigerants the evolution of the pressure drop with the overall condenser length for the same system configuration used to draw the trends in Figure 5.22. It was decided to report in Figure 5.23 only the pressure drop in the condensing section, due to its considerably greater contribution compared to the one of the subcooling

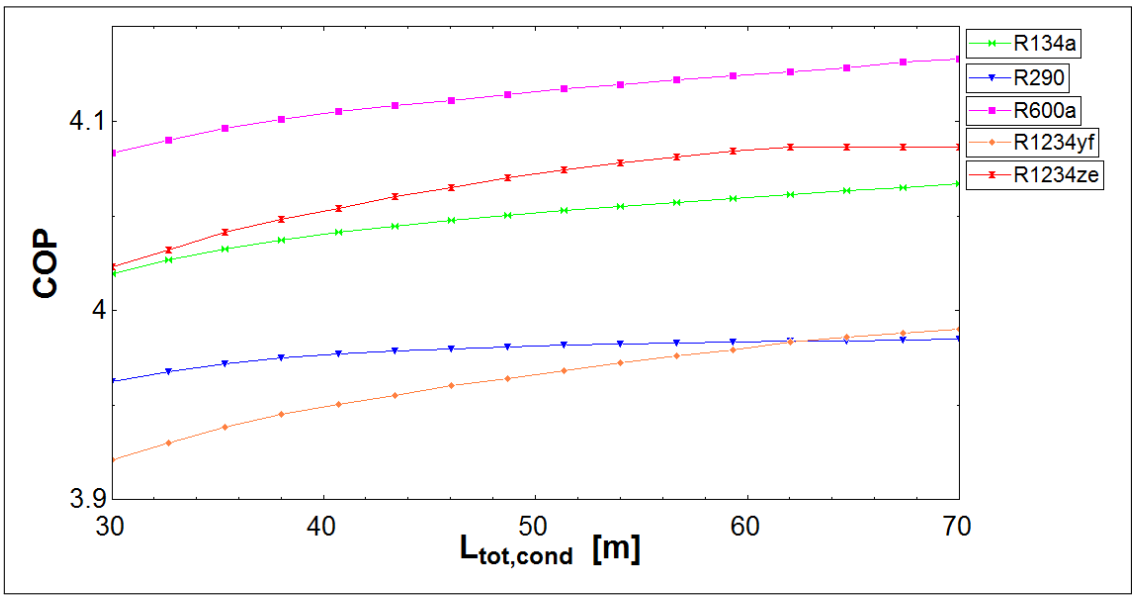

Figure 5.22: COP as a function of the condenser length for the system working with different refrigerants.

and desuperheating sections.
Figure 5.23 shows that the two refrigerants R1234yf and R1234ze are characterised by the highest pressure drop in the condensing section. Also for the pressure drop, the system working with R1234ze presents a flat trend after a condenser length of 62 m, for the same reasons to justify its trend in Figure 5.22. On the other hand, the pressure drop in the condensing section of the refrigerant R290 is the smallest. To explain these trends for the different refrigerants, it must be mentioned that the pressure gradient in the condensing section, computed applying the Muller-Steinhagen and Heck correlation [46], is a function of the refrigerant mass flow rate, as show in Appendix B.1.2. Higher mass flow rates imply higher values for the monophase frictional pressure gradients for the vapour and liquid phases, enhancing the frictional pressure gradient. As previously explained by observing Figure 5.20, the mass flow rate is higher for refrigerants with lower latent heat of vaporization. This justifies the trends of Figure 5.23

5.4.1 Safety aspects

In this section, the safety classification for the different refrigerants is reported as well as some practical considerations mentioned by Mariam Jarahnejad [72]. Before stating the toxicity and flammability behaviour of the different refrigerants, it is relevant to report in Figure 5.24 the safety classification of the refrigerants, according to ANSI/ASHRAE Standard 34-2007 [73]. The safety classes for the refrigerants analysed in the current study is presented in Table 5.7.
The hydrocarbons refrigerant considered in this study, i.e. R290 and R600a, are classified as highly flammable and in a range of low toxicity. These refrigerants are compatible to work

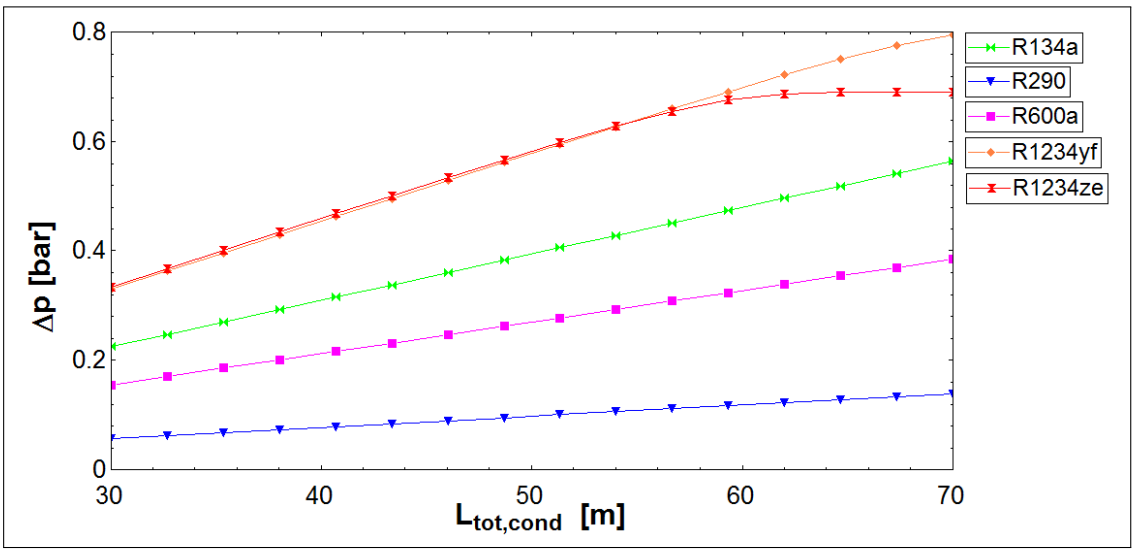

Figure 5.23: Pressure drop in the condensing section as a function of the condenser length for the system working with different refrigerants.

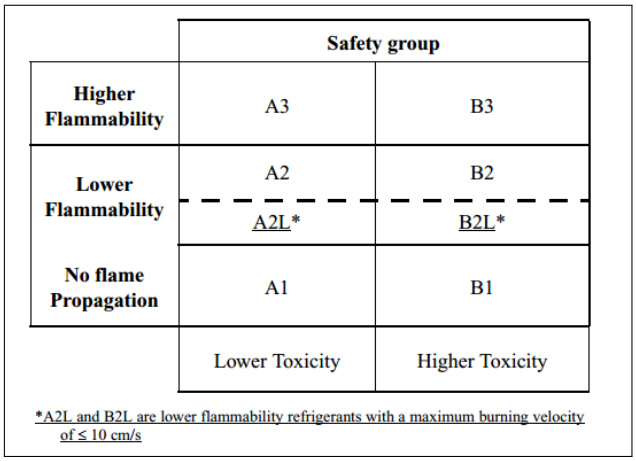

Figure 5.24: Safety classification of refrigerants according to ASHRAE Standard 34-2007 [73].

Table 5.7: Safety classes of the analysed refrigerants.

Propane (R290)	A3
Isobutane (R600a)	A3
R134a	A1
R1234ze	A2L
R1234yf	A2L

with almost all lubricants (a part the ones containing silicate and silicone) commonly used in refrigeration applications. According to Mariam Jarahnejad [72], nowadays they are applied in

several domestic refrigerators.
HFO-1234ze is non-flammable, increasing its suitability in domestic applications. However, overheating, flames and sparks can cause fire and consequently the risks of corrosion and toxic decomposition. Mariam Jarahnejad [72] stated that the products of the pyrolysis of HFC-1234ze contain hazardous products such as hydrogen fluoride and fluorocarbons. Moreover, it is suggested to avoid any reaction with alkali metals. In case of leakage, this refrigerant does not damage the biodiversity. However the biodegradability of R1234ze is not easy.
Finally, HFO-1234yf is characterised by the same safety classification of HFC-1234ze. According to Mariam Jarahnejad [72], this refrigerant at high temperature can be decomposed forming hydrofluoric acid (HF) and carbonyl fluoride(COF2), which is converted to CO and CO_2 in case of contact with water. It is also a stable and neutral gas whose polymerization is not harmful. Due to its difficult biodegradability, it should not be discharged in the ambient. Mariam Jarahnejad [72] also mentioned some bases, acids and oxidizing agents not compatible with this refrigerant.

5.5 Analysis of the other runs

The previous investigations were focused on the analysis of the performances of the forth run of the heating up process. In this chapter, some relevant results concerning Run 1, 2 and 3 will be provided. Again, as previously done, the three system configurations firstly described in Section 5.2 will be considered.
As mentioned in Chapter 3, it was decided to base the initial investigation on run 4 because of its worse performances compared to the other phases of the heating up process. The goodness of this assumption is demonstrated in Table 5.8, in which the system COP for the four runs is reported.
The relative increase of the COP compared to the COP of Case 1 is depicted in Figure 5.25.

Table 5.8: COP of the four runs of the heating up process.

COP			
	Case 1	Case 2	Case 3
Run 1	3.62	3.66	3.65
Run 2	4.10	4.12	4.14
Run 3	4.83	4.85	4.88
Run 4	5.61	5.61	5.65

The figure shows that for all the runs the percentage variation of the COP is very limited for the analysed configurations. Moving from Run 4 to Run 1, the COP of Case 2 compared to the one of Case 1 shows an almost linear reduction, meaning that the benefit gained from the reduced diameter is lowered for lower hot water temperatures. Differently, the %COP variation for Case 3 shows an inverted U-shaped trend, with a peak in Run 2.

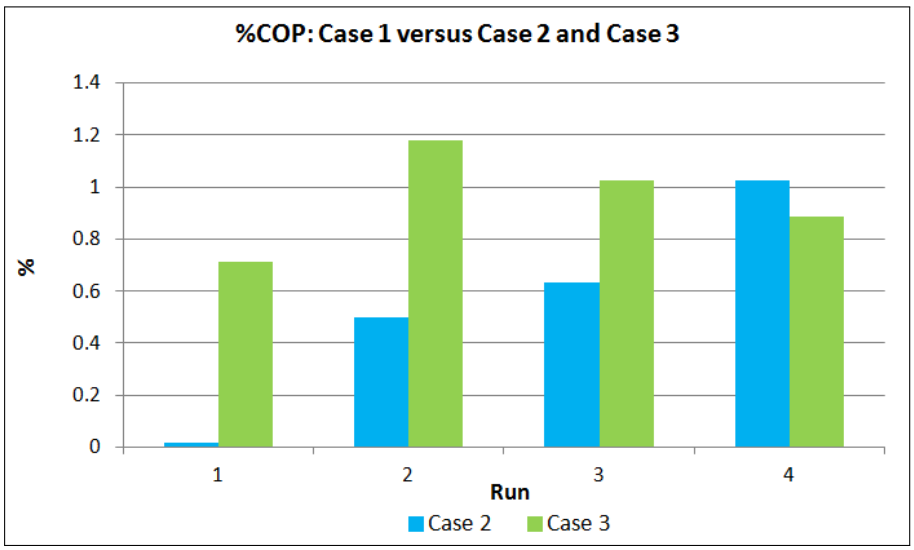

Figure 5.25: Relative variation of the COP of Case 2 and and Case 3 compared to the COP of Case 1.

It was then decided to show the main differences between the cycle parameters of the three system configurations during the four runs. First of all, different shares of the overall condenser area among the three sections were observed. More in details, while the area of the condensing section for Case 1 is subjected to minor variations during the four runs, for Case 2 and 3 it shows a considerable reduction. For a graphical visualization of this fact, the percentage share of the overall condenser area between the three sections of the condenser is depicted for the 4 runs in Figure 5.26 for Cases 1 and 2. Case 3 is not presented because it is characterised by a behaviour very similar to the one of Case 2. Figures 5.26a and 5.26b highlights that the greatest discrepancy occurs between the forth and the third run. Case 1 shows marginal variations, while in Case 2 the area of the condensing section is sharply reduced causing a considerable increase of the area of the subcooler. For a better understanding of this behaviour, a comparison between the transition from Run 4 to Run 3 for Case 1 and Case 2 is firstly assessed. More in details, the variations occurring in the expression of the LMTD in the condensing sections are considered (Equation 3.7 applied to the condensing section). For both Case 1 and 2, the heats transferred in the condensing section and the U values are subjected to similar variations moving from Run 4 to Run 3. Consequently, the deciding parameter to justify the variation in the condensing area is the logarithmic mean temperature difference. For Case 1 it is increased by 8 % from Run 4 to Run 3, while Case 2 shows a much bigger increase amounting to 57 %. Consequently, due to the similarity of the variation of $\dot{Q}_{cond}$ between Case 1 and 2, the heat transfer area of the condensing section strongly decreases in Case 2 while it is characterised by a minor fluctuation for Case 1.

After the observation of this evidence, it is also relevant to investigate the variations of some relevant parameters for Case 2 from Run 4 to Run 3. Some main parameters for the forth and the third run for Case 2 are summarized in Table 5.9. The reduction of $\dot{Q}_{desup}$ and the

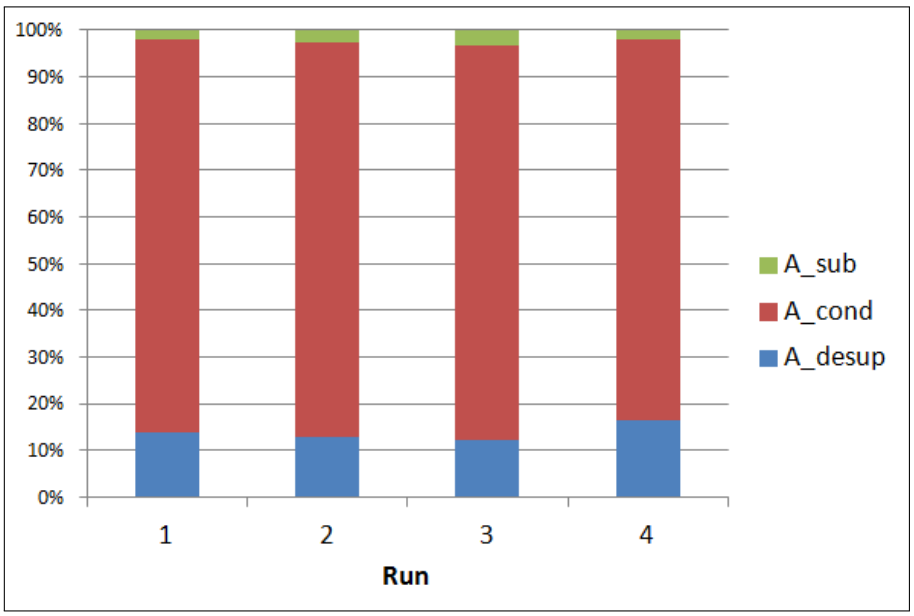

(a) Percentage variation of the areas in the three sections of the condenser during the four runs for Case 1.

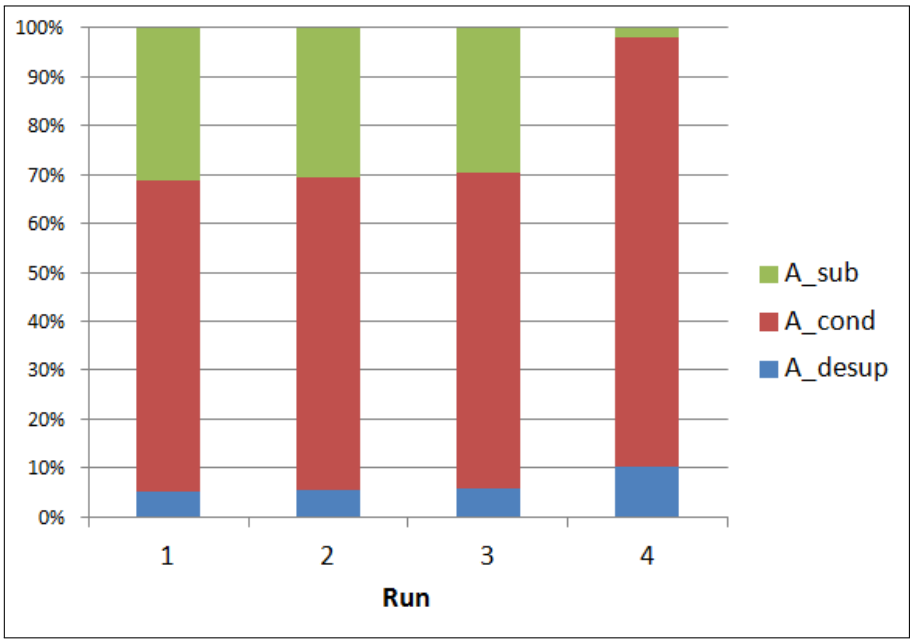

(b) Percentage variation of the areas in the three sections of the condenser during the four runs for Case 2.

Figure 5.26

increase of $\dot{Q}_{cond}$ are caused by the variation of the enthalpy differences caused by the shape of the Andrews thermodynamic diagram for lower condensing pressure, shown for the two

Table 5.9: Comparison between some main parameters for Run 4 and Run 3 for Case 2.

	Run 4	Run 3
$\dot{m}_r$ $[kg/s]$	0.0066	0.0067
$\dot{Q}_{desup}$ $[W]$	283.2	255.5
$\dot{Q}_{cond}$ $[W]$	1011	1085
$\dot{Q}_{sub}$ $[W]$	51.3	50.2
U_{desup} $[W/m^2K]$	561.4	539.3
U_{cond} $[W/m^2K]$	953.3	898.3
U_{sub} $[W/m^2K]$	489.3	469.4
Δp_{desup} $[bar]$	0.14	0.09
Δp_{cond} $[bar]$	0.96	0.84
Δp_{sub} $[bar]$	0.003	0.05

considered Runs in Figure 5.27. In fact, as shown in Table 5.9, the refrigerant mass flow rate is subjected to minor variations. All the U values are decreased for the third run and the one in the condensing section shows the biggest reduction. The reason for this drop lays in the heat transfer coefficients water side for all the three sections of the condenser. They are sharply reduced from Run 4 to Run 3 due to the lower wall temperatures, which are directly proportional to the Rayleigh numbers and consequently to the Nusselt numbers. To give a numerical prove of the lower wall temperatures, it is worthy to mention the discharge temperatures from the compressor for Run 4 and Run 3: they are respectively 90°C and 80°C. The condensing section is subjected to the highest reduction in U value because the dominant and prevailing resistance to the heat exchange is in the water side. For the desuperheating and subcooling sections, the refrigerant in its single phase is the dominant resistance. The variations of the pressure drops for the three sections of the condenser reflect the trends of the share of the overall condenser area shown in Figure 5.26b.

In fact, the pressure drop of each section is directly proportional to the length of the corresponding section: a reduction of the area of the section implies a lower length resulting in smaller pressure drop. Table 5.9 shows that the pressure drops in the desuperheating and condensing sections are decreased moving from Run 4 to Run 3, while the pressure drop in the subcooler is raised. The changes of the pressure drops are aligned with the variations of the logarithmic mean temperature difference mentioned in the previous paragraph. More in details, while the Pinch Point for Run 4 is at the beginning of the condensing section (or at the end of the desuperheating section), for Run 3 the minimum temperature difference between the water and the refrigerant profiles shifts to the end of the subcooling section.

The reason for these trends lay in Figure 5.28a, in which the T-Q diagrams of Case 2 for Run 3 and Run 4 are plotted. The initial water temperatures in the figure were shifted to 0°C to facilitate the comparison. Figure 5.28b depicts the same comparison between the T-Q diagrams of Case 1 for Run 3 and Run 4. Both the figures show that the temperature profile for the water is characterised by different slopes for the forth and the third run. This is due to the different water mass flow rates given as input for the two runs, as summarised in Table 4.1.

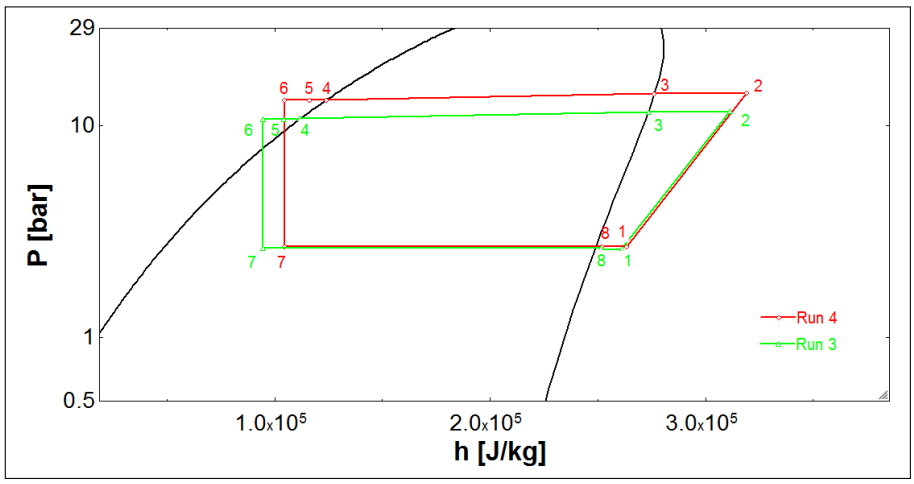

Figure 5.27: Pressure-enthalpy diagrams for Run 3 and Run 4 of Case 2.

More in details, the smaller mass flow rate of Run 4 causes a steeper trend for the temperature profile of the water if compared to Run 3. Both for Case 1 and Case 2, this fact results in a reduction of the temperature difference between the water and the refrigerant at the end of the subcooling section moving from Run 4 to Run 3. However, for Case 1 the Pinch Point remains at the end of the desuperheating section (or beginning of the condensing section) in both Run 4 and Run 3 due to the small contribution of the pressure drops. On the other hand, for Case 2, moving from Run 4 to Run 3, the different slopes of the two water profiles cause a shift of the Pinch Point from the end of the desuperheating section to the end of the subccoling section because of the higher pressure drops involved. It is difficult to notice this shift in Figure 5.28a due to the small temperature differences involved. For Run 3 of Case 2, the temperature difference at the end of the subcooler is 0.1 K, while the one at the end of the desuperheating section is 0.4 K. This very small values can be explained considering the small mass flow rates of water involved, which can cause the water temperature and the refrigerant one to be very close. However, experimental measurements would be required to detect the reliability of this result.

At this point, it is interesting to verify the reason why, despite the similar mass flow rates presented in Table 4.1, Run 1 and Run 4 are still characterised by different shares of the overall condenser area between the three sections (Figure 5.26b). The T-Q diagrams comparing Run 4 and Run 1 for Case 2 is shown in Figure 5.29a. Again all the temperatures are shifted down to 0°C. The figure shows a higher overall heat transfer for the first run, again cause by the shape of the Andrews thermodynamic diagram. The temperature profiles of the water have similar slopes as expected. The main difference between the two T-Q diagrams is the considerable higher pressure drop in the condensing section for Run 1. For this reason, it was decided to plot in Figure 5.29b the evolution with the vapour quality of the pressure gradient in the condensing section calculated by applying the Muller-Steinhagen and Heck

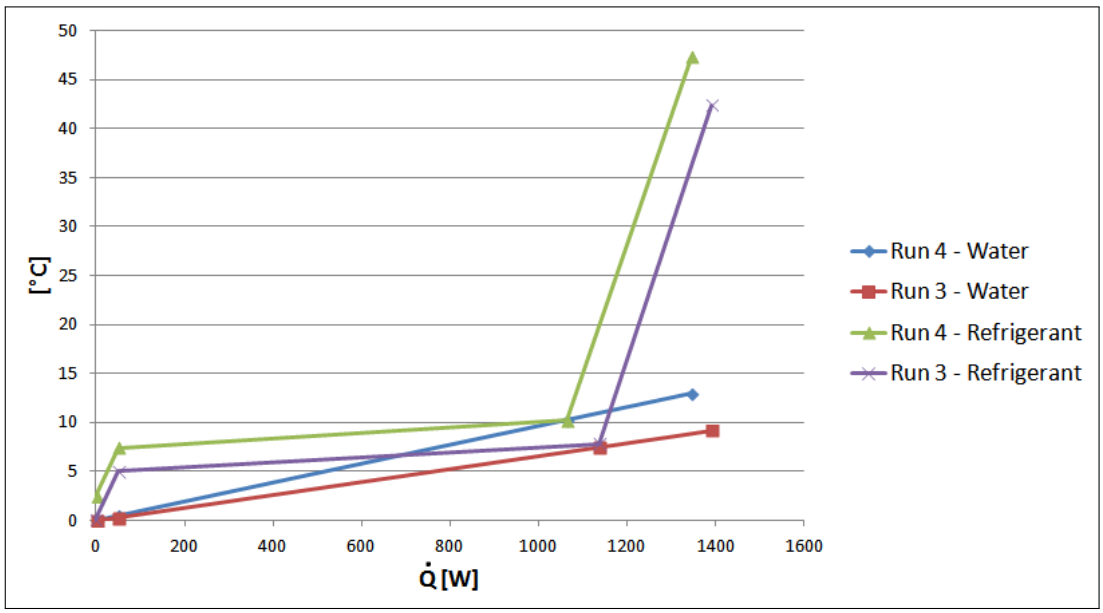

(a) T-Q diagrams for Run 4 and Run 3 of Case 2.

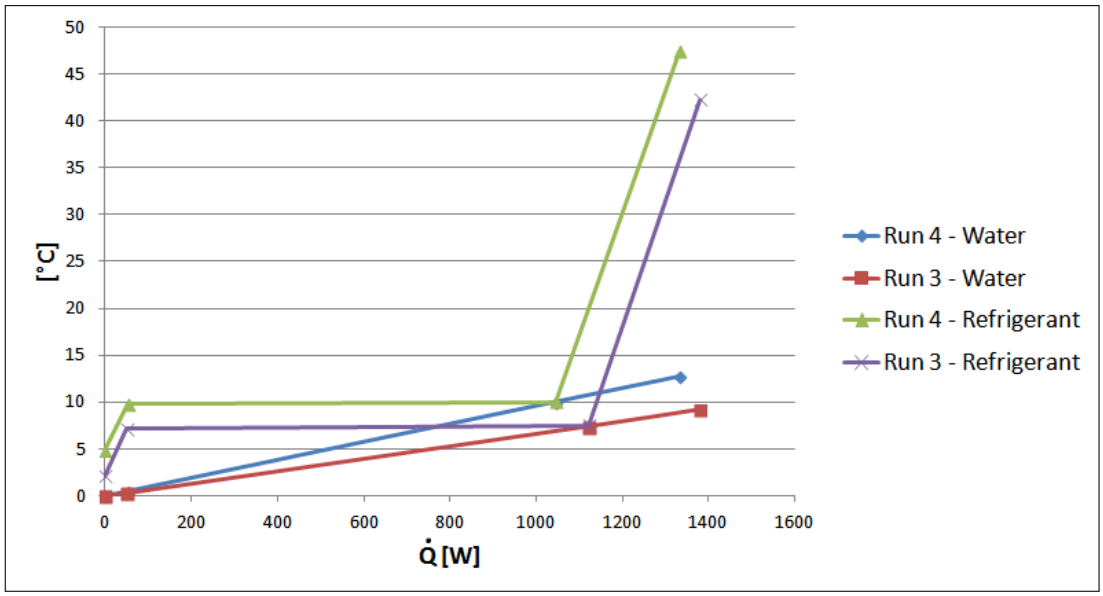

(b) T-Q diagrams for Run 4 and Run 3 of Case 1.

Figure 5.28

correlation [46]. The equations applied are reported in Section B.1.2 of Appendix B. Run 1 shows a considerable higher pressure gradient compared tu Run 4. These trends were found to be due to the difference between the densities of the vapour phase for the two runs: it is almost halved moving from Run 4 to Run 1. This is consequence of the lower condensing pressure for Run 1. The lower vapour density causes an increase of the monophase frictional

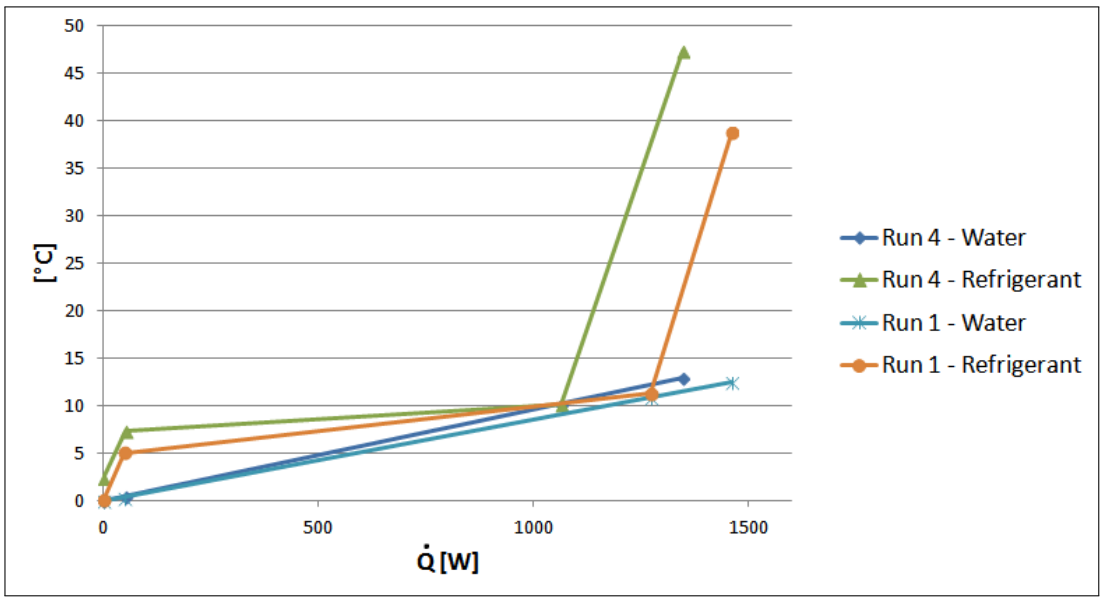

(a) T-Q diagrams for Run 4 and Run 1 of Case 2.

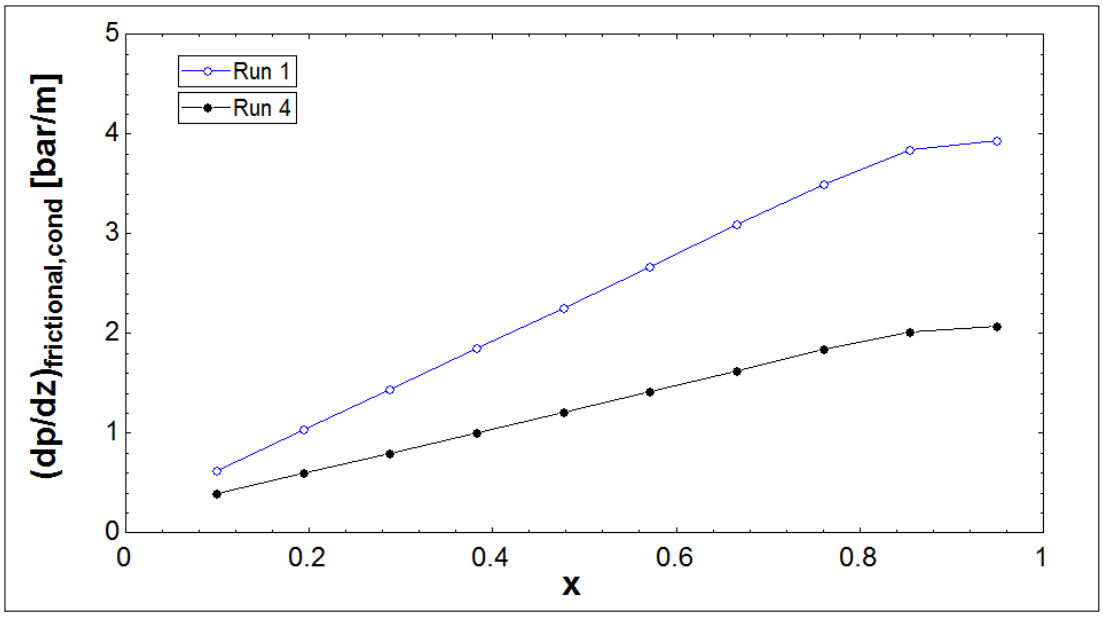

(b) Evolution with the vapour quality of the pressure gradient in the condensing section calculated by applying the Muller-Steinhagen and Heck correlation for Run 4 and Run 1 of Case 2..

Figure 5.29

pressure gradient for the vapour phase, which raises the two-phase frictional pressure gradient.

Other differences found concern the heat transferred in the condensing and desuperheting

section and the compressor work for the three Cases. However, the reasons for these differences was mentioned previously during the report and they are only briefly summarised in this section. The heat transferred in the condensing section is increased lowering the condenser diameter due to the higher enthalpy difference. Through all the runs, Case 3 shows the highest amount of heat released in the condenser section and the lowest compressor work due to the slightly better isentropic efficiency of the compressor. On the other hand, Cases 1 and 2 are characterised by a greater heat transferred in the desuperheater due to the presence of the internal heat recovery unit.

6 Results from dynamic simulations

In this chapter the findings from the dynamic simulations conducted in the Dymola environment are presented. Before explaining the main results derived from the investigations, a validation of the model described in Section 3.2 through experimental results is proposed.

6.1 Validation of the model

As aforementioned, experimental data are used to validate and to adjust some parameters of the tank model, such as the mass fraction of water which is assumed to be recirculated in the tank (r) and the heat loss to the ambient. Taking into account the indications from the steady-state investigations about the distance from the bottom of the tank at which each section of the condenser starts (y) for the actual system configuration, it was decided to distribute the desuperheater, the condenser and the subcooler in the different layers of the tank as summarised in Table 6.1. The overall heat transferred in the condensing section was divided by three to account that it is distributed to three different nodes. This distribution was kept constant for all the heating up process because no relevant variations of the parameter y were observed for the existing system configuration (Case 1).

The heat transferred from each section of the condenser to the hot water in the tank was

Table 6.1: Distribution of the three sections of the condenser in the tank nodes.

Section of the condenser	*Nodes*
Desuperheating	14
Condensing	15-16-17
Subcooling	18

implemented in the model by deriving some correlations relating the heat released and the water temperature in the tank. More in details, the heat transferred through each section was related to the corresponding average water temperature of the section, considering the outputs from the four runs previously analysed. Also the compressor work was introduced in the model

by means of correlations derived from the steady state simulations. Further explanations and the correlations for the different system configurations analysed are presented in Appendix C. Finally, before presenting the results, the location of the temperature sensor required to implement the thermostatic control strategy needs to be specified. It was initially positioned in node 17, the last layer of the condensing section. The upper limit for the temperature in layer 17, i.e. the set point temperature, was set to 52°C, meaning that when the water reaches this temperature at that layer the heat pump switches off.

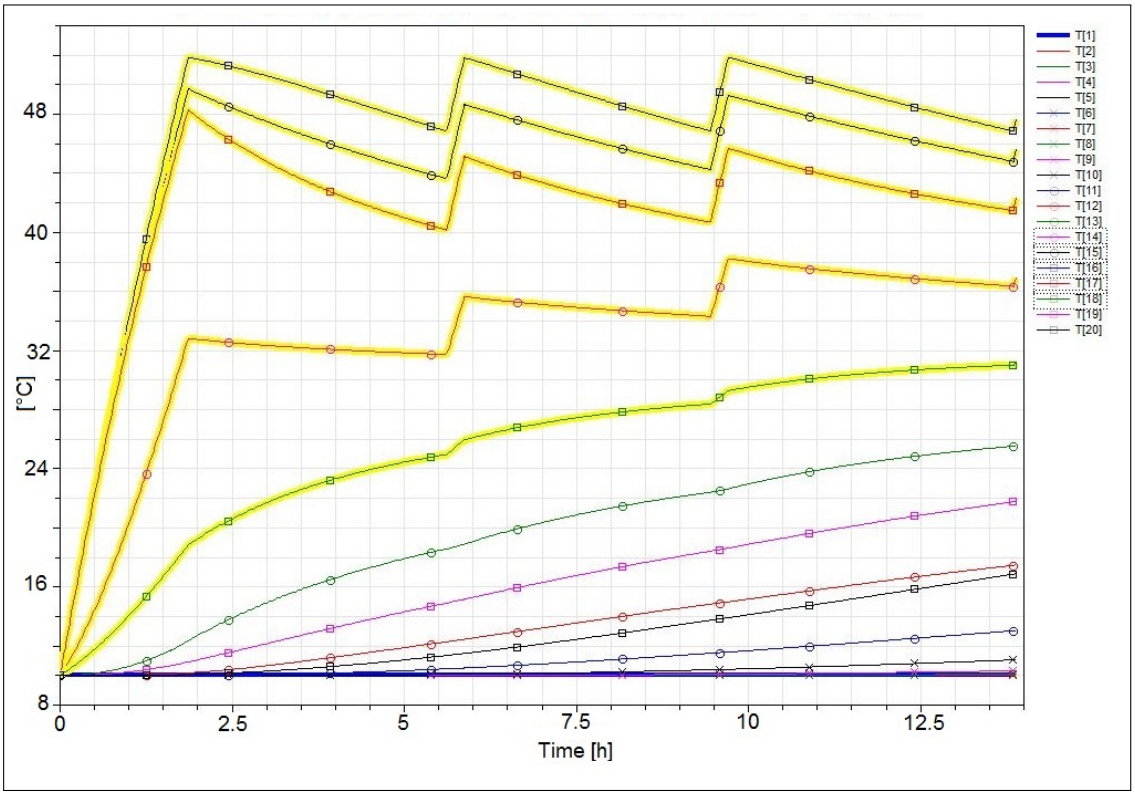

Figure 6.1: Temperature distribution in the nodes of the tank in case of $r = 0\%/s$ and $U_{amb} = 0$ W/m^2K.

Initially, no heat loss to the ambient was considered and a nil water recirculation in the tank was assumed. The resulting temperature distribution in the 20 layers of the tanks is depicted in Figure 6.1. It was decided to highlight with yellow the water temperatures in the tank around the condenser and with blue the water temperature at the top node of the tank. The figure shows that the absence of water recirculation in the tank model causes an excessive and unrealistic thermal stratification between the nodes. More in details, the water temperatures of layers 15-16-17 are subjected to a rapid increase due to the considerable heat transferred in the condensing section. The temperatures in layers 14 and 18, respectively where the desuperheater and the subcooler are located, show a more limited increase because of the

reduced heat released by the refrigerant in its single phase. The temperatures in the two layers below the condenser (19 and 20) and in the four layers above the condenser (10, 11, 12 and 13) are slightly raised due to the contribution of the conduction between adjacent layers. Finally, all the layers between the ninth and the first are characterised by a constant temperature of 10°C, which is the uniform temperature inside the tank before starting the heating up process.

Other simulations were performed varying r. They are presented in Appendix D. It was observed that even for a value of 0.5 %/s, the mixing between the layers plays a noticeable effect on the temperature distributions. The value for the fraction of water recirculating in the tank ensuring a good agreement with experimental results was 10 %/s. Later, it was noticed that the heat loss to the ambient influences the shape of the temperature profiles during the heating up process. A greater contribution of the heat loss implies a more concave trend for the temperature distributions. The reason for this effect is explained in Appendix D. A satisfactory match between experimental results and predicted results from the model was achieved setting U_{amb} to 7 W/m^2K, as shown in Figure 6.2. Figure 6.2a depicts the temperature distributions in all the 20 nodes setting r and U_{amb} respectively to 10 %/s and 7 W/m^2K. Figure 6.2b shows a comparison between the experimental data provided by Metro Therm and the predicted temperature profiles in nodes 10 and 17, calculated by setting the same starting water temperature of the experiments. Layers 10 and 17 were selected as representative respectively for the temperatures at the middle and at the bottom of the tank. As mentioned in Chapter 4, several experimental results were given by the company. For the implementation of the four runs in the steady-state simulations, it was chosen to consider the data characterised by the highest temperature difference between the bottom and the middle of the tank. This represents a worst-case condition and was suitable to detect possible improvements of the COP. On the other hand, for the validation of the model, it is relevant to refer to the most probable situation, i.e. the one which was observed to occur with a certain repetitiveness. This condition, noticed in many experimental data, is the one depicted in Figure 6.2b for the experimental data, with limited temperature differences between T_9 and T_{10}. Figure 6.2b does not include numerical indications in the axis. This choice was done in order to respect the confidentiality agreement and avoid to directly show the provided data.

It is relevant to compare *predicted* T_{10} with *experimental* T_9 and *predicted* T_{17} with *experimental* T_{10}. For what concerns the first comparison, a maximum discrepancy of 11% was observed, applying Equation 3.31. The highest percentage difference between the two temperatures for the latter comparison was 14%, with respect to the temperature lift of the water starting from 10°C. Acceptable values for the discrepancy between experimental and predicted results found in the literature are up to 20% [16] [74] [26], consequently the model can be considered successfully validated. Moreover, it can be seen that the predicted temperature profiles from the tank model replicate with satisfactory agreement the slightly concave trend of the experimental data. Figure 6.2a depicts that all the temperature profiles from node 17 to node 1 are characterised by this concave trend and are quite homogeneous. An exception to this

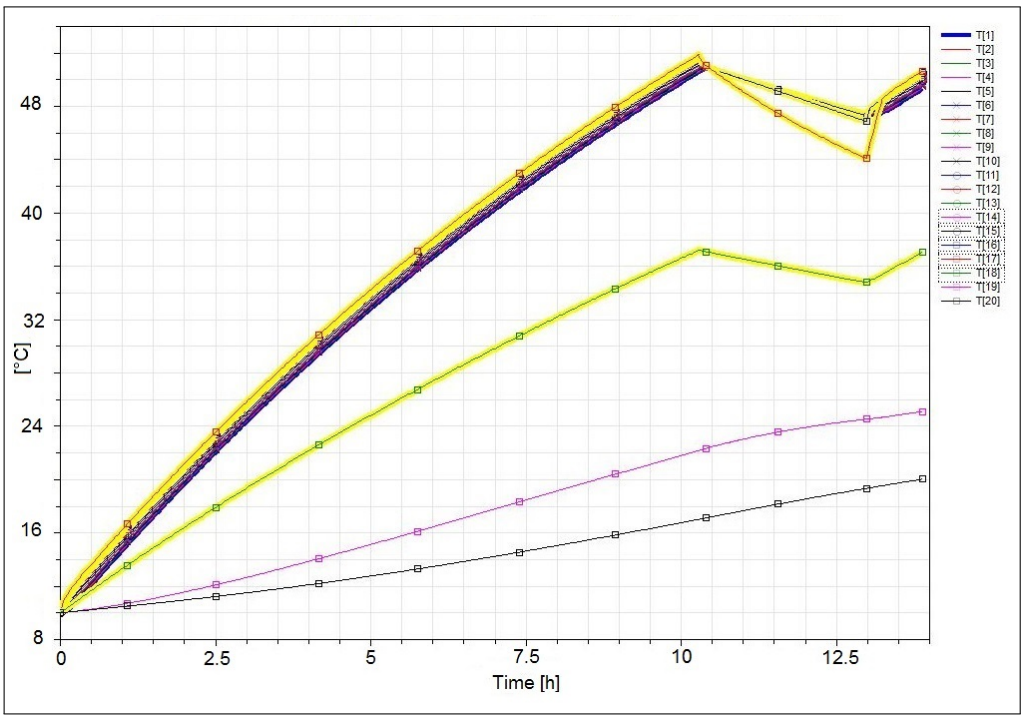

(a) Temperature distribution in the nodes of the tank in case of $r = 10\%/s$ and $U_{amb} = 7\ W/m^2K$.

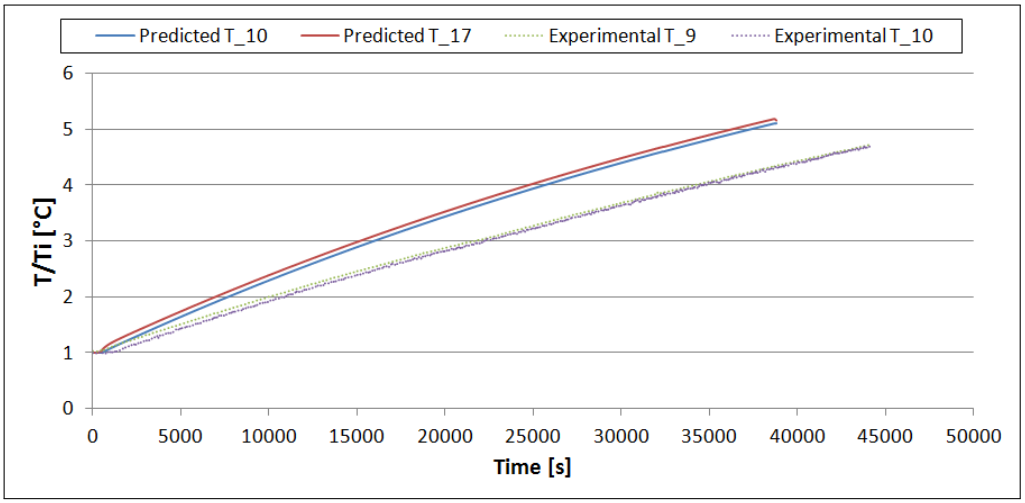

(b) Comparison between the experimental data concerning the evolution of the temperatures T_9 and T_{10}, and the predicted temperature profiles in node 10 and 17.

Figure 6.2

homogeneity is represented by the evolution of the temperatures in layers 18, 19 and 20. In fact the temperature distributions in the last three nodes of the tank show considerably lower values. This is an expected results if the heat transfer mechanism summarised in Figure 3.3 is applied to the bottom of the tank. During all the heating up process, no water recirculation

is permitted in the three layers in the lower part of the tank. In fact, if node 19 is considered the middle node in Figure 3.3, i.e. node i, it is clear that both the conditions $T_i < T_{i-1}$ and $T_{i+1} < T_i$ occur. Moreover, also the water mixing between layer 18 and layer 17 is not allowed due to the higher temperature of layer 17. Consequently, node 18 is slightly heated up thanks to only contributions of the heat transferred through the subcooling section of the condenser and through the conduction from the above layer. Layers 19 and 20 are subjected to a limited temperature raise because of the heat conduction between adjacent layers. The validity of this consideration is proved also by experimental measurements performed by the company on the really bottom part of the tank. It is consequently evident that the temperature sensor measuring T_{10} was not placed in the last three layers of the tank during the tests. Its position in layer 17, considered in the model, is proved to be a valid assumption.
However, a careful examination of Figures 6.2b highlights a slight difference. In the predicted temperature distributions from the model, the warmest node is node 17 and the water temperatures from layer 16 to layer 1 are progressively decreased. Consequently T_{17} is higher than T_{10} in Figure 6.2a. On the other hand, from the experimental results it emerges that the temperature in the middle of the tank (T_9) is higher than the one in the bottom of the tank T_{10}. It was not possible to achieve this condition in the model because the heat transfer through the condensing section occurs between layers 15 and 17, and consequently they are characterised by the highest temperatures. Probably, the buoyancy effect in the real tank plays a major role causing higher water temperatures ascending in the tank. However, despite this discrepancy, the model can still be considered reliable and, as it emerges from a comparison between Figures 6.1 and 6.2a, the inclusion of the water recirculation in the tank considerably increase its realism.

It is also relevant to discuss the reason why in the model node 17 shows the highest temperature even though the same amount of heat is transferred through the condensing section in nodes 15, 16 and 17. To explain this result it is necessary again to refer to the heat transfer mechanism depicted in Figure 3.3. Layer 18 is not considered in this discussion because, as aforementioned, it does not receive any contribution from the water mixing between nodes. On the other hand, node 16 is receiving and consequently delivering energy from both the adjacent nodes. The same situation is occurring for node 15. For the two aforementioned layers all the four energy transfers depicted in Figure 3.3 are occurring. More in details, node 15 is delivering to node 14 and node 16 the same amount of energy. However, the energy deficit caused by the mixing with node 14 overcomes the energy gain due to the heat exchange with layer 16. In other words, node 15 is "cooled down" by layer 14 more than the extent in which it is "heated up" by node 16 because of the low temperature of node 14. The same reasoning can be applied to node 16, whose temperature is reduced due to the interaction with layer 15. However, due to the fact that layer 15 is warmer than layer 14, the energy deficit for node 16 is less disadvantageous than the one of node 15. The same consideration can be applied also for layer 17, concluding that node 17 is characterised by the least disadvantageous energy deficit with the above layer (node 16). This justifies its highest temperature in the model.

6.2 Comparison between the heating up processes

After the model has been validated, it was used to compare the three system configurations described in Chapter 5.2. An assumption was required at this stage in order to simplify the model implementation. The distribution of the three sections of the condenser in the tank nodes is kept as described in Table 6.1 for all the cases. However, a more proper formulation of the model should take into account that due to the considerable variation of the areas of the three sections of the condenser proved in Section 5.5, also the repartition of the nodes should vary. This would require an additional if-statement increasing the complexity of the model. Moreover, it must be specified that the correct amount of heat is transferred through each section of the condenser thanks to the correlations described in Appendix C. In fact, they take into account the evolution of the areas in the condenser sections.

The first comparison between the three system configurations analysed can be based on the COP_{avg} at the end of the heating up process. This parameter takes into account the overall energies involved during the heating up process. All the cases show a COP_{avg} of 5: no differences were observed. This result is not aligned with what presented in Figure 5.25, in which some differences in the COP were spotted for the four runs. In order to understand the reason for this discrepancy, a simulation of the heating up process without considering the heat loss to the ambient was run ($U_{amb} = 0$). This simulation showed some slight differences and confirmed the results of Figure 5.25. At the end of the heating up process, Case 3 shows a slightly better COP_{avg} than Case 1, i.e. around 1%. Case 2 is characterised again by almost the same COP_{avg} of Case 1: as in Figure 5.25 the instantaneous COP for the last phase of the heating up process is slightly enhanced, but this does not affect significantly the COP_{avg}. This observation implies that Case 3 is subjected to slightly higher heat loss to the ambient than the other cases and that the contribution of the heat loss levels the variations in the COP_{avg} between the different system configurations.

The next investigation was conducted in order to detect if different ambient temperatures can cause some variations of the COP_{avg}. The average monthly temperatures for the locations of Copenhagen and Paris summarised in Table 5.4 are again considered. More in details, the heating up process was simulated for the most extreme value: -1°C (January-February in Copenhagen). This was the value considered for the supplied air temperature at the evaporator. The correlations for the compressor work and the heat transferred in the three sections of the condenser were derived in the same way explained in Appendix C, considering the same assumptions described in Section 5.2. Moreover, for the assessment of the heat loss to the ambient, from the aforementioned outdoor temperatures it was required to find the corresponding temperature in the basement where the heat pump is again assumed to be placed. The application of one of the correlations developed by Armstrong et al. [75] was considered suitable for this purpose. In fact, in that study the basement foundation surface

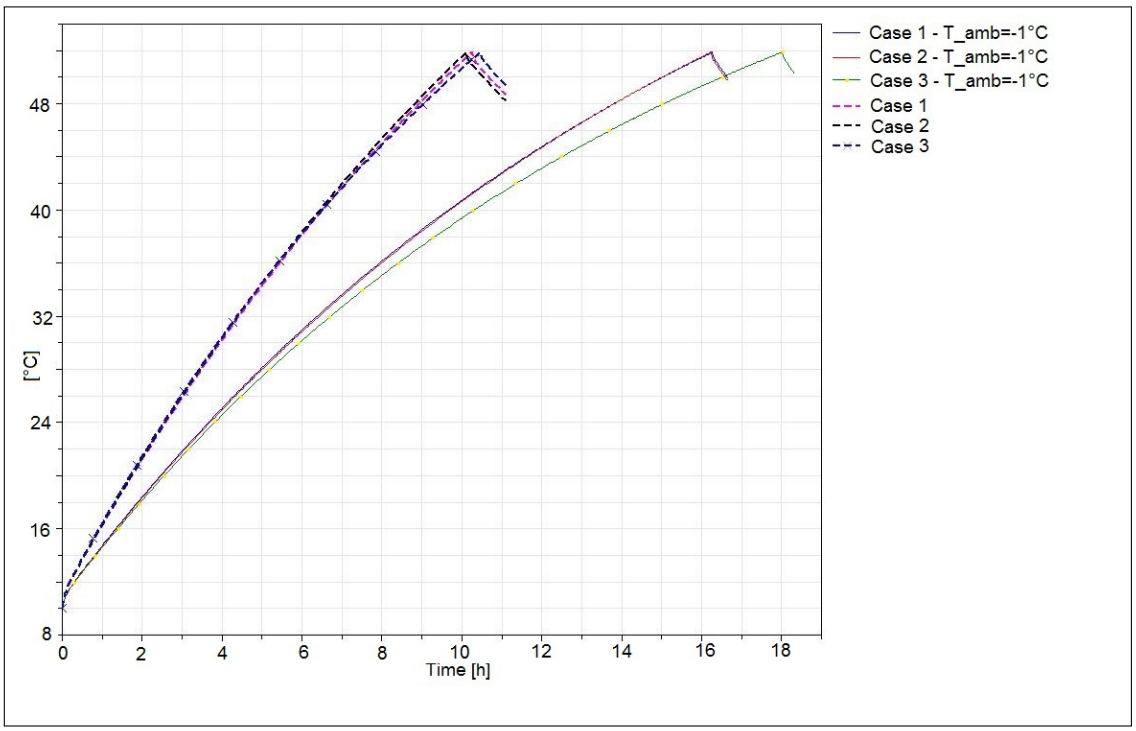

Figure 6.3: Evolution of the temperature profile in node 17 during the heating up process for the three cases considering both a T_{amb} of 7°C and -1°C.

temperatures and ground temperatures where monitored for 7.5 years in a Canadian reference house. Some correlations were developed in order to relate the foundation surface temperature to the outdoor temperature. Due to the location of the evaporator on the top of the tank for the analysed system, it was chosen to apply Equation 6.1, which was derived measuring with a thermocouple the temperature at the top of the interior of the basement wall.

$$T_{basement} = 0.0061\,T_{amb} + 0.4932\,T_{amb} + 6.7018 \tag{6.1}$$

The corresponding values of the basement temperatures for T_{amb} of -1°C is 6.2°C. The heating process process derived implementing these new values is compared with the original one in which the air is supplied to the evaporator at 7°C and the temperature in the basement is 20°C.

Table 6.2: COP_{avg} of the overall heating up process for the the three considered system configurations for an ambient temperature of -1°C.

System configuration	COP_{avg}
Case 1	3.94
Case 2	3.91
Case 3	3.85

The COP_{avg} for the case with ambient temperature of -1°C at the end of the heating up process is shown in Table 6.2 for the three cases. The table shows again small differences between the different cases. The actual system configuration emerged to offer the best COP_{avg}, 2.3% higher than one of Case 3. The reason for this difference mainly lays in the heat transferred in the desuperheating section of the condenser. Despite the slightly higher heat transfer in the condensing section and the slightly lower compressor work of Case 3, the detriment due to the smaller heat transfer in the desuperheating section caused by the lack of the IHEX is prevailing causing a lower COP_{avg}. A graphical representation of the aforementioned results is offered in Appendix E. This fact also considerably raises the duration of the heating up process, as shown in Figure 6.3. The figure depicts the evolution of the temperature profile in node 17 during the heating up process for the three cases considering both a T_{amb} of 7°C (Case 1, Case 2 and Case 3 in the figure) and -1°C (Case 1 - $T_{amb} = -1$°C, Case 2 - $T_{amb} = -1$°C and Case 3 - $T_{amb} = -1$°C in the figure). Figure 6.3 also shows that the lower temperature in the basement in case of ambient temperature of 1°C causes higher heat loss to the ambient resulting in a more concave trend.

6.2.1 Water temperature up to 60°C and position of the sensor

In this section the first goal is to estimate the reduction of the COP_{avg} if the heat pump is required to heat up the domestic hot water up to 60°C. The system performances are expected to decrease due to the higher pressure ratio involved. This investigation is relevant because, as aforementioned in the report, some countries can require some periodical thermal disinfestation of the water stored in a tank. Moreover, in some manufacturer catalogues, such us the one proposed by the company A.O. Smith [76], it is mentioned that commercial air to water heat pump water heaters can easily and efficiently maintain hot water temperatures in the tank up to 60°C.
Due to the small magnitude of the parameter variations for the three considered system configurations, it was preferred to investigate the influence of different set point temperatures only on the actual system configuration, Case 1, chosen as representative also for the other cases. The variation of the COP_{avg} with the set temperature introduced in the model to implement the control strategy is depicted in Figure 6.4. In other words, the x-axes shows the temperature at which the heat pump is switched off (T_{stop}), and consequently the temperature at which the heating up process is concluded. The figure shows an almost linear reduction. The COP_{avg} is reduced approximately by 10% if the set point temperature is reduced from 52°C to 60°C. Anyway, the numerical values of Figure 6.4 show that the heating up process of the hot water up to 60°C can still be performed efficiently by the heat pump.
Another idea was to plot the reduction of the COP_{avg} as a function of the set point temperature for different heights of the sensor in the hot water tank. In fact, the current investigation and all the previous ones were conducted keeping the sensor controlling the operation of the heat pump in layer 17. However, the very small variations achieved with this sensitivity analysis discouraged to present these results. The reason for the small magnitude of the variations lay in the proximity of the temperature profiles from node 17 to node 1 depicted in Figure 6.2a.

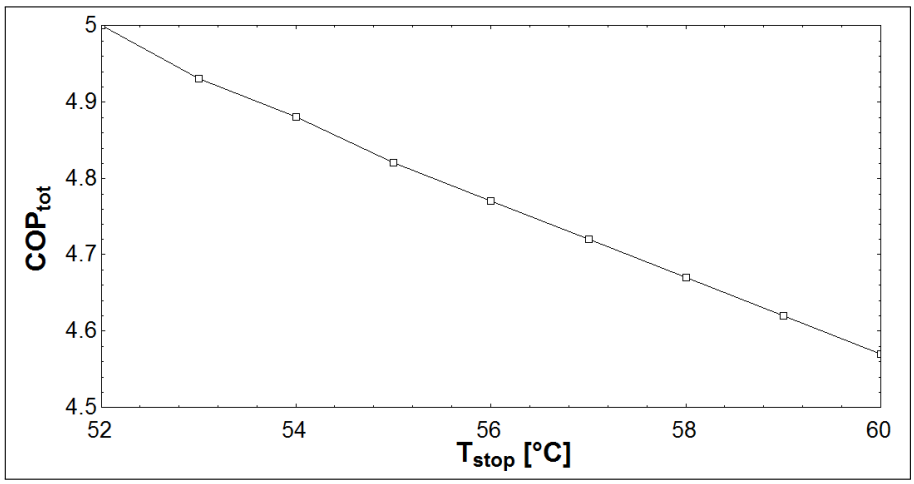

Figure 6.4: Evolution of the COP_{avg} with the stop temperature for the heat pump for Case 1.

6.2.2 Sensitivity analysis on the compressor work correlation

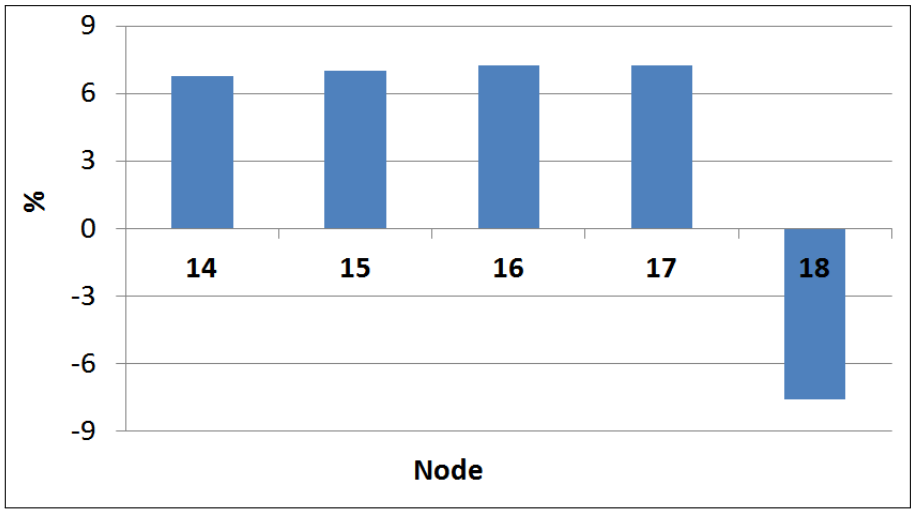

Figure 6.5: Sensitivity analysis on the compressor work in the dynamic model.

As explained in Appendix C, the compressor work is implemented in the Dymola model by means of correlations resulting from the simulations of the four runs in the EES model. More in details, the compressor work is expressed in the dynamic model as a function of the average water temperature throughout the overall condenser. Looking at Table 6.1, it means that the mentioned average water temperature is considered between layer 14 and 18. However, as shown in Figure 6.2a, the temperature profile in node 18 is way lower compared to the one in the other four nodes. It was consequently decided to investigate the extent in which this assumption affects the compressor work. The sensitivity analysis was conducted on Case 1, the actual system configuration. The same correlation showed in Figure C.10 is applied.

The compressor work calculated over the average water temperature between layers 14 and 18 is considered as reference value. The relative difference between this benchmark and the compressor work calculated as a function of the water temperature in each node between 14 and 18 is presented in Figure 6.5. The comparison was performed considering the cumulative overall energy [J] required to the compressor at the end of the heating up process. As it emerges from the figure, the compressor work is subjected to considerable fluctuations. These variations follow the indications of Figure 6.2a: higher values for the temperature profiles imply higher compressor works. More in details, a discrepancy of 14% is observed if the compressor work is calculated as a function of T_{17} instead of T_{18}.

6.3 Comparison between the tapping cycle L

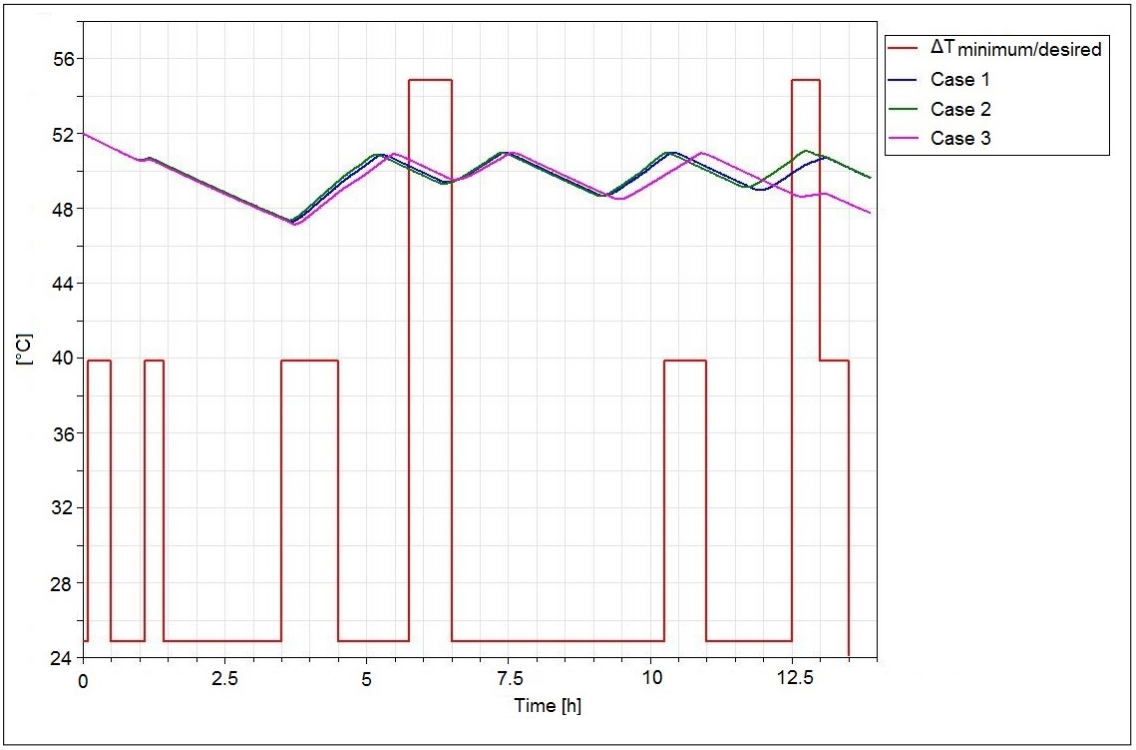

Figure 6.6: Evolution with the time of the temperature in node 1 during tapping cycle L and $\Delta T_{minimum}$ or $\Delta T_{desired}$ for the three considered system configurations.

In this section the results deriving from the implementation of the tapping cycle L, as described in Section 4.5, are presented. As aforementioned in that section, Standard DS/EN 16147 [32] specifies some energy requirement and minimum/desired temperature difference for the water to be met for every tapping. Even though the fulfilment of the energy requirements is not considered in this work, it is relevant to verify at least if the water temperature in the top of the tank meets the $\Delta T_{minimum}$ or $\Delta T_{desired}$ (which are not distinguished) for the tappings mentioned in Table 4.2. The evolution with the time of the temperature in node 1, the upper

layer of the tank, is shown in Figure 6.6 together with the $\Delta T_{minimum}$ or $\Delta T_{desired}$ (red line) for the three considered system configurations. As it is evident from the figure, the temperature in node 1 meets the requirements on the ΔT during all the tapping cycle a part for two time steps: from hour 5.75 to 6.5 and from hour 12.5 to 13. However, this fact was predictable considering that in the corresponding tapping for these two time steps is the dish washing, which requires a temperature lift of 45 K for the water. According to the Standard, the missing temperature difference should be provided by an additional electrical resistance heater (COP=1) which is not considered in this report. Figure 6.6 suggests that Case 3 should be the system configuration subjected to the highest penalisation in the system COP, if the electrical resistance heater is taken into account. In fact, while from hour 5.75 to 6.5 the temperature profiles are quite close, from hour 12.5 to 13 Case 3 shows a significant lower temperature at the top of the tank compared to the other cases.

After this preliminary investigation, the COP_{avg} for the three cases are summarised in Table 6.3. The cumulative energies used to find these values include all the contribution until hour 13.5, in which the tapping cycle ends. Also in this case the magnitude of the variations is very limited. Case 2 offers an enhancement of the COP_{avg} of 0.9% compared to Case 1 due to higher heat transferred in the overall condenser during all the tapping cycle (the compressor work is almost the same for the two cases). Case 3 basically does not cause any variation on the considered parameter.

Table 6.3: COP_{avg} of the tapping cycle L for the the three considered system configurations.

System configuration	COP_{avg}
Case 1	4.46
Case 2	4.50
Case 3	4.48

7 Experimental results

In this chapter, the experimental results derived from the tests conducted in the in-house laboratory of the company are reported. Both the findings from the steady-state and dynamic simulations suggested that very limited variations in terms of COP can be observed with the two system configurations analysed. Consequently, the main advantages of a reduced diameter lays in the cost savings. At the moment of choosing the system configuration to be tested, a key factor was the need to find quickly in the market the condenser tube required. First of all, the material was changed from aluminium to copper because of the easier availability of the latter. This variation, implemented in the steady-state model, resulted to cause nil variations in the system performances due to the small conductance in the tube wall. Two condenser tube outer diameters satisfied the criteria of easy provision: 8 mm and 6 mm. Both of them had a tube thickness of 1 mm. It was preferred to test the latter option due to the higher attractiveness in terms of cost savings. The following choice concerned the tube length to be tested. Again the steady-state simulations indicated that the system COP is varying marginally with the tube length. Consequently, it was preferred to keep the actual condenser length of 54 m because in this way no changes in the production line would be required. In fact, at the moment the machine is automated to cut the condenser tube every 54 m. The characteristics of the tested condenser tube are summarized in Table 7.1. For the rest of report, this system configuration will be named Case 4.

Table 7.1: Characteristics of the tested condenser tube (Case 4).

Material	Copper
$D_{out,c}$ [mm]	6
s [mm]	1
L_c [m]	54
$A_{tot,c}$ [m^2]	0.85

It was then decided to keep the internal heat recovery unit in the system. This choice was

caused by the lack of significant improvements caused by the exclusion of this component. Moreover, Figure 6.3 proves that the absence of the IHEX can considerably prolong the duration of the heating up process for low ambient temperatures.
Before presenting the test conditions and the findings from the experiments, it is worthy to propose again the sketch of the system, shown in Figure 7.1a. Moreover, a picture of the heat pump used for the tests is also presented in Figure 7.1b.

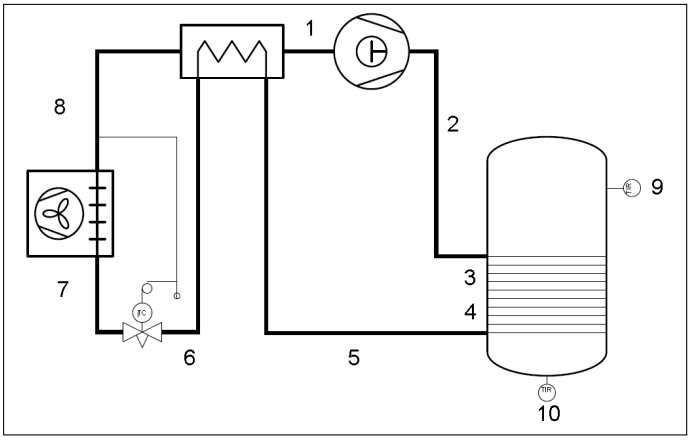

(a) PI diagram of the METROAIR AQUA.

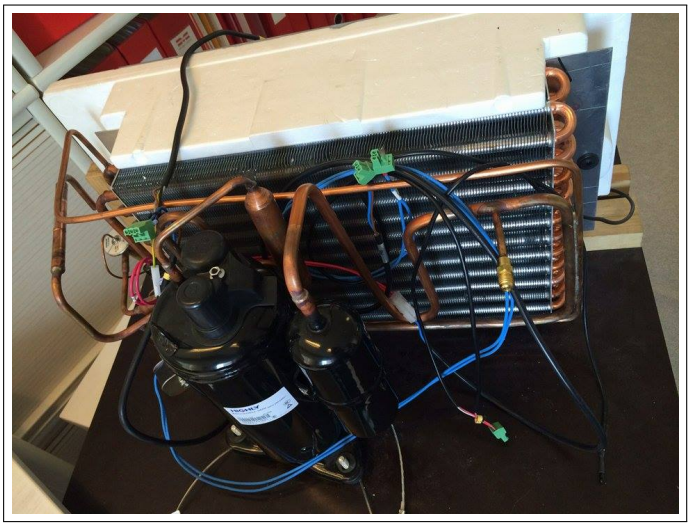

(b) Picture of the heat pump used for the tests.

Figure 7.1

For what concerns the test conditions, it needs to be specified that the air was supplied at the evaporator at 7°C. The set point temperature for the heat pump was fixed to 45°C in order to shorten the duration of the heating up process. The temperature in the higher part of the tank

is expected to be higher than 45°C due to the heating phenomena occurring in the tank. The temperature in the hot water tank was measured at the bottom and at the middle of the tank, respectively 23 cm and and 78 cm above the lowest point of the tank. The temperature sensor used is a PT100 sensor class A. The uncertainty of the instrument is:

$$Uncertainty = 0.15 + 0.002|T| \tag{7.1}$$

where the temperature T must be expressed in [°C].

Before performing the test, it was considered worthy to implement a simulation first with EES and then with Dymola to determine the expectations from the tests. The performances of the heating up process obtained with Case 4 and Case 1 needed to be compared. To accomplish this goal, the four runs were implemented in the steady-state model for Case 4 as presented in Chapter 4. Then, similarly to what described in Appendix C, the correlations were derived from the four runs in order to include in the dynamic model the compressor work and the heat transferred in the three sections of the condenser. The set point temperature for the heating up process was set to 50°C in the model. This value is higher than the 45°C considered for the tests. However, as aforementioned, the temperature in the middle/top of the tank is expected to be higher than 45°C in the tests, justifying the choice to set a temperature of 50°C in the model. The results indicate that Case 4 shortens the heating up process compared to Case 1. The evolution of the temperature profile in node 10 for the two cases under investigation is depicted in Figure 7.2. The choice to report the temperature distribution in node 10 lays in the fact that the test measurements consider the temperature in the middle of the tank. Even though the set point temperature was set to 50°C, the predicted temperature reached in layer 10 at the end of the heating up process is slightly lower than this value. This is due to the heating phenomena occurring inside the tank: the heat pump stops running when the temperature in node 17 reaches 50°C. Figure 7.2 highlights that the duration of the heating process is reduced by almost 30 minutes for Case 4 compared to Case 1. This means that the heat transferred in the overall condenser is increased. The COP is enhanced by 2% compared to the original system configuration.
To sum up, the expectations from the test are to observe a faster heating up process and a slight improvement of the COP.

A comparison between the experimental results concerning the temperature profiles at the middle and at the top of the tank during the heating up processes for the original system configuration (Case 1) and for Case 4 is presented in Figure 7.3. In the figure T_9 and T_{10} represents respectively the temperature in the middle and in the bottom of the tank, as shown in Figure 2.1. The values on the y-axis are dimensionless due to the confidentiality agreement with the company. More in details the temperature at each time step is expressed as the ratio of its nominal value and the temperature at the time 0 (i.e. T_i). The same strategy is adopted also for Figure 7.4. The figure partially confirm the expectations. The heating up process for Case 4

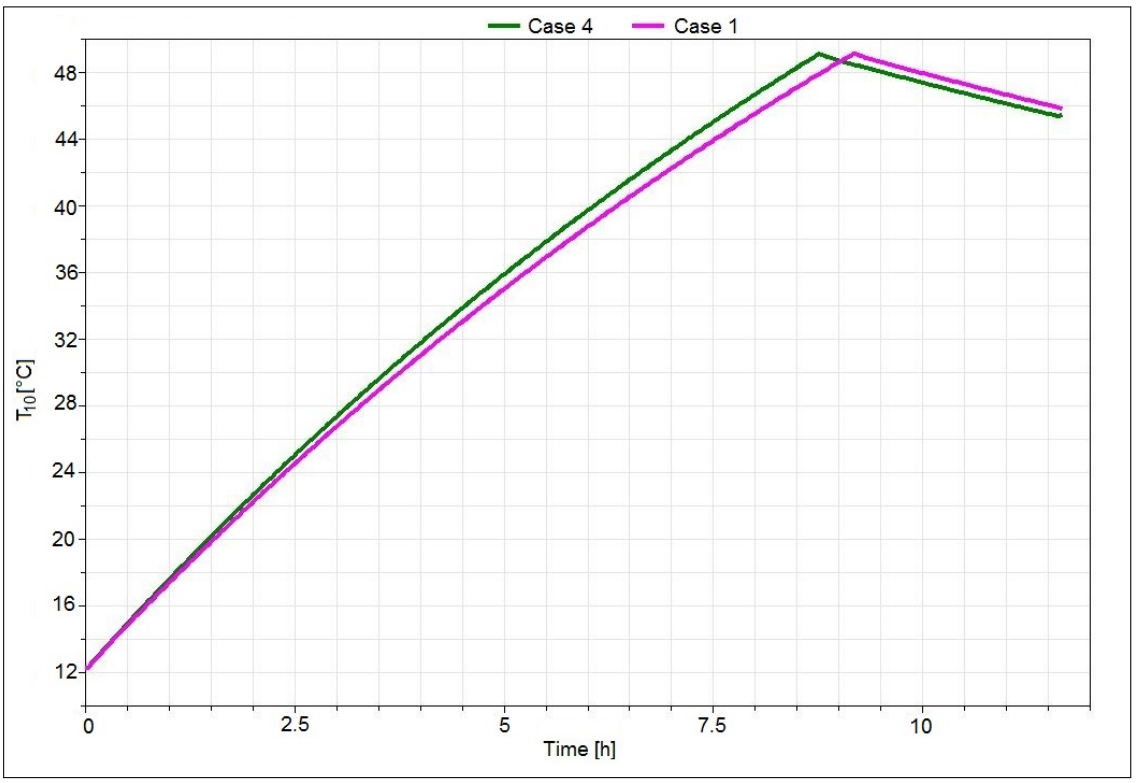

Figure 7.2: Evolution of the temperature profile in node 10 for Case 1 and Case 4.

is faster than Case 1, as expected. However the extent of the time reduction is almost 1.5 hours, triple than the 0.5 hours predicted by the model. This difference can be explained considering Figure 6.2b. This figure shows that the predicted time required to accomplish the heating up process is lower than the experimental one. This is probably due to an overestimation of the heat transferred from the condenser to the domestic hot water. Even though in the previous chapter it was stated that the discrepancy between predictions and experiments was acceptable, this differences justify the inconsistency between Figure 7.2 and Figure 7.3.

Another fact emerging from Figure 7.3 is the considerably higher temperature difference between the middle and the bottom of the tank for Case 4. The explanation for this fact can be found in Figure 6.2a. It depicts that the bottom layers of the tank, due to the lack of mixing effect between the layers, are colder than the other nodes. In the tests, due to the lower diameter of Case 4 compared to Case 1, the condenser ends at a higher height from the bottom of the tank. Moreover, similarly to what shown in Figure 5.26b for Case 2 and as verified in the steady-state simulations for Case 4, the subccoling section occupies a larger portion of the overall condenser for Case 4. Consequently it is expected that, if the sensor measuring T_{10} is placed at the same height for both the cases, for Case 4 the sensor is already in the region in the bottom of the tank where the water recirculation is nil. This explains the higher gap between the temperature profiles in the middle and in the bottom of the tank.

The faster heating up process is expected to result in an enhancement of the COP because of

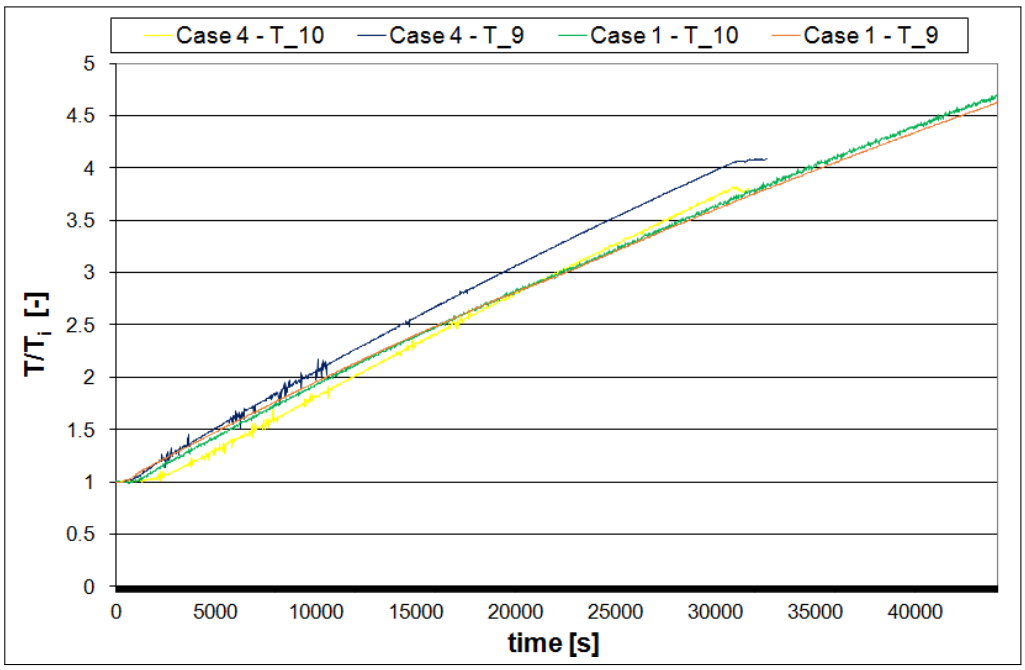

Figure 7.3: Comparison between the temperature profiles from experimental results for Case 1 and Case 4.

the higher heat released in the condenser. However, a verification of this fact was not possible due to fact that the heat transferred from the condenser and the compressor work were not measured.

It was also decided to take advantage of the experimental data to further validate the model. More in details, among the two additional temperature profiles provided, it was considered relevant to compare the temperature profile in the middle of the tank and to disregard the one in the bottom of the tank. This is due to the fact that in the tank model a constant distribution on the nodes of the desuperheating, condensing and subcooling section is assumed, and the increase of the height from the bottom of the tank at which the condenser ends is not considered for the smaller diameter. This additional validation is proposed in Figure 7.4 in which the predicted temperature distribution in node 10 is compared to the experimental results for the temperature in the middle of the tank (T_9). The two lines depicting the temperature profile $\pm$ the uncertainty calculated applying Equation 7.1 are not presented because they would complicate the understanding of the figure. The figure highlights that the model can predict accurately the temperature profile: the maximum discrepancy is lower than 5%, with respect to the temperature lift of the water starting from 10°C. From a comparison with Figure 6.2b, it emerges that the accuracy of the model is increased for smaller condenser areas, even if for both the cases it is acceptable. As shown in Figure 5.9 for the system COP and consequently for the heat transferred from the condenser to the domestic hot water, many assumptions affect

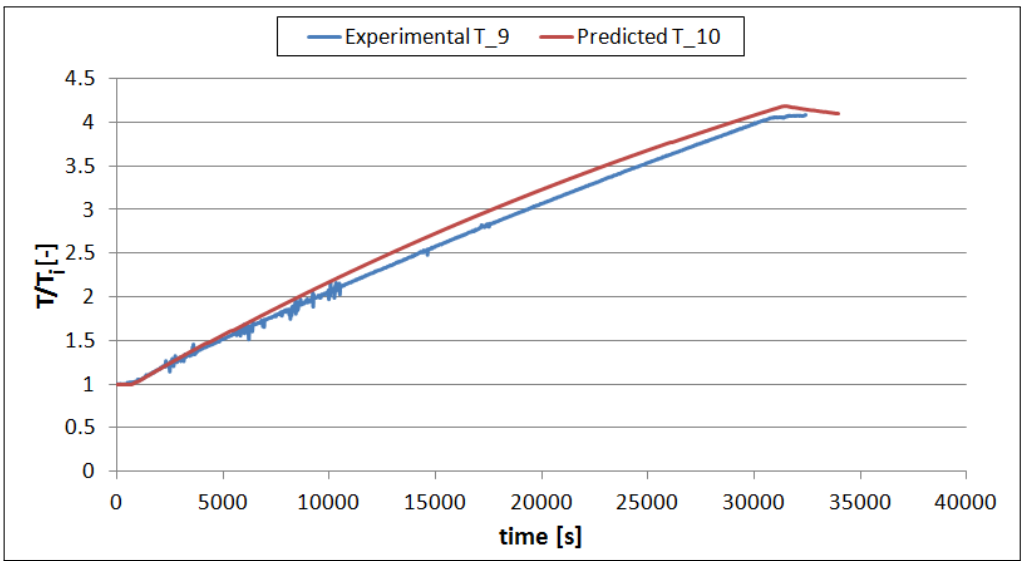

Figure 7.4: Further validation of the model.

the outputs from the models. A possibility can be that the assumed values are closer to the real values for smaller condenser areas rather than for bigger geometries. Further investigations and tests need to be done to verify this fact.

Finally, it was decided to quantify the economical benefit implied by the reduced diameter applying Equation 4.4. Moving from an outer diameter of 9.95 mm to one of 6 mm, the cost of the condenser per unit of length is reduced from 1.13 €/m to 0.74 €/m. Considering the condenser length of 54 m for both cases, the extent of the expenditure reduction is 34%. This data does not take into account the reduction of the condenser tube thickness: it is 1.4 mm for the actual tube and 1 mm for the new tested configuration. This fact is expected to be reflected in an even higher cost reduction for Case 4.

8 Discussion

In this chapter the main findings from this study as well as the main limitations of the models implemented are presented. In the last section, some possibilities to further improve the system are presented.

8.1 Main findings

From the analysis conducted with the steady-state model implemented in EES, minor variations were observed in the system COP varying the condenser tube length and diameter and excluding the internal heat recovery unit. These indications are not aligned with the experimental data shown by Zhang et al. [19], in which significant improvements of the system COP were observed in the heating up process modifying the condenser tube length for an air source heat pump water heater. More in details, two tank sizes were considered, i.e. 150 l and 200 l, and the COP showed an inverted U trend varying the condenser length. The COP reached its maximum value respectively for condenser length of 50 m and 70 m. For the smallest tank, the extent of the COP increase was approximately 50% if the tube length was varied from 20 m to 50 m. The differences between these results and the findings from the present study can be due to the different sizes of the tanks and also of the systems compared: Zhang et al. [19] considered a heating load of 3.4 kW while in the present study the heating capacity never exceeds 1.4 kW. Moreover, a different refrigerant is applied in the two cases (R22 instead of R134a) and the condenser is immersed in the tank in the heat pump studied by Zhang et al. [19]. On the other hand, the findings from the current study concerning the condenser length are close to the indications provided by Imbrahim et al. [16], in which again an ASHPWH with immersed condenser working with R22 is studied. The outcomes from this research on the heating up process indicate than a COP improvement of approximately 6% can be achieved by increasing the condenser length from 40 m to 100 m. The depicted trend of the COP enhancement with the condenser length is concave for an outer diameter of 9.9 mm. The same conclusion can be drawn looking at Figure 5.5 for the two cases with and without internal heat exchanger for a condenser tube diameter of 9.95 mm.

For what concerns the reduction of the condenser tube diameter, a considerable beneficial effect on the condensation heat transfer coefficient resulted from the simulations, as shown in Figure 5.2. This enhancement is confirmed in the literature. For example, Yan et al. [77] proved through experimental investigations that the heat transfer coefficient during condensation of R134a averaged over the refrigerant quality was increased by 10% using a pipe diameter of 2 mm instead of 8 mm. A smaller diameter results also in higher pressure drop in the tube, which raises the condensing pressure but at the same time increases the enthalpy difference in the condensing section. There is consequently a trade off between the two contributions, which results in a maximum for the COP as shown in Figure 5.14, if a constant condenser length is maintained. However, as previously mentioned, the magnitude of the COP variations are very limited.
The removal of the internal heat recovery emerged to cause a reduction of the heat transfer in the superheating section of the condenser due to the lower enthalpy at the compressor discharge. However, also in this case, negligible effects were observed on the system COP. The limited effects on the system of the IHEX are aligned with the discussions proposed by Domaski et al. [25]. They stated that this additional heat exchanger can be beneficial in case of poor performances of the system, but it can result in insignificant variations if the system is already characterised by a good COP.

The attractiveness of the studied configurations is increased if the economical point of view is taken into account. For example a system configuration without IHEX, a condenser length of 70 m and an outer tube diameter of 6.95 mm can reduce the expenditures by 20%.

Another possible configuration considered for the condenser was the application of minichannel condenser. A sharp enhancement of the refrigerant side condensing heat transfer coefficient was noted, but the detriment caused by the huge pressure drops was prevailing. However, it was also noticed that disregarding the pressure drop minichannel condensers become really attractive. The studied minichannel geometry, with an outer diameter of 3.4 mm, can lower the cost of the condenser per unit of length by 57%. In the aforementioned study conducted by Imbrahim et al. [16] a numerical comparison between two minichannel condensers and a macrochannel one is assessed. The pressure drops in the heat exchangers are neglected in the mentioned analysis. The minigeometries result in limited COP improvements, around 2%, but they enable a refrigerant charge reduction from 1.4 kg to 0.4 kg and an increase of the compactness of the heat exchanger.

For what concerns the analysis of alternative refrigerants as drop-in replacement for 134a for the forth run of the heating up process, both the effects of the new refrigerants on the system COP and on the volumetric flow rate at the suction of the compressor are considered. First of all it was observed that all the four alternative refrigerants are suitable to replace R134a in the system. For what regards their performances, R600a showed the highest increase of

COP compared to the system working with R134a, but at the same time it was characterised by the greatest increase of volumetric flow rate. This means that this solution is expected to be not worthy from the economical point of view. On the other hand, the system working with R290, despite the slight reduction of the COP, enables a reduction of more then 20 % of the volumetric flow rate.

For what concerns the tank model built in the Dymola environment, a good and satisfactory agreement with experimental results was proved. This good match between predictions and experiments was achieved using a simple one dimensional model. According to Han et al. [54], one dimensional models have difficulties in the prediction of the flow structure inside the tank, especially in case of elaborated tank structure and high flow rate involved. Consequently, after 1990 most of the researches focused on two or three dimensional models. However, these models considerably increase the complexity of the model and the computational efforts required. Han et al. [54] also stated that also with more complex models, the thermal stratification and the mixing within the tank are not easy to be replicated because they are affected by operating conditions which are not possible to be described in the model. In other words, it is difficult to replicate some of the phenomena happening in the real systems. Celador et al. [51] adopted a one dimensional model to simulate the thermal stratification in hot water tanks for the simulation of combined heat and power plants. The authors justified this choice mentioning that, even though two and three dimensional models are more exhaustive, a one dimensional model can be considered a good compromise between the accuracy of the predictions and the time required for computation. The findings from the current study confirm the validity of this statement.
For a better understanding of the real intensity of the mixing inside the hot water tank, the *Instantaneous Profile Method* methodology proposed by Caldwell et al. [78] can be applied. It consists on the measurement of the temperatures at every sensor at two different times ($t-\Delta t$ and t) and on the record of the inlet flow rate during the considered time step. Using as starting value the measurement at time $t-\Delta t$, the temperature at time t can be predicted without taking into account any effect of mixing. The predicted temperature profile and the experimental one can then be compared to detect the extent of the mixing intensity.
The dynamic model was then applied to verify the conclusions deriving from the steady-state simulations and to perform some more investigations. The dynamic simulations confirmed that the three system configurations analysed are characterised by similar performances in terms of COP both during the heating up process and the tapping cycle L. Only the dynamic simulation shown in Figure 6.3 for an ambient temperature of -1°C, showed a detriment for the system in case of removal of the internal heat exchanger. Moreover, the model was used to verify the extent of the COP reduction in case of heating up of the domestic hot water until 60°C. A linear decreasing trend of the system COP was observed for higher stop temperatures of the heating up process. Finally, the variation of the height in the tank in which the sensor controlling the operation of the heat pump is placed does not affect the system COP of the heating up process due to the proximity of the temperature profiles in the tank (Figure 6.2a).

It needs also to be discussed that the small magnitude of the COP variations and the uncertainties of the model presented in Chapter 5.2 make difficult to state the realism of the small COP enhancements or decreases emerging from the investigations. What can be concluded from this work is that the studied modifications of the condenser and the internal heat recovery do not result in noticeable effects on the system COP. Moreover, the thermodynamic analysis conducted are useful to understand what happens in the system when the two previously mentioned components are changed or removed in case of the IHEX.
Anther possible investigation which can be conducted on the condenser consists on evaluating the system performances in case of micro plate condenser, as mentioned in Section 2.1 proposed by Danfoss.

8.2 Main limitations of the models

A general limitation of the steady-state model is represented by the assumption concerning the UA value of the evaporator. In further investigations the correlations for the heat transfer coefficient in the evaporator need to be applied to the model. This would enable the optimization of the area of the evaporator and the possibility to derive some considerations about the fan power. Moreover, a temperature difference of 5 K was assumed in the subcooler for all the runs. This fact is not expected to be replicated in the real behaviour in the system. However, both Figure 5.9 and the good matching between experiments and predictions in the dynamic simulations testify to the low impact of this assumption. Experimental measurements in different parts of the condenser tube can help to detect the real evolution of the temperature difference in the subcooler during the heating up process.
The economical evaluations were based on the prices found in the manufacturer catalogue for a single condenser tube. In reality, in case of stock purchase the expenditures can be decreased affecting the cost savings offered by solutions with smaller diameters. Moreover, the assumed cost of the internal heat recovery unit was not the real one. The expenditure caused by the welding process of the tubes need to be evaluated in further investigations.
For what concerns the analysis on alternative refrigerants, the reliability of the investigation is limited by the assumption of introducing a fake compressor. It was not possible to find in manufacturers catalogues data for real compressors working with the alternative refrigerants considered in this analysis. Consequently, further investigations need to be done trying to get access to these data. This would give the possibility to verify the reliability of the findings from the analysis conducted in this paper.
A limitation of the tank model lays in the correlations used to calculate the heat transfer in the condensing sections and the compressor work. They were derived from the linear interpolations of the results from the four runs implemented in the steady-state model. This limitation does not allow the possibility to extract many thermodynamic considerations from the dynamic model. A more detailed investigation should model also the heat pump in Dymola and synchronize it with the model built for the hot water tank. However, it was chosen to build

the former model in EES due to the better familiarity with its programming language. As a consequence, the values for the average COP reported in Chapters 6 and 7 need to be verified comparing the predicted compressor work with the experimental one. In fact, while the predicted heat transferred through the condenser are expected to be quite realistic due to the good agreements between the temperature profiles, the predictions for the compressor work need an experimental validation. The sensitivity analysis conducted on the compressor work, depicted in Figure 6.5, shows that this parameter is characterised by considerable fluctuations if it is expressed as a function of the temperature in different nodes in the tank. Moreover, another critical parameter which can largely alter the compressor work is the isentropic efficiency of the compressor, as shown in Figure 5.11.

8.3 System improvements

As previously mentioned, there is not so much room for COP enhancement looking at the condenser and at the internal heat recovery unit. An inexpensive and attractive solution to improve the system COP can be represented by the replacement of the expansion valve with a two-phase ejector. It is a device which uses the Venturi effect of a converging-diverging nozzle to transform the pressure energy of the moving fluid into kinetic energy. More in details, the ejector takes advantage of the kinetic energy of the high-pressure refrigerant, which is the motive fluid. This energy is exploited to partially compress the saturated vapour at the evaporator outlet, reducing the pressure lift required to the compressor. This solution would enable a reduction of the thermodynamic losses caused by the throttling process occurring in the expansion device [79]. Moreover, due to the absence of moving parts and the small dimensions, this device can be easily applicable to existing systems. The two-phase ejector is more advantageous in case of high pressure lift in the cycle and consequently many application on transcritical CO_2 cycles can be found in the literature. However, some applications of this device can be found also in refrigeration systems using R134a as working fluid. For example, Chaiwongsa et al. [80] experimentally investigated the performances of a refrigeration cycle applying a two-phase ejector as expansion device. The research focused on verifying the influence of different parameters, such as the diameter of the motive nozzle and the temperatures of the heat sink and heat source, on the system COP and other relevant parameters (the cooling capacity, the compressor ratio). The authors does not give an indication of the COP enhancement caused by the application of the two-phase ejector compared to the original system. For transcritical CO_2 cycles the two-phase ejector can raise the system COP of approximately 20% compared to the system applying an expansion valve [81] [82].

Another possible alternative to the actually used thermostatic expansion valve is the application of an electronic expansion valve. The thermostatic expansion valve is characterised by some limitations. First of all it requires a minimum pressure drop between the condenser and the evaporator. Moreover, it is necessary to maintain a minimum superheating to avoid

hunting. The electronic expansion valve controls the amount of refrigerant flowing in the evaporator applying a pressure and temperature sensor placed at the outlet at the evaporator. The elaboration of the signals is performed by a regulator, which controls the opening of the valve in real time mode [83]. Lazzarin et al. [83] experimentally evaluated the possibility to replace a thermostatic expansion valve with an electric one considering as case study the refrigeration system of a supermarket located in the North of Italy. The system consisted of two different circuits: a low temperature one (evaporation temperature of -34°C and 75 kW of refrigeration capacity) and a medium one (evaporation temperature of -13.5°C and 325 kW of refrigeration capacity). The working fluid was R404A. The electronic expansion valve enabled lower superheating and more steady operation for the system. Noticeable energy savings offered by the installation of the electronic expansion valve resulted from the investigation. In case of medium-temperature circuit, the amount of electricity required throughout all the year was reduced from 719278 kWh to 424746 kWh. For the case with low-temperature circuit, the system working with a thermostatic expansion vale required 397386 kWh, while the one applying the electric expansion valve needed 295250 kWh of electricity during the year.

For what concerns the replacement of the reciprocating compressor actually included in the cycle, Grace et al. [84] verified through experimental tests that a hermetic scroll compressor can be a valid alternative. The authors experimentally analysed the performances of the two compressors in a water-water chiller facility using R404A as working fluid. The results indicated that the scroll compressor was characterised by equal or greater COP and cooling capacities compared to the reciprocating one. The advantage of the scroll compressor was higher for greater condensing temperatures: for a T_c of 35°C the COP was on average 10% higher for the tested 90 minutes.

9 Conclusions

In this study a domestic hot water heat pump was modelled and optimised in terms of COP focusing on the condenser. First of all the heating up process of the domestic hot water in the tank was simulated by a steady state model. Due to the nonlinear trend of the process, it was chosen to focus the initial investigations on the last portion of the water temperature lift because of its poorer COP. Different condenser tube lengths and outer diameters were simulated both for the system inclusive and exclusive of the internal heat recovery unit. Despite the small magnitude of the COP variations, two alternative system configurations were selected: both of them with a condenser outer diameter and length of respectively 6.95 mm and 70 m, one with internal heat recovery unit and the other one without this additional component. The effects on the heat transfer coefficients and on the pressure drops were evaluated. Then, the variations of the system COP were evaluated also for other portions of the heating up process, resulting again in limited variations. Anyway, the outputs from these investigations in terms of compressor work and heating capacity were used to build a dynamic model, in which the heat transfer phenomena and in particular the water recirculation inside the tank were taken into account. The dynamic model was validated comparing the predicted and experimental temperature profiles in the tank for two sets of data. For the existing system configuration, a maximum discrepancy of 14%, with respect to the temperature lift of the water starting from 10°C, was observed between experiments and predictions. For a system configuration characterised by a reduced condenser tube diameter, the highest gap between the considered temperature profiles was lower than 5%, considering the temperature raise of the water starting from an initial temperature of 10°C. In both the cases, a good agreement between predicted and experimental data was confirmed, implying that the built models can be a good solution to replace the more expensive experimental tests. The dynamic simulations confirmed the closeness of the performances between the actual system configuration and the two proposed solutions both during the overall heating up process and the tapping cycle L. Moreover, an average COP reduction of 10% was observed in case of heating up of the domestic hot water until 60°C instead of 52°C. The height in the tank of the temperature sensor performing the on/off control function on the compressor did not influence the system performances due to the proximity of the temperature profiles in the different nodes of the

tank.

The steady-state simulation of the last portion of the heating up process was also used to evaluate the applicability of minichannel condensers and of alternative refrigerants to replace R134a. The minigeometry analysed was characterised by too penalizing pressure drops and not suitable for the existing condenser configuration wrapped around the hot water tank as a single tube. This could be solved by arranging the condenser with more circuits. However, system arrangements aiming to reduce their impact are expected to reverse the judgement on minichannel condensers. The most attractive alternative refrigerant on the existing system configuration from an economical point of view was R290, reducing the compressor volumetric flow rate. On the other hand, the system working with R600a resulted in the highest COP enhancement but it is expected to be unattractive from the economical point of view.

At the end, experimental investigations were performed comparing the actual system configuration with one having a condenser outer tube diameter of 6 mm. It was not possible to test one of the two previously mentioned configurations due to the difficult provision of these condenser tubes. The condenser length was kept unchanged to 54 m during the test and the internal heat recovery unit was included in the cycle. The new configuration was observed to shorten the heating up process by 1.5 hour. The real COP was not measured, but according to the predictions the COP is expected to improve by 2 %. The calculated reduction in terms of expenditure for the condenser tube in terms of material, according to the data found in a manufacturer catalogue, was found to be 34% for the reduced diameter.

To conclude, it can be said that the present study proved that there is not much room for improvement for the system COP of the domestic hot water heat pump focusing on the actual condenser arrangement and the internal heat recovery unit. Further investigations can evaluate possible improvements or replacements for the expansion valve, the rotary compressor or the evaporator, or can apply a micro plate heat exchanger as condenser.

Bibliography

[1] Eurostat, 2013. URL http://ec.europa.eu/eurostat/tgm/table.do?tab=table&init=1&language=en&pcode=t2020_rk200&plugin=1.

[2] Abel S. Vieira, Rodney A. Stewart, and Cara D. Beal. Air source heat pump water heaters in residential buildings in australia: identification of key performance parameters. *Energy and Buildings*, 91:148–162, 2015.

[3] John J. Conti, Paul D. Holtberg, Joseph A. Beamon, A. Micheal Schaala, Glen E. Sweetnam, and Andy S. Kydes. Annual energy outlook 2009 with projections to 2030. Technical Report -, Energy Information Administration, Washington, DC, 20585, 2009.

[4] Lukas G. Swan and V. Ismet Ugursal. Modeling of end-use energy consumption in the residential sector: A review of modeling techniques. *Renewable and Sustainable Energy Reviews*, 13:1819–1835, 2009.

[5] Jihoon Min, Zeke Hausfather, and Qi Feng Lin. A high-resolution statistical model of residential energy end use characteristics for the united states. *Journal of Industrial Ecology*, 14(5):791–807, 2010.

[6] Luis Pérez-Lombarda, José Ortiz, and Christine Pout. A review on buildings energy consumption information. *Energy and Buildings*, 40:394–398, 2007.

[7] H. Singh, A. Muetze, and P.C. Eames. Factors influencing the uptake of heat pump technology by the uk domestic sector. *Renewable Energy*, 35:873–878, 2010.

[8] Emer Dennehy and Martin Howley. Energy in the residential sector. Technical Report -, Sustainable energy authority of Ireland, Wilton Place, Bublin 2, Ireland, 2013.

[9] John J. Contia, Paul D. Holtberg, James R. Diefenderfer, Sam A. Napolitano, A. Michael Schaal, James T. Turnure, and Lynn D. Westfall. Annual energy outlook 2014 with projections to 2040. Technical Report -, Energy Information Administration, Washington, DC, 20585, 2014.

[10] Center for climate and energy solutions, 2009. URL http://www.c2es.org/technology/factsheet/ResidentialBuildingEnd-Use#5.

[11] Water heating. URL https://www.dmme.virginia.gov/DE/LinkDocuments/HandbookWaterHeating.pdf.

[12] Danish Energy Agency. Guide to ecodesign and energy labelling requirements for electric heat pump water heaters and electric conventional water heaters. Technical Report -, Danish Energy Agency, Amaliegade 44 DK 1256 Copenhagen K, 2014.

[13] Delta energy & environment, 2015. URL http://www.c2es.org/technology/factsheet/ResidentialBuildingEnd-Use#5.

[14] European Union. Directive 2009/28/ec of the european parliament and of the council of 23 april 2009 on the promotion of the use of energy from renewable sources and amending and subsequently repealing directives 2001/77/ec and 2003/30/ec (text with eea relevance). Technical Report -, Official Journal of the European Union, Plateau du Kirchberg, B.P. 1601, L-2929 Luxembourg, 2009.

[15] Xiaoyu Liu, Siu-Kit Lau, and Haorong Li. Optimization and analysis of a multi-functional heat pump system with air source and gray water source in heating mode. *Energy and Buildings*, 69:1–13, 2013.

[16] Oussama Ibrahim, Farouk Fardoun, Rafic Younes, and Hasna Louahlia-Gualous. Air source heat pump water heater: dynamic modeling, optimal energy managment and mini-tubes condensers. *Energy*, 64:1103–1116, 2013.

[17] *Domestic hot water heat pump – Manual METROAIR AQUA and METROAIR AQUA Sl*. Metro Therm A/S, January 2014.

[18] Alberto Cavallini, Luca Doretti, Marko Matkovic, and Luisa Rossetto. Update on condensation heat transfer and pressure drop inside minichannels. *Heat Transfer Engineering*, 24(4):74–87, 2006.

[19] J. Zhang, R. Z. Wang, and J. Y. Wu. System optimization and experimental research on air source heat pump water heater. *Applied Thermal Engineering*, 27(2007):1029–1035, 2006.

[20] Per Henrik Pedersen. Gwp alternatives to hfcs in refrigeration. Environmental Projekt no. 1425 -, Miljøstyrelsen, Strandgade 29 1401, København K, 2012.

[21] Luis R. Bernardo, Henrik Davidsson, and Björn Karlsson. Retrofitting domestic hot water heaters for solar water heating systems in single-family houses in a cold climate: A theoretical analysis. *Energies*, 5(10):4110–4131, 2012.

[22] Muhammad Asmail Eleiwi. An experimental study on a vapour compression refrigeration cycle by adding internal heat exchanger. *Journal of Eng. Sciences*, 15(4):63–78, 2008.

[23] Gustavo Pottker and Pega Hrnjak. Experimental investigation of the effect of condenser subcooling in r134a and r1234yf air-conditioning system with and without internal heat exchanger. *International Journal of Refrigeration*, 50:104–113, 2015.

[24] W. V. Payne, E. A. Silk, and P. A. Domaski. A water-to-water heat pump using hydrocarbon and hydrofluorocarbon zeotropic mixtures with and without an internal heat exchanger. *United States Department of Commerce*, Gaithersburg, MD 20899, 2000.

[25] P. A. Domaski, D.A. Didion, and J.P. Doyle. Evaluation of suction line-liquid line heat exchange in the refrigeration cycle. *International Refrigeration and Air Conditioning Conference*, Paper 149, 1992.

[26] J.J. Guo, R.Z. Wang J.Y. Wu, and S. Li. Experimental research and operation optimization of an air-source heat pump water heater. *Applied Energy*, 88:4128–4138, 2011.

[27] G.L. Morrison, T. Anderson, and M. Behnia. Seasonal performance rating of heat pump water heaters. *Solar Energy*, 76:147–152, 2004.

[28] Kingspan, 2015. URL http://www.kingspansolar.ie/pdf/Aeromax%20Plus.pdf.

[29] Dimplex, 2015. URL http://www.dimplex.de/fileadmin/dimplex/downloads/produktschrift_syst/en/25-WW_4S_engl.pdf.

[30] Stiebel eltron, 2015. URL http://www.stiebel-eltron-usa.com/accelera.html.

[31] Phnix, 2015. URL http://www.phnixexp.com/.

[32] European Committee for standardization. Ds/en 16147 - heat pumps with electrically driven compressors - testing and requirements for making of domestic hot water units. Standard -, CEN, Avenue Marnix 17, B-1000 Brussels, 2010.

[33] Danfoss, 2015. URL http://www.danfoss.com/.

[34] Shan Kui, Li Shuhong, and Zhang Xiaosong. Water heater compound with ground source heat pump. *Proceedings of ISES World Congress*, Vol. I – Vol. V:2542–2546, 2007.

[35] S. A. Klain EES. *version V9.698-3D*. Dassault Systèmes, University of Wisconsin-Madison, 2014.

[36] DYMOLA. *version 2015 FD01 (32-bit)*. Dassault Systèmes, 78946 Vélizy, Villacoublay Cedex, France, 2015.

[37] Modelon, 2013. URL http://www.modelon.com/products/dymola/.

[38] Eric Granryd et.al. *Refrigeration Engineering*. Royal Institute of Technology, KTH, 2011.

[39] MATLAB. *version 8.4.0 (R2014b)*. The MathWorks Inc., Natick, Massachusetts, 2014.

[40] F. W. Dittus and L. M. K. Boelter. Heat transfer in automobile radiators of the tubular type. *International Communications in Heat and Mass Transfer*, 12(1):3–22, 1985.

[41] Frank P. Incropera, David P. DeWitt, Theodore L. Bergman, and Adrienne S. Lavine. *Fundamentals of Heat and Mass Transfer*. Wiley, March 10,2006.

[42] Søren Knudsen. *Investigation and optimisation of heat storage tanks for low-flow SDHW systems*. PhD thesis, Technical University of Denmark, 2004.

[43] Marko Matkovic, Alberto Cavallini, Davide Del Col, and Luisa Rossetto. Experimental study on condensation heat transfer inside a single circular minichannel. *International Journal of Heat and Mass Transfer*, 52:2311–2323, 2009.

[44] Alberto Cavallini, Davide Del Col, Luca Doretti, Marko Markovic, Luisa Rossetto, Claudio Zilio, and Giuseppe Censi. Condensation in horizontal smooth tubes: a new heat transfer model for heat exchanger design. *Heat Transfer Engineering*, 27(8):31–38, 2006.

[45] M. M. Shah. A general correlation for heat transfer during film condensation inside pipes. *International Journal of Heat and Mass Transfer*, 22(-):547–556, 1979.

[46] M.B. Ould Didi, N. Kattan, and J.R. Thome. Prediction of two-phase pressure gradients of refrigerants in horizontal tubes. *International Journal of Refrgieration*, 25(-):935–947, 2002.

[47] A. Cavallini, L. Rossetto, M. Matkovic, and D Del Col. A model for frictional pressure drop during vapour–liquid flow in minichannels. *International Conference Thermophysical Properties and Transfer Processes of Refrigerants, 31 August–2 September, Vicenza, Italy*, -(-):71–78, 2005.

[48] A. Cavallini, D. Del Col, M. Matkovic, and L. Rossetto. Frictional pressure drop during vapour–liquid flow in minichannels: Modelling and experimental evaluation. *International Journal of Heat and Fluid Flow*, 30(-):131–139, 2009.

[49] Cynthia Ann Cruickshank. *Evaluation of a stratified multi-tank thermal storage for solar heating applications*. PhD thesis, Queen's University, Kingston, Ontario, Canada, 2009.

[50] Newton B. J. *Modelling of Solar Storage Tanks*. PhD thesis, M.Sc. Thesis, University of Wiscons in-Madison, 1995.

[51] A. Campos Celador, M. Odriozola, and J.M. Sala. Implications of the modelling of stratified hot water storage tanks in the simulation of chp plants. *Energy Conversion and Management*, 52(-):3018–3026, 2011.

[52] Shyu R.J., Lin J.Y., and Fan L.J. Thermal analysis of stratified tanks. *ASME, Solar Energy Engineering*, 22(-):55–61, 1989.

[53] Vijay Dwivedi. *Thermal Modelling and Control of Domestic Hot Wate Tank*. PhD thesis, M.Sc. Thesis, University of Strathclyde, 2009.

[54] Y.M. Han, R.Z. Wang, and Y.J. Dai. Thermal stratification within the water tank. *Renewable and Sustainable Energy Reviews*, 13:1014–1026, 2009.

[55] Adriàn Mota-Babiloni, Joaquìn Navarro-Esbrì, Angel Barragàn, Francisco Molè, and Bernardo Peris. Theoretical comparison of low gwp alternatives for different refrigeration configurations taking r404a as baseline. *International Journal of Refrigerantion*, 44:81–90, 2014.

[56] X-rates, 2015. URL http://www.x-rates.com/calculator/?from=AUD&to=EUR&amount=1.

[57] Rapid fab, 2015. URL http://www.fab.net.au/rapidfab.htm.

[58] C. Aprea, M. Ascani, and F. De Rossi. A criterion for predicting the possible advantage of adopting a suction/liquid heat exchanger in refrigeration system. *Applied Thermal Engineering*, 19:329–336, 1998.

[59] Doucette industries inc, 2015. URL http://doucetteindustries.com/.

[60] Yemada Taitel and A. E. Dukler. A model for predicting flow regime transitions in horizontal and near horizontal gas-liquid flow. *AlChE Journal*, 22(1):47–55, 1976.

[61] World weather online, 2015. URL http://www.worldweatheronline.com/.

[62] S. G. Kandlikar and W. J. Grande. Evolution of microchannel flow passages - thermohydraulic performance and fabrication technology. *Heat Transfer End*, 24(1):3–17, 2003.

[63] Sanhua, 2013. URL https://www.sanhuaeurope.com/wo/en/.

[64] Richard A. Perkins and Marcia L. Huber. Measurement and correlation of the thermal conductivity of 2,3,3,3-tetrafluoroprop-1-ene (r1234yf) and trans-1,3,3,3-tetrafluoropropene (r1234ze(e)). *J. Chem. Eng. Data*, 56(12):4868–4874, 2011.

[65] Sho Fukuda, Chieko Kondou, Nobuo Takata, and Shigeru Koyama. Low gwp refrigerants r1234ze(e) and r1234ze(z) for high temperature heat pumps. *International Journal of Refrigeration*, 40(-):161–173, 2014.

[66] Thomas J. Leck. Evaluation of hfo-1234yf as a potential replacement for r-134a in refrigeration applications. *3rd IIR Conference on Thermophysical Properties and Transfer Process of Refrigerants, Boulder, CO*, 2009.

[67] D. Del Col, D. Torresin, and A. Cavallini. Heat transfer and pressure drop during condensation of the low gwp refrigerant r1234yf. *International Journal of Refrigeration*, 33: 1307–1318, 2010.

[68] J. Navarro-Esbrì, J.M. Mendoza-Miranda, A. Mota-Babiloni, A. Barragàn-Cervera, and J.M. Belman-Flores. Experimental analysis of r1234yf as a drop-in replacement for r134a in a vapor compression system. *International Journal of Refrigeration*, 36:870–880, 2013.

[69] Mahmood Mastani Joybari, Mohammad Sadegh Hatamipour, Amir Rahimi, and Fatemeh Ghadiri Modarres. Exergy analysis and optimization of r600a as a replacement of r134a in a domestic refrigerator system. *International Journal of Refrigeration*, 36: 1233–1242, 2013.

[70] E. Navarro, I.O. Martìnez-Galvan, J. Nohales, and J. Gonzàlvez-Macia. Comparative experimental study of an open piston compressor working with r-1234yf, r-134a and r-290. *International Journal of Refrigeration*, 36:768–775, 2013.

[71] Danfoss. Danfoss compressors - practical application of refrigerant r290 propane in small hermetic systems, 2014.

[72] Mariam Jarahnejad. *New Low GWP Synthetic Refrigerants*. PhD thesis, M.Sc. Thesis, KTH School of Industrial Engineering and Management - Division of Applied Thermodynamics and Refrigeration SE-100 44 STOCKHOLM, 2012.

[73] William F. Walter et al. Designation and safety classification of refrigerants. Standard 34-2007, ANSI/ASHRAE, 1791 Tullie Circle NE, Atlanta, GA 30329, Approved by the ASHRAE Standards Committee on January 23, 2010; by the ASHRAE Board of Directors on January 27, 2010; and by the American National Standards Institute on February 24, 2010.

[74] Fu L., Ding G., and Zhang C. Dynamic simulation of air-to-water dual-mode heat pump with screw compressor. *Appl Therm Eng.*, 88(11):4128–4138, 2003.

[75] Armstrong M. M., Ruest K., and Swinton M. C. Assessing the impact of cold climate on basement temperatures. Report B-6042.2, Canadian Centre for Housing Technology, M20, Montreal Road, Ottawa, Ontario, Canada K1A OR6, 2011.

[76] A.o. smith, 2015. URL http://www.hotwater.com/lit/spec/com_elec/aosze15000.pdf.

[77] Yi-Yie Yan and Tsing-Fa Lin. Condensation heat transfer and pressure drop of refrigerant r134a in a small pipe. *International Journal of Heat and Mass Transfer*, 42:697–708, 1999.

[78] Jeffrey S. Caldwell and William P. Bahnfleth. Identification of mixing effects in stratified chilled-water storage tanks by analysis of time series temperature data. *Inclusion in Ashrae transaction 1998*, 104, 1998.

[79] Kornhauser A. A. The use of an ejector as a refrigerant expander. *International Refrigeration and Air Conditioning Conference*, Paper 82, 1990.

[80] Praitoon Chaiwongsa and Somchai Wongwises. Experimental study on r-134a refrigeration system using a twp-phase ejector as an expansion device. *Applied Thermal Engineering*, 28:467–477, 2008.

[81] H. T. Ozaki and H. Takeuchi. Regeration of expansion energy by ejector in co_2 cycle. *Proceedings of the 6th IIR-Gustav Lorentzen Conference on Natural Working Fluids, Glasgow*, 2004.

[82] G. E. D. Li. Transcritical co_2 refrigeration cycle with ejector-expansion device. *Int. J. Refr.*, 28:766–773, 2005.

[83] Renato Lazzarin, Daniele Nardotto, and Marco Noro. Electronic expansion valves vs. thermal expansion valves. *ASHRAE Journal*, pages 34–38, 2009.

[84] I. Grace, D. Datta, and S. A. Tassou. Comparison of hermetic scroll and reciprocating compressor operating under varying refrigerant charge and load. *International Compressor Engineering Conference*, Paper 1518, 2002.

[85] A. Cavallini, G. Censi, D. Del Col, L. Rossetto, L. Doretti, and G.A. Longo. Experimental investigation on condensation heat transfer and pressure drop of new hfc refrigerants (r134a, r125, r32, r410a, r236ea) in a horizontal tube. *Int. J. Refrigeration*, 24(-):73–87, 2001.

[86] Paleev I. I. and Filippovich B. S. Phenomena of liquid transfer in two-phase dispersed annular flow. *International Journal of Heat and Mass Transfer*, 9(10):1089–1093, 1966.

A $\dot{m}_r$ and compressor η_{is}

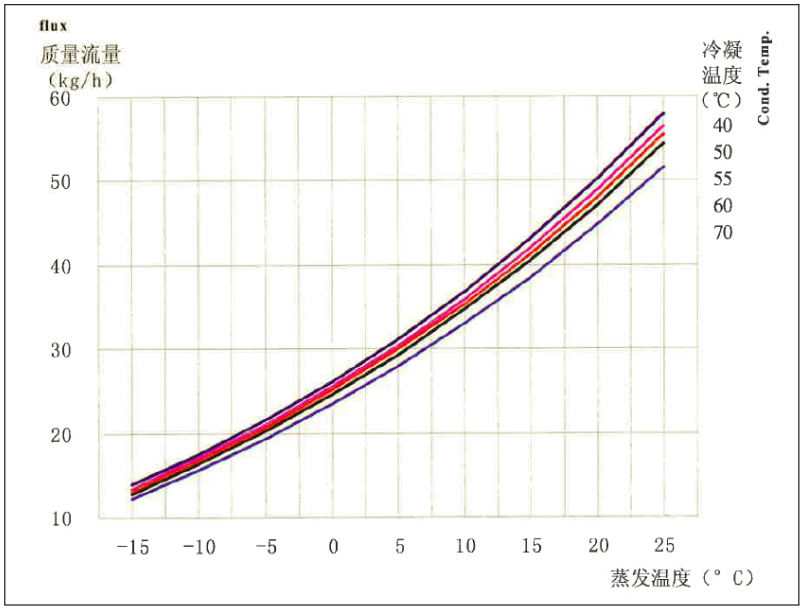

Figure A.1: Refrigerant mass flow rate as a function of condensing and evaporating temperatures [17].

For the calculation of the compressor isentropic efficiency and refrigerant mass flow rates, it was required to build up a simple EES model in which the test conditions and the points extrapolated from Figures A.1 and A.2 were included. The test conditions are specified in Table A.1.

The values of the refrigerant mass flow rates and the heating capacity were approximately estimated from Figures A.1 and A.2 for several combinations of evaporating and condensing temperatures. The four aforementioned values were given as input in the EES code, together with the test conditions. It was then possible to calculate the enthalpy and the entropy of the refrigerant at the suction of the compressor. First the expression for the refrigerant mass flow rate was derived from Figure A.1. Then it was applied for the computation of the isentropic

efficiency: the isentropic compression was compared with the compression process required to meet the heating capacity given as input. In this way it was possible to detect the values of the isentropic efficiency as a function different condensing and evaporating temperatures. All these values for the refrigerant mass flow rate and the compressor isentropic efficiency were introduced in Matlab with the goal to create the interpolating function presented in the main body of the report.
The constants z_i and o_i required respectively in Equations 3.4 and 3.5 to calculate the isentropic efficiency of the compressor and the refrigerant mass flow rate are presented in Tables A.2 and A.3.

Table A.1: Test conditions for the compressor

ΔT_{sub} [K]	8.3
ΔT_{sup} [K]	10

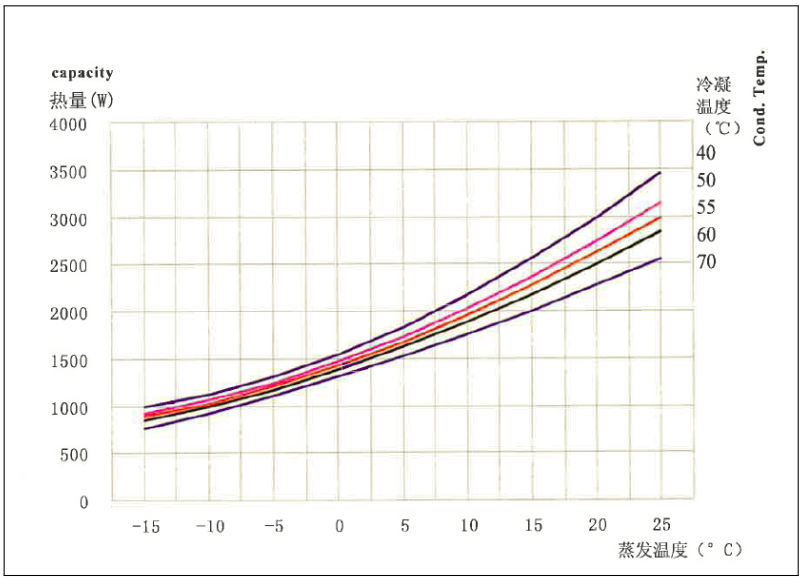

Figure A.2: Heating capacity as a function of condensing and evaporating temperatures [17].

Table A.2: Constants used for calculating the compressor isentropic efficiency

z_1	-517.1
z_2	-0.03627
z_3	5.555
z_4	0.00436
z_5	-0.009884
z_6	-0.01396
z_7	$-4.396 \cdot 10^{-6}$
z_8	$-6.312 \cdot 10^{-7}$
z_9	$1.888 \cdot 10^{-5}$
z_{10}	$8.931 \cdot 10^{-6}$

Table A.3: Constants used for calculating the refrigerant mass flow rate

o_1	0.0546
o_2	0.0004367
o_3	-0.001089
o_4	$-3.457 \cdot 10^{-7}$
o_5	$-8.947 \cdot 10^{-7}$
o_6	$3.004 \cdot 10^{-6}$

B Correlations

In this Appendix a detailed explanation of the correlations implemented in the model for the heat transfer coefficients and the pressure drop is provided. As explained in Chapter 3, it is necessary to distinguish between the correlations applied for macrochannels and the ones used for microchannels.

B.1 Macrochannels

B.1.1 Heat transfer coefficient

For the calculation of the heat transfer coefficient refrigerant side in the condensing section it was chosen to apply the Shah's correlation [45]. In the following, the considerations presented in the original paper will be repeated to provide an understanding about the way in which the correlation was developed.
Through the analysis of various data derived from horizontal, vertical downflow and upflow orientations, it was observed that Equation B.1 is valid in absence of bubble nucleation and if the tube surface is kept wetted by the liquid.

$$\Psi = \frac{1.8}{Co^{0.8}} \tag{B.1}$$

where Ψ and Co are:

$$\Psi = \frac{\alpha_{TP}}{\alpha_1} \tag{B.2}$$

$$Co = \left(\frac{1}{x} - 1\right)^{0.8} \left(\frac{\rho_G}{\rho_L}\right)^{0.5} \tag{B.3}$$

In Equations B.2 and B.3, ρ_L and ρ_G stand respectively for the density of liquid and density of water, x is the thermodynamic vapour quality, α_{TP} is the two phase condensing or boiling

heat transfer coefficient, α_1 is the superficial heat transfer coefficient of the liquid phase and it is calculated as:

$$\alpha_1 = \alpha_L(1-x)^{0.8} \tag{B.4}$$

where α_L is the heat transfer coefficient assuming that all the mass is flowing as liquid, calculated applying the Dittus-Boelter equation.
Then, a comparison between the aforementioned equations and experimental data suggested that a slight change of the term Co would be beneficial for the correlation. Consequently a new parameter Z is introduced and defined as in Equation B.5, where p_r is the reduced pressure.

$$Z = \left(\frac{1}{x} - 1\right)^{0.8} p_r^{0.4} \tag{B.5}$$

A further analysis of varied data, proved that Equation B.6 gave the best fit.

$$\Psi = 1 + \frac{3.8}{Z^{0.95}} \tag{B.6}$$

If Equations B.2, B.4 and B.5 are considered, Equation B.6 can be rewritten as:

$$\alpha_{TP} = \alpha_L \left[(1-x)^{0.8} + \frac{3.8x^{0.76}(1-x)^{0.04}}{p_r^{0.38}}\right] \tag{B.7}$$

The original paper also presents a methodology to estimate the mean heat transfer coefficient from Equation B.7. As an approximation, the validity of Equation B.8 can be assumed. In the Equation, α_{TPL} is the local two phase heat transfer coefficient and L is the length of the tube in which the analysed condensation process occurs.

$$\alpha_{TPL} = \frac{1}{L}\int_0^L \alpha_{TPL} dL \tag{B.8}$$

At this point, two assumptions are presented by the author:

- the transport properties of liquid phase and the pressure are subjected to negligible changes along the length of the pipe;
- Equation B.8 gives a quite accurate definition of mean heat transfer coefficient.

Thanks to these two assumptions, the local two phase heat transfer coefficient from L_1 to L_2 can be derived by integrating Equation B.7 as:

$$\alpha_{TPM} = \frac{\alpha_L}{L_2 - L_1}\int_{L_1}^{L_1} \left[(1-x)^{0.8} + \frac{3.8x^{0.76}(1-x)^{0.04}}{p_r^{0.38}}\right] dL \tag{B.9}$$

Assuming that the vapour quality varies linearly with the pipe length, expanding the second term in Equation B.9 applying the binomial theorem and neglecting small terms, it is possible

to rewrite Equation B.9 as:

$$\alpha_{TPM} = \frac{\alpha_L}{(x_2 - x_1)} \left[-\frac{(1-x)^{1.8}}{1.8} + \frac{3.8}{p_r^{0.38}} \left(\frac{x^{1.76}}{1.76} - \frac{0.04x^{2.76}}{2.76} \right) \right]_{x_1}^{x_2} \tag{B.10}$$

If the variation of the vapour quality is from 1 to 0, Equation B.10 becomes:

$$\alpha_{TPM} = \alpha_L \left(0.55 + \frac{2.09}{p_r^{0.38}} \right) \tag{B.11}$$

Equation B.11 was used in the report to calculate the average heat transfer coefficient through the condensing process. Shah observed that if the heat transfer coefficient is calculated at $x = 0.5$ applying Equation B.7, and it is then compared with the result of Equation B.11, the difference amounts only to 5%.

B.1.2 Pressure drop

The frictional pressure gradient in the condensing section for macrogeometries was calculated by applying the Muller-Steinhagen and Heck correlation [46]. In this section, the equations are reported, mainly because they are used to calculate the trends depicted in Figure 5.29b. In the following equations, the subscript g indicates that all the mass is assumed to flow as vapour, while the subscript l indicates that all the refrigerant is hypothesized to be flowing as liquid.

$$f_g = \frac{0.079}{Re_g^{0.25}} \tag{B.12}$$

$$f_l = \frac{0.079}{Re_l^{0.25}} \tag{B.13}$$

$$\left(\frac{dp}{dz} \right)_g = f_l \frac{2\dot{m}_r^2}{D_{in,c}\rho_g} \tag{B.14}$$

$$\left(\frac{dp}{dz} \right)_l = f_l \frac{2\dot{m}_r^2}{D_{in,c}\rho_l} \tag{B.15}$$

$$\left(\frac{dp}{dz} \right)_{frictional} = \left\{ \left(\frac{dp}{dz} \right)_l + 2 \left[\left(\frac{dp}{dz} \right)_g - \left(\frac{dp}{dz} \right)_l \right] x \right\} (1-x)^{1/3} + \left(\frac{dp}{dz} \right)_g x^3 \tag{B.16}$$

B.2 Minichannels

B.2.1 Heat transfer coefficient

For the calculation of the heat transfer coefficient in the condensing section in case of minichannels, it was chosen to apply the heat transfer model developed by Cavallini et al. in [44]. Also in this case, a more detailed description of the model is presented following the considerations of the original article.
The moving engine for the development of this model, is the observation of the parameters which affect the heat transfer coefficient in a horizontal pipe. The saturation temperature, the mass velocity, the vapour quality and the pipe geometry show an influence on the heat transfer coefficient. On the other hand, its dependence on the temperature difference ΔT was not always verified, but it occurs if gravity is the dominant force. Consequently, the authors distinguish two flow regimes: a ΔT-dependent one and a ΔT-independent one. This requires an unique transition criterion. The validation of the model, performed considering experimental data, suggests that Equation B.17 well represents the transition line, expressing the gas velocity J_G (or the transition dimensionless gas velocity J_G^T) as a function of the Martinelli's parameter X_{tt}.

$$J_G^T = \left\{ \left[\frac{7.5}{4.3X_{tt}^{1.111}+1} \right]^{-3} + C_T^{-3} \right\}^{-1/3} \tag{B.17}$$

where $C_T = 1.6$ for hydrocarbons and $C_T = 2.6$ for other refrigerant. Due to the fact that R134a is a HFC refrigerant, a value of 2.6 was used for C_T.
For the development of the equations for the heat transfer model, data sets from Cavallini et al.[85] were used. For the ΔT-independent flow regime, occurring when $J_G > J_G^T$, a two-phase multiplier correcting the liquid phase heat transfer coefficient is considered as shown in Equation B.18.

$$\alpha_A = \alpha_{LO}\left[1 + 1.128x^{0.8170}\left(\frac{\rho_L}{\rho_G}\right)^{0.3685}\left(\frac{\mu_L}{\mu_G}\right)^{0.2363}\left(1-\frac{\mu_L}{\mu_G}\right)^{2.144} Pr_L^{-0.100}\right] \tag{B.18}$$

For the ΔT-dependent flow regime, occurring when $J_G < J_G^T$, the heat transfer coefficient, expressed by Equation B.19, is related to α_A and to a fully-stratified flow heat transfer coefficient α_{STRAT}.

$$\alpha_D = \left[\alpha_A\left(\frac{J_G^T}{J_G}\right)^{0.8} - \alpha_{STRAT}\right]\left(\frac{J_G}{J_G^T}\right) + \alpha_{STRAT} \tag{B.19}$$

$$\alpha_{LO} = \frac{0.023 Re_{LO}^{0.8} Pr_L^{0.4} k_L}{D} \tag{B.20}$$

$$\alpha_{STRAT} = 0.725\left\{1+0.741\left[\frac{(1-x)}{x}\right]^{0.3321}\right\}^{-1}\left[\frac{k_L^3\rho_L(\rho_L-\rho_G)gh_{LG}}{\mu_L D\Delta T}\right]^{0.25}+(1-x^{0.087})\alpha_{LO} \quad \text{(B.21)}$$

where h_{LG} corresponds to the latent heat.
In Chapter 3, in the main body of the report, it was decided to mention only Equation B.18 due to the fact that only ΔT-dependent flow regime was observed in this study. The authors also state that all the flow regimes typical of the process of condensation are included in the model:

- *Annular flow* is contained in Equation B.18.
- *Stratified-wavy flow* and *Stratified-smooth flow* are both covered by Equation B.19. The transition between wavy to smooth stratified flow is represented in the linear interpolation comprised in Equation B.19 and when the smooth flow occurs, the T-dependent component is the prevailing one.
- *Slug flow* is represented by both Equations B.18 and B.19. Due to the ΔT-independent nature, the transition line described by Equation B.17 is conceived to be inclusive of a weak effect of T in Equation B.19 when the development of slug flow occurs.

B.2.2 Pressure drop

For what concerns the estimation of the frictional pressure drop in minichannels, the model derived through the observation of experimental data and described by Cavallini et al. [47] was considered. It is presented in the following.
The frictional pressure gradient can be calculated through Equation B.22 for $J_G > 2.5$.

$$\left(\frac{dp}{dz}\right) = \frac{\Phi_{LO}^2 2 f_{LO} G^2}{D_h \rho_L} \quad \text{(B.22)}$$

where the friction factor f_{LO} is referred to surfaces with negligible surface roughness and is expressed as shown in Equation B.23 for any Re_{LO}.

$$f_{LO} = 0.046 Re_{LO}^{-0.2} = 0.046\left(\frac{GD_{hydraulic}}{\mu_L}\right)^{-0.2} \quad \text{(B.23)}$$

The others parameters included in Equation B.22 can be evaluated applying the following equations.

$$\Phi_{LO}^2 = Z + 3.595 FH(1-E)^W \quad \text{(B.24)}$$

$$W = 1.398 p_R \quad \text{(B.25)}$$

$$Z = (1-x)^2 + x^2 \frac{\rho_L}{\rho_G} \left(\frac{\mu_G}{\mu_L}\right)^{0.2} \tag{B.26}$$

$$F = x^{0.9525}(1-x)^{0.414} \tag{B.27}$$

$$H = \left(\frac{\rho_L}{\rho_G}\right)^{1.132} \left(\frac{\mu_G}{\mu_L}\right)^{0.44} \left(1 - \frac{\mu_G}{\mu_L}\right)^{3.542} \tag{B.28}$$

The entrained liquid fraction E needs to be calculated using Equation B.29 as presented by Paleev and Filippovich [86].

$$E = 0.015 + 0.44 log \left[\left(\frac{\rho_{GC}}{\rho_L}\right)\left(\frac{\mu j_g}{\sigma}\right)^2 10^4\right] \tag{B.29}$$

$$if\ E \geq 0.95 \qquad E = 0.95 \tag{B.30}$$

$$if\ E \leq 0 \qquad E = 0 \tag{B.31}$$

where j_G is the superficial gas velocity, σ is the surface tension and ρ_{GC} is the homogeneous gas core density, calculated as:

$$\rho_{GC} = \left(\frac{x + (1-x)E}{\frac{x}{\rho_G} + \frac{(1-x)E}{x}}\right) \tag{B.32}$$

which in case of $\rho_L >> \rho_G$ can be simplified to:

$$\rho_{GC} \approx \rho_G \left(1 + \frac{(1-x)E}{x}\right) \tag{B.33}$$

The model was also extended for $J_G < 2.5$, but this extension is not reported in this report because only values of J_G greater than 2.5 were observed.

C Correlations for the dynamic simulations

As mentioned in Chapter 6, the heat transferred through each section of the condenser to the hot water tank was implemented in the tank model deriving some correlations from the steady state simulations. More in details, some correlations relating the heat transferred in each section of the condenser with the corresponding average water temperature of each section were extrapolated. Three system configurations were considered:

- *Case 1*: condenser diameter 9.95 mm, condenser length 54 m , with IHEX.
- *Case 2*: condenser diameter 6.95 mm, condenser length 70 m , with IHEX.
- *Case 3*: condenser diameter 6.95 mm, condenser length 70 m , without IHEX.

The correlation for the heat transferred in the desuperheating, condensing and sucooling sections for three aforementioned geometries are depicted in Figures C.1, C.2, C.3, C.4, C.5, C.6, C.7, C.8 and C.9 . The figures show the four points resulting from the steady state simulations, the linear interpolation adopted through Excel and the corresponding equation. The temperatures are expressed in K due to the fact they are expressed in K in Dymola and consequently the correlations required this unit of measure.

Moreover, as mentioned in Chapter 6, also the compressor work for the three system configurations was introduced in the model by considering some correlations. It was correlated with the average water temperature in the condenser as shown in Figures C.10, C.11 and C.12.

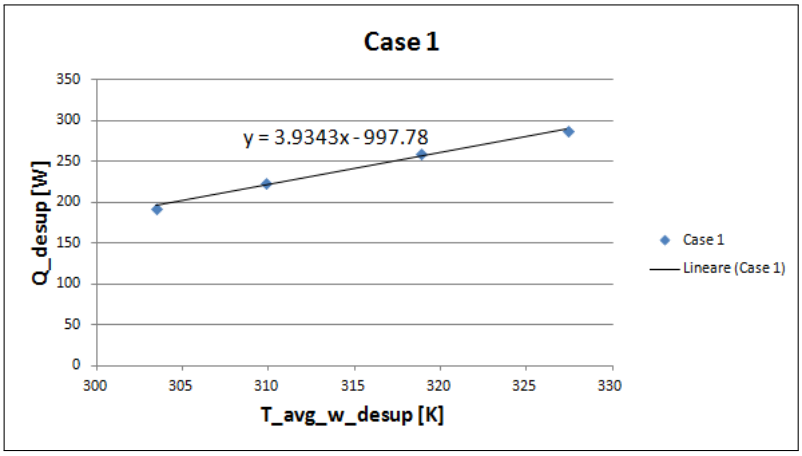

Figure C.1: Correlation for the heat transfer in the desuperheating section for Case 1.

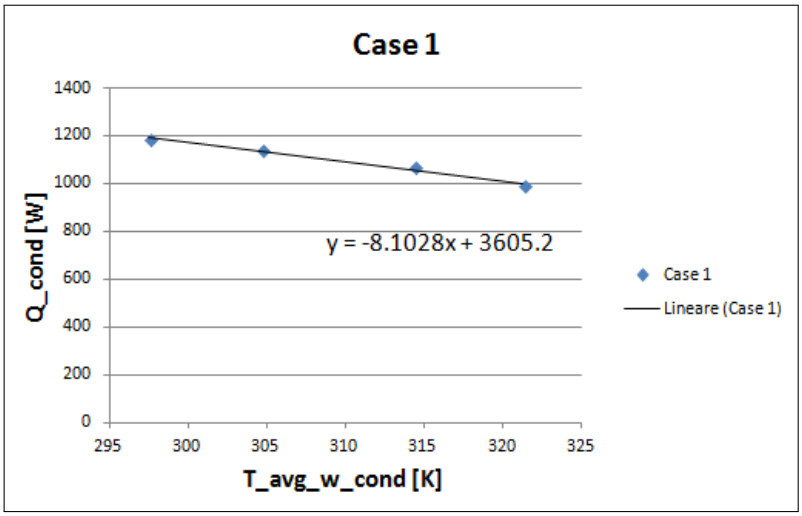

Figure C.2: Correlation for the heat transfer in the condensing section for Case 1.

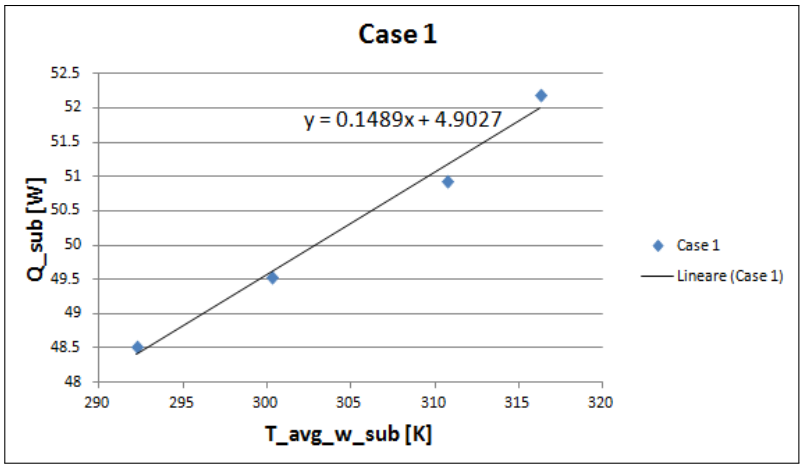

Figure C.3: Correlation for the heat transfer in the subcooling section for Case 1.

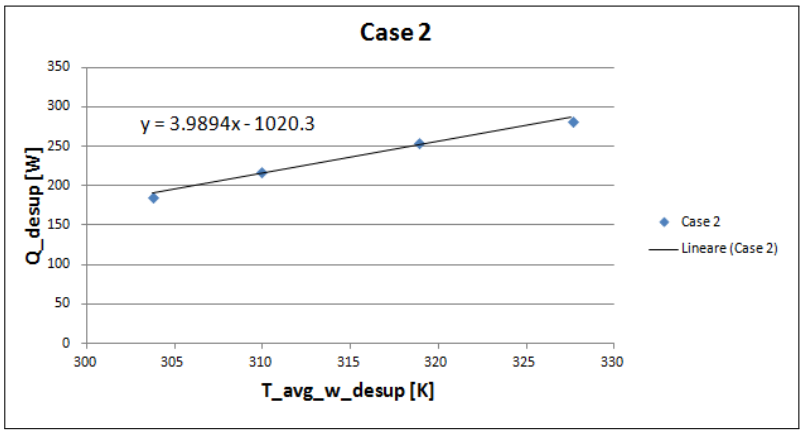

Figure C.4: Correlation for the heat transfer in the desuperheating section for Case 2.

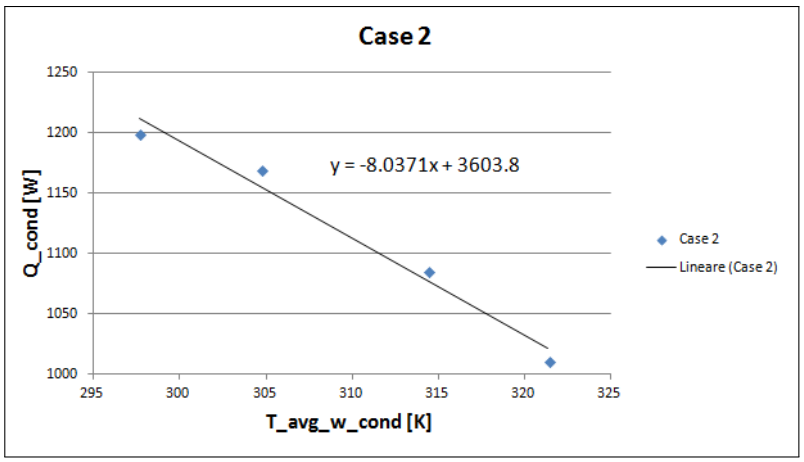

Figure C.5: Correlation for the heat transfer in the condensing section for Case 2.

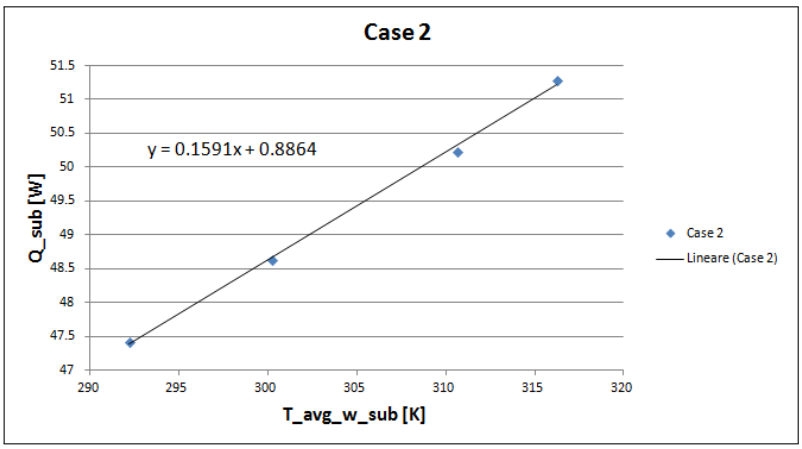

Figure C.6: Correlation for the heat transfer in the subcooling section for Case 2.

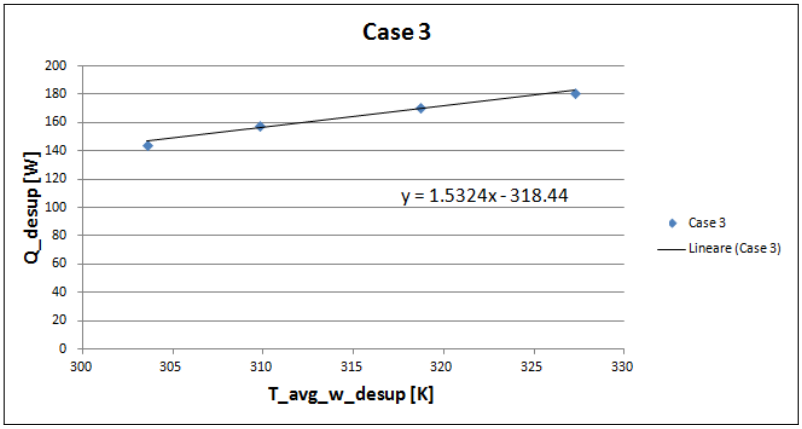

Figure C.7: Correlation for the heat transfer in the desuperheating section for Case 3.

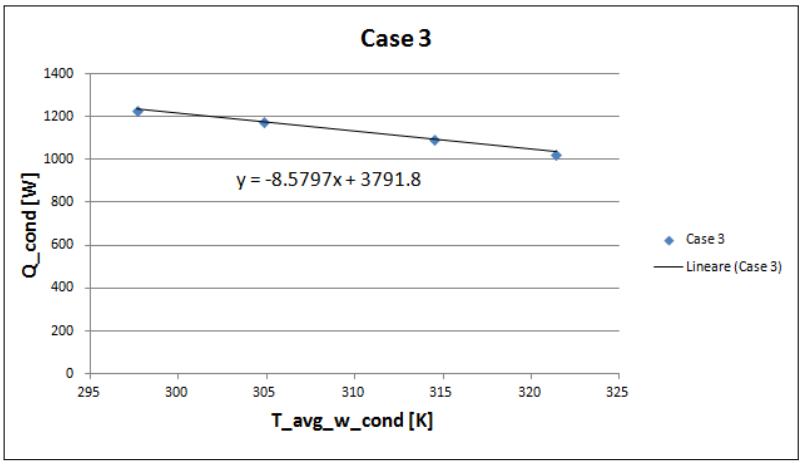

Figure C.8: Correlation for the heat transfer in the condensing section for Case 3.

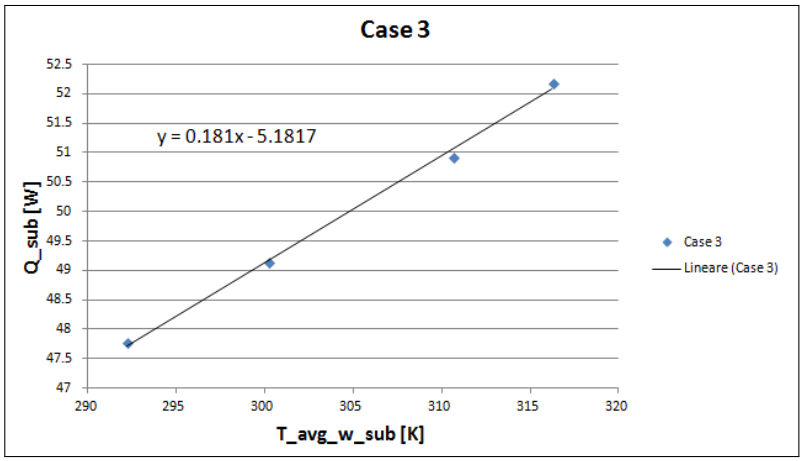

Figure C.9: Correlation for the heat transfer in the subcooling section for Case 3.

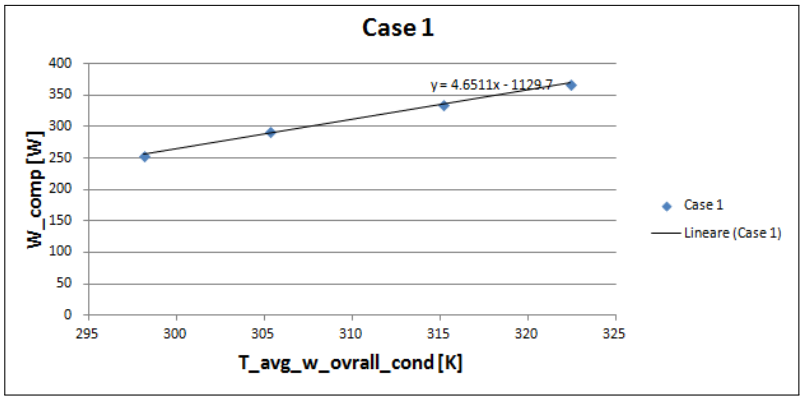

Figure C.10: Correlation for the compressor work for Case 1.

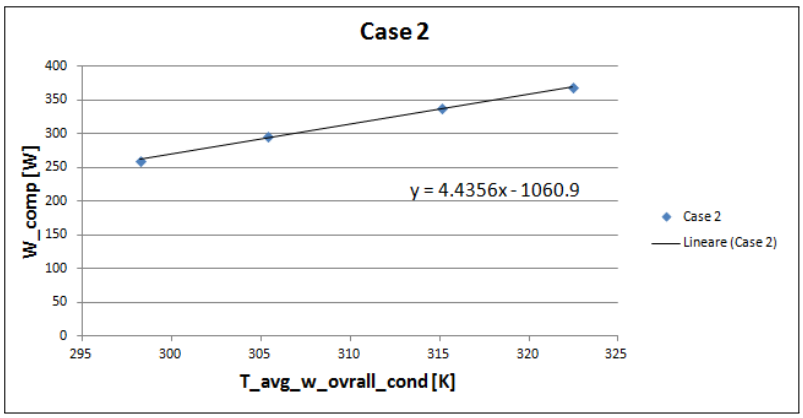

Figure C.11: Correlation for the compressor work for Case 2.

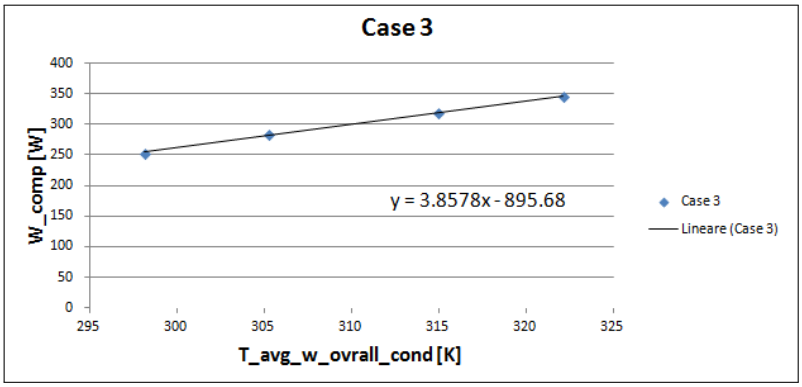

Figure C.12: Correlation for the compressor work for Case 3.

D Variation of the water recirculation

In this chapter some other temperature distributions resulting from the tank model varying the extent of water recirculation (r) are presented. In Figure 6.1 of Chapter 6 it was observed than a nil water recirculation in the tank causes an excessive thermal stratification of the hot water in the tank. Considerable variations in the temperature profiles are shown even for very low value of the amount of water recirculating. Figure D.1 depicts the temperature distributions in the 20 nodes of the tank for r equals to 0.5 %/s. The temperature across the condenser wrapped around the tank are highlighted with yellow, while the temperature in the top layer of the tank is highlighted with blue. In the figure the heat loss to the ambient was set to zero. A comparison between Figures D.1 and 6.1 highlights the considerable extent of the mixing between the nodes even for limited values of water recirculating. It can already be observed that the temperatures in layers 18-19 and 20 are considerably lower than the ones in the rest of tank, as largely explained in Chapter 6. Moreover, the temperature in node 17 is the warmest as it again explained in Chapter 6.

Additionally, in the main body of the report was explained that the inclusion in the model of the heat loss with the ambient causes a more concave trend of the temperature profiles. This fact is evident comparing Figure D.2 with Figure 6.2a. In both of them the same amount of water recirculation is considered (r=10 %/s), but the former is characterised by nil heat losses with the ambient while the latter considers the heat loss ($U_{amb} = 7W/m^2K$). The concave trend caused by the heat loss can be explained with the fact that they are proportional to the temperature difference between the water inside the tank and the ambient temperature. The latter was set to 20°C as specified in Standard [32], while the former varies during the heating up process. For water temperatures lower than 20°C the heat loss represents a "gain" for the system due to the positive contribution of the term $U_{amb,i}A_{s,i}(T_{amb} - T_i)$ in Equation 3.28. This justifies the sharper trend of the temperature profiles for low water temperatures in the tank. On the other hand, for water temperature higher than 20°C the heat loss to the ambient becomes an actual loss for the system, reducing the slope of the temperature profiles for high water temperatures.

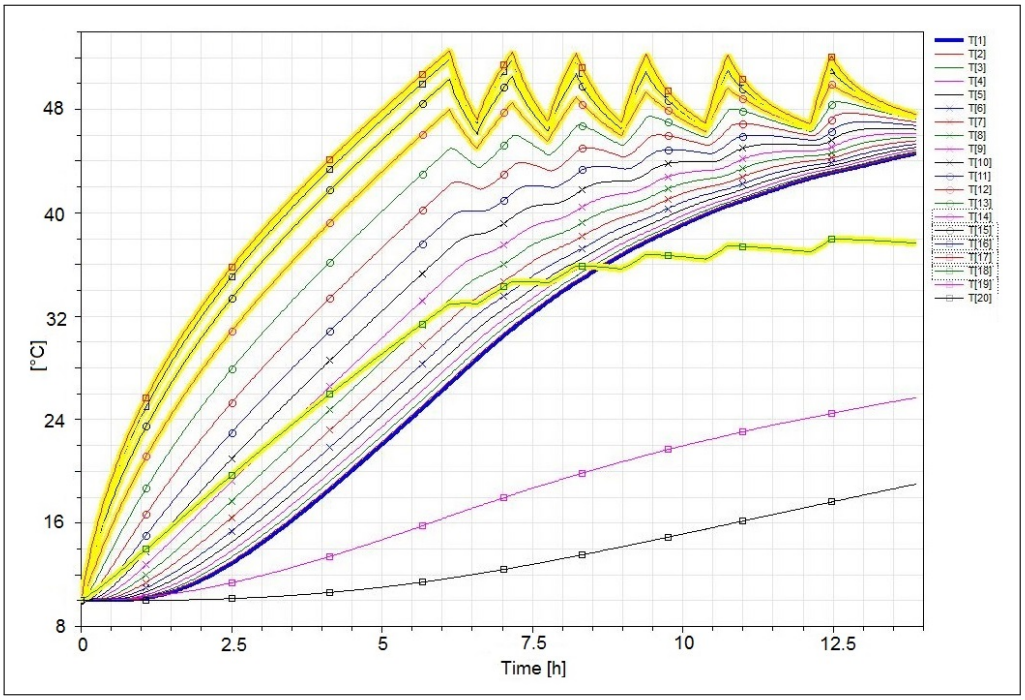

Figure D.1: Temperature distribution in the nodes of the tank in case of $r = 0.5\%/s$ and $U_{amb} = 0\ W/m^2K$.

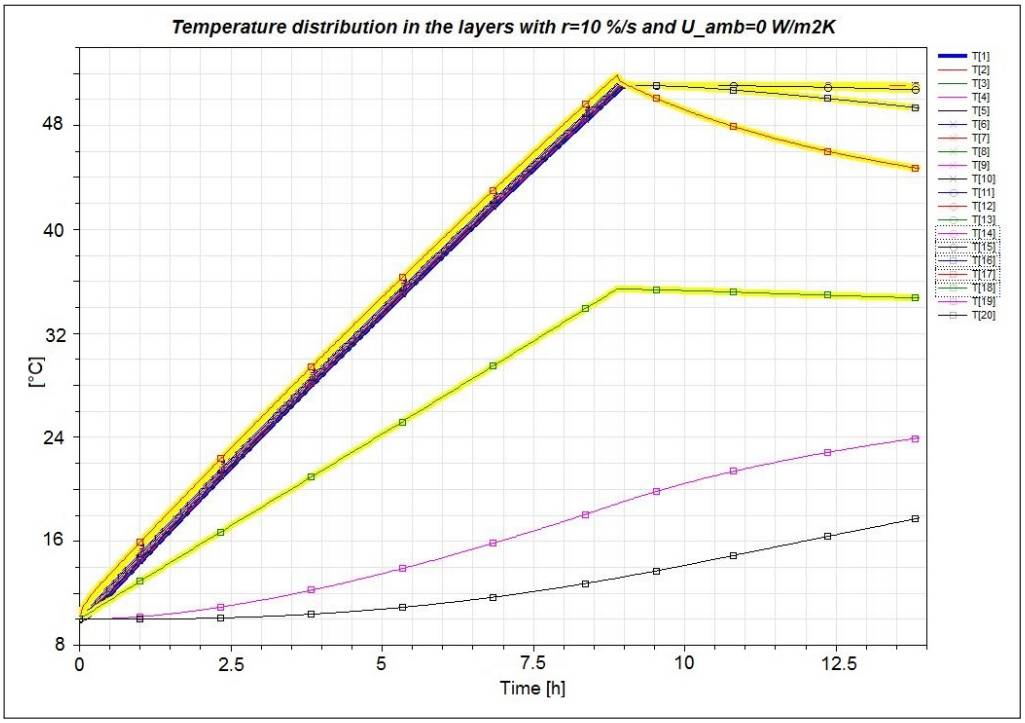

Figure D.2: Temperature distribution in the nodes of the tank in case of $r = 10\%/s$ and $U_{amb} = 0\ W/m^2K$.

E Heating up process with $T_{amb} = -1$°C

In this chapter a graphical representation of some results concerning the heating up process with $T_{amb} = -1$°C for the three system configurations considered are presented. A brief explanation of these results was provided in Section 6.2. Table 6.2 shows the COP_{avg} for the three considered cases. Case 1 shows the highest COP_{avg} and the increase compared to Case 3, i.e. 2.3%, was a surprising result. The reason for this discrepancy must be found in the different heat transferred in the desuperheating section, caused by the presence of the heat recovery unit in Case 1, which affect the overall heat transfer in the condenser ($Q_{tot-cond}$) as depicted in Figure E.1. The dotted lines depict the heat transfer in the desuperheating section, while the continuous ones show the overall heat released to the water in the condenser. More in details the Figure shows that the gap between Q_{desup} is increasing with time, causing the same effect on $Q_{tot-cond}$. In the previous simulations, Case 3 showed results comparable with the other cases thanks to the higher heat transferred in the condensing section which overcame the reduced heat released by the desuperheater. However, for an ambient temperature of -1°C, the slightly higher heat transferred in the condensing section does not compensate the significantly smaller Q_{desup}. The heat transferred in the other sections of the condenser and the compressor work were not plotted due to the very small magnitude of the variations, causing the almost overlapping of the curves.
Case 1 and Case 2 are characterized by very similar results due to the fact that they are both inclusive of the IHEX.

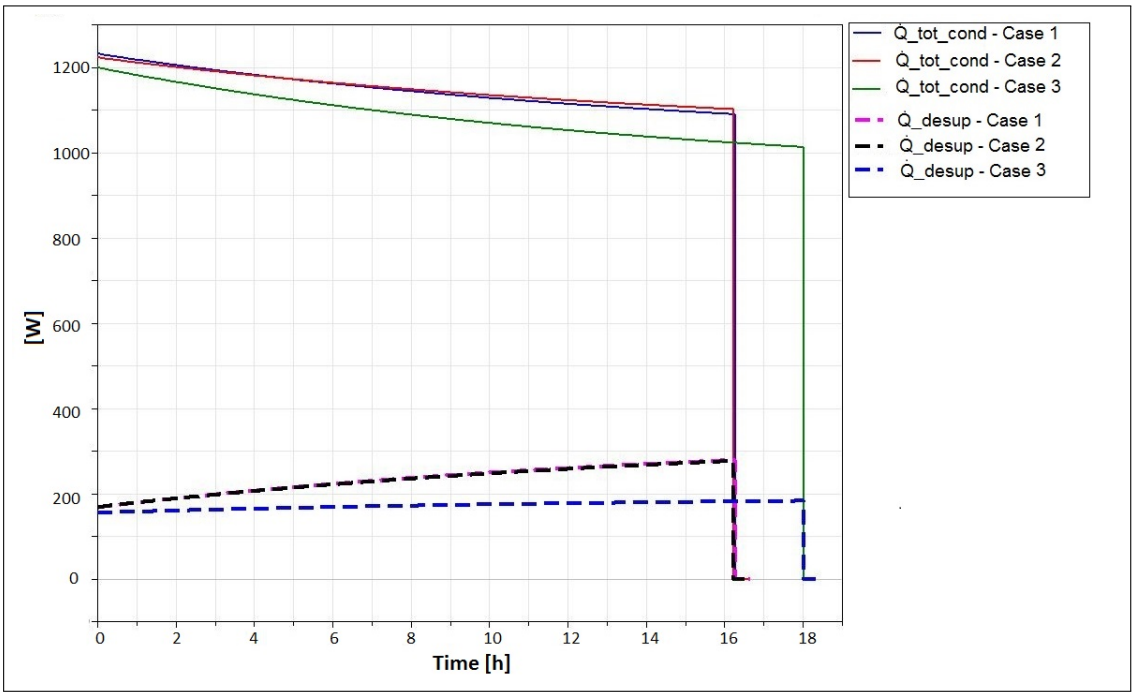

Figure E.1: Heat transferred in the desuperheatinging section and in the overall condenser during the heating up process for the three system configurations with an ambient temperature of -1°C.

F EES code

In this chapter the EES code and a screen shot of the diagram window used to run the model are presented.

```
"!************************************************************************"
"Procedure heat transfer coefficient water"
"!************************************************************************"
Procedure hwater(T_in_w, T_out_w, T_wall, L, H, D_out_tank: h_w)

p_amb=1.013
g=9.81
T_w_avg=(T_out_w+T_in_w)/2
Beta=1/T_w_avg
mu_w=Viscosity(Water,T=T_w_avg , P=p_amb)
rho_w=Density(Water,T=T_w_avg , P=p_amb)
Pr_w=Prandtl(Water,T=T_w_avg,P=p_amb)
k_w=Conductivity(Water,T=T_w_avg,P=p_amb)
Gr_w=(g*Beta*(T_wall-T_w_avg)*rho_w^2*L^(3))/(mu_w^(2))
Ra_w=Gr_w*Pr_w  "Rayleigh number"

Nuss_w=(0.186*(H/D_out_tank)+2.285)*(Ra_w*(D_out_tank/H)^4)^(0.26)
h_w=Nuss_w*k_w/L
end

"!************************************************************************"
"Procedure isentropic efficiency compressor"
"!************************************************************************"
Procedure Compressor(T_e, T_c: eta_is)

p00 = -517.1
p10 = -0.03627
p01 =    5.555
p20 = 0.00436
p11 = -0.009884
```

```
p02 =   -0.01396
p30 = -4.396e-06
p21 =   -6.312e-07
 p12 =  1.888e-05
p03 =  8.931e-06
x_pol=T_c
y=T_e

eta_is = p00 + p10*x_pol + p01*y + p20*x_pol^2 + p11*x_pol*y + p02*y^2 +
  p30*x_pol^3 + p21*x_pol^2*y + p12*x_pol*y^2 + p03*y^3
end

"!!!!!!!!!!!!!!!!!!!!!!!!!!!!!!!!!!!!!!!!!!!!!!!!!!!!!!!!!!!!!!!!!!!!!!!!!!!"
"Procedure mass flow rate compressor"
"!!!!!!!!!!!!!!!!!!!!!!!!!!!!!!!!!!!!!!!!!!!!!!!!!!!!!!!!!!!!!!!!!!!!!!!!!!!"
Procedure mr(T_e, T_c: m_r)

p00 = 0.0546
p10 = 0.0004367
p01 =   -0.001089
p20 = -3.457e-07
p11 = -8.947e-07
p02 =  3.004e-06

x=T_c
y=T_e

m_r  =p00 + p10*x + p01*y + p20*x^2 + p11*x*y + p02*y^2

end

"!!!!!!!!!!!!!!!!!!!!!!!!!!!!!!!!!!!!!!!!!!!!!!!!!!!!!!!!!!!!!!!!!!!!!!!!!!!"
"Procedure Dittus-Boelter correlation"
"!!!!!!!!!!!!!!!!!!!!!!!!!!!!!!!!!!!!!!!!!!!!!!!!!!!!!!!!!!!!!!!!!!!!!!!!!!!"
Procedure Dittus(R$,T[2], T[3], p_c,D_in,m_r: h_r)

A_cross=pi*D_in^(2)/4
T_r_avg=(T[2]+T[3])/2
Pr_r=Prandtl(R$,T=T_r_avg,P=p_c)
rho_r=Density(R$,T=T_r_avg,P=p_c)
mu_r=Viscosity(R$,T=T_r_avg,P=p_c)
k_r=Conductivity(R$,T=T_r_avg,P=p_c)  "in W"
v_r=m_r/(A_cross*rho_r)
Re_r=rho_r*v_r*D_in/mu_r

Nus_r=0.023*Re_r^(0.8)*Pr_r^(0.3) "n=0.3 for cooling (Dittus-Boelter
  correlation)"
```

```
h_r=Nus_r*k_r/D_in
end

"*************************************************************************************"
"Procedure deltap desuperheater and subcooler"
"*************************************************************************************"
Procedure deltapcalc(R$,T[2], T[3], p_c,D_in,m_r,L: DELTAp)

A_cross=pi*D_in^(2)/4
T_r_avg=(T[2]+T[3])/2
Pr_r=Prandtl(R$,T=T_r_avg,P=p_c)
rho_r=Density(R$,T=T_r_avg,P=p_c)
mu_r=Viscosity(R$,T=T_r_avg,P=p_c)
k_r=Conductivity(R$,T=T_r_avg,P=p_c)  "in W"
v_r=m_r/(A_cross*rho_r)
Re_r=rho_r*v_r*D_in/mu_r

f=0.158/(Re_r^0.25)
DELTAp=f*rho_r*v_r^2*L/D_in*10^(-5)


end


"*************************************************************************************"
"Procedure Shah correlation"
"*************************************************************************************"
Procedure Shah(R$,p_c, m_r,D_in: h_r_cond)

p_critic=P_crit(R$)
p_r=p_c/p_critic
A_cross_cond=pi*D_in^(2)/4
mu_l=Viscosity(R$,x=0 , P=p_c)
rho_l=density(R$,x=0 , P=p_c)
k_l=Conductivity(R$, x=0, P=p_c)
Pr_l=Prandtl(R$, x=0, P=p_c)
v_l=m_r/(A_cross_cond*rho_l)
Re_lo=rho_l*v_l*D_in/mu_l
h_L_SHAH=0.023*Re_lo^0.8*Pr_l^0.4*k_l/D_in
h_r_cond=h_L_SHAH*(0.55+2.09/p_r^0.38)
end

"*************************************************************************************"
"Procedure Gnieliski correlation"
"*************************************************************************************"
Procedure Gnieliski(R$,T[5],T[4],p_c, m_r,D_in: h_r_sub)
```

```
T_r_avg_sub=(T[5]+T[4])/2
A_cross_sub=pi*D_in^(2)/4
Pr_r_sub=Prandtl(R$,T=T_r_avg_sub,P=p_c)
rho_r_sub=Density(R$,T=T_r_avg_sub,P=p_c)
mu_r_sub=Viscosity(R$,T=T_r_avg_sub,P=p_c)
k_r_sub=Conductivity(R$,T=T_r_avg_sub,P=p_c)  "in W"
v_r_sub=m_r/(A_cross_sub*rho_r_sub)
Re_r_sub=rho_r_sub*v_r_sub*D_in/mu_r_sub
f_sub=(0.790*ln(Re_r_sub)-1.64)^(-2)
Nus_r_sub=((f_sub/8)*(Re_r_sub-1000)*Pr_r_sub)/(1+12.7*(f_sub/8)^(1/2)*(Pr_r_sub^(2/3)-1))
h_r_sub=Nus_r_sub*k_r_sub/D_in
end



"*************************************************************************************"
"INPUT DATA"
"*************************************************************************************"
"********** Gravity*******"
g=9.81
"********** Refrigerant*******"
R$ = 'R134a'
"********** Tank ********"
H=1.4   "Tank height"
D_out_tank=0.660   "Tank outer diameter"
L=0.43     "Starting height for the condenser"
"***********Condenser*********"
D_in=D_out-thickness  "Inner diameter"
"***********Heating capacity*********"
T_avg_w=(T_in_w+T_out_w)/2 "Average water temperature"
p_amb=1.013
Cp_w=Cp(Water,T=T_avg_w , P=p_amb)



"***********************************************************************"
"EVAPORATOR"
"************************************************************************"
"************ Energy balances**************"
Q_e=m_air*Cp_air*(T_air_in-T_air_out)  "Air side"
Cp_air=Cp(Air,T=T_avg_air)
T_avg_air=(T_air_in+T_air_out)/2

Q_e=m_r*(h[8]-h[7])  "Refrigerant side"
"************ LMTD*************************"
Q_e=UA_evap*DELTAT_ml_evap
dT[7]=T_air_in-T_e
```

```
dT[8]=T_air_out-T_e
DELTAT_ml_evap=(dT[7]-dT[8])/ln(Arg_evap)
Arg_evap=dT[7]/dT[8]
"*************Cycle properties***************"
p_e=P_sat ( R$, T=T_e)
p[7]=p_e
p[8]=p_e
T[8]=T_e+DELTAT_superheating
h[8]=Enthalpy(R$, T=T[8], p=p[8])


"*********************************************************************"
"ITERNAL HEAT RECOVERY UNIT"
"*********************************************************************"
h[1]-h[8]=h[5]-h[6]
Effectiveness=(T[1]-T[8])/(T[5]-T[8])
h[1]=Enthalpy(R$, p=p_e, T=T[1])
T[5]=T[4]-DELTAT_subcooling
h[5]=Enthalpy(R$, p=p[5], T=T[5])
T[6]=Temperature(R$, p=p[6], h=h[6])
p[6]=p[5]
p[5]=p[4]-DELTAp_sub
p[1]=p_e



"*********************************************************************"
"COMPRESSOR"
"*********************************************************************"
"**********Refrigerant mass flow rate*****************"
Call mr(T_e, T_c: m_r)
"**********Thermodinamic state compressor discharge**"
s[1]=Entropy(R$, p=p_e, T=T[1])
T[2]=Temperature(R$, p=p_c, h=h[2])
p[2]=p_c
h_2_is=Enthalpy(R$, p=p[2], s=s[1])
eta_is=(h_2_is-h[1])/(h[2]-h[1])
Call Compressor(T_e, T_c: eta_is)
"**********Compressor work*****************************"
W_comp=m_r*(h[2]-h[1])

*********************************************************************"
"CONDENSER"
"*********************************************************************"
 p_c=P_sat(R$ ,T=T_c)
A_cond_tot=pi*L_tot_cond*D_in
```

```
"**********************DESUPERHEATER************************************"
"*********Thermodynamic state points**********"
Q_desup=m_r*(h[2]-h[3])
h[3]=Enthalpy(R$, p=p[3], x=1)
p[3]=p_c-DELTAp_desup
T[3]=T_sat(R$,P=P[3])
"*********Temperature water side*************"
Q_desup=m_w*Cp_w*(T_out_w-T_in_w_desup)
"*********LMTD*****************************"
Q_desup=U_desup*A_desup*DELTAT_ml_desup
A_desup=pi*L_desup*D_in
dT[3]=T[3]-T_in_w_desup
dT[2]=T[2]-T_out_w
DELTAT_ml_desup=(dT[3]-dT[2])/(ln(Arg))
Arg=dT[3]/dT[2]
1/(U_desup)=((1/(h_r_desup)+1/(h_w_desup)+R_wall_desup*pi*D_out))
R_wall_desup=(ln(D_out/D_in))/(2*pi*k_al_desup)  "Wall resistance"
k_al_desup=Conductivity(Aluminum, T=T_wall_desup)  "Aluminum thermal
  conductivity at T_wall"
"*********Newton's law of cooling to find T_wall*****"
Q_desup=A_desup*h_r_desup*(T_r_avg_desup-T_wall_desup)
T_r_avg_desup=(T[2]+T[3])/2
"********Heat transfer coefficient water side*********"
Call hwater(T_in_w_desup, T_out_w, T_wall_desup, L, H, D_out_tank: h_w_desup)
"********Heat transfer coefficient refrigerant side***"
Call Dittus(R$,T[2], T[3], p_c,D_in,m_r: h_r_desup)
"*********UA*****************************************"
UA_desup=U_desup*A_desup

"**********************CONDENSENSING SECTION******************"
"*************Thermodynamic state points**************"
Q_cond=m_r*(h[3]-h[4])
h[4]=Enthalpy(R$, p=p[4], x=0)
p[4]=p[3]-DELTAp_cond
T[4]=T_sat(R$,P=P[4])
"************Temperatures water side******************"
Q_cond=m_w*Cp_w*(T_in_w_desup-T_in_w_cond)
"************LMTD*************************************"
Q_cond=U_cond*A_cond*DELTAT_ml_cond
dT[4]=(T[4]-T_in_w_cond)
DELTAT_ml_cond=(dT[4]-dT[3])/(ln(Arg2))
Arg2=(dT[4])/(dT[3])
A_cond=pi*L_cond*D_in
1/(U_cond)=((1/(h_r_cond)+1/(h_w_cond)+R_wall_cond*pi*D_out))
R_wall_cond=(ln(D_out/D_in))/(2*pi*k_al_cond)  "Wall resistance"
k_al_cond=Conductivity(Aluminum, T=T_wall_cond)
```

```
"**************Newton's law of cooling to find T_wall***********"
Q_cond=A_cond*h_r_cond*(T_r_avg_cond-T_wall_cond)
T_r_avg_cond=(T[3]+T[4])/2
"*************Heat transfer coefficient water side**************"
Call hwater(T_in_w_cond, T_in_w_desup, T_wall_cond, L_2, H, D_out_tank:
  h_w_cond)
n=L_desup/(pi*D_out_tank)
L_2=L-n*D_out
"****************Heat transfer coefficient refrigerant side -
  SHAH*************"
Call Shah(R$,p[3], m_r,D_in: h_r_cond)
"**************UA************************************************"
UA_cond=U_cond*A_cond


"*********************************SUBCOOLER*********************************************"
"*************Thermodynamic state points**********************"
Q_sub=m_r*(h[4]-h[5])
Q_sub=m_w*Cp_w*(T_in_w_cond-T_in_w)
"*************LMTD************************************************"
L_sub=L_tot_cond-L_desup-L_cond
Q_sub=U_sub*A_sub*DELTAT_ml_sub
dT[5]=T[5]-T_in_w
DELTAT_ml_sub=((dT[5])-dT[4])/(ln(Arg3))
Arg3=dT[5]/dT[4]
A_sub=pi*L_sub*D_in
1/(U_sub)=((1/(h_r_sub)+1/(h_w_sub)+R_wall_sub*pi*D_out))
R_wall_sub=(ln(D_out/D_in))/(2*pi*k_al_sub)  "Wall resistance"
k_al_sub=Conductivity(Aluminum, T=T_wall_sub)
"**********Newton's law of cooling to find T_wall***************"
Q_sub=A_sub*h_r_sub*(T_r_avg_sub-T_wall_sub)
T_r_avg_sub=(T[5]+T[4])/2
"**********Heat transfer coefficient water side****************"
Call hwater(T_in_w, T_in_w_cond, T_wall_sub, L_3, H, D_out_tank: h_w_sub)
n_2=L_cond/(pi*D_out_tank)
L_3=L_2-n_2*D_out
"************Heat transfer coefficient refrigerant side - Gnielinski****"
Call Gnieliski(R$,T[5],T[4],p[4], m_r,D_in: h_r_sub)
"************UA*****************************************"
UA_sub=U_sub*A_sub

"*************************************************************************"
"EXPANSION VALVE"
"*************************************************************************"
h[6]=h[7]

"*************************************************************************"
```

```
"COP"
"************************************************************************"
Q_c=Q_sub+Q_desup+Q_cond
COP=Q_c/W_comp




"************************************************************************"
"PRESSURE DROP"
"************************************************************************"
"DESUPERHEATER"
Call deltapcalc(R$,T[2], T[3], p[2],D_in,m_r,L_desup: DELTAp_desup)


"CONDENSER"
DELTAP_cond=DELTAP_2phase_horiz('R134a', G_J, p[3], D_in, L_cond, x_i, x_o)
x_i=1
x_o=0
G_J=m_r/A_cross_cond
A_cross_cond=pi*D_in^(2)/4

"SUBCOOLER"
Call deltapcalc(R$,T[4], T[5], p[4],D_in,m_r,L_sub: DELTAp_sub)
```

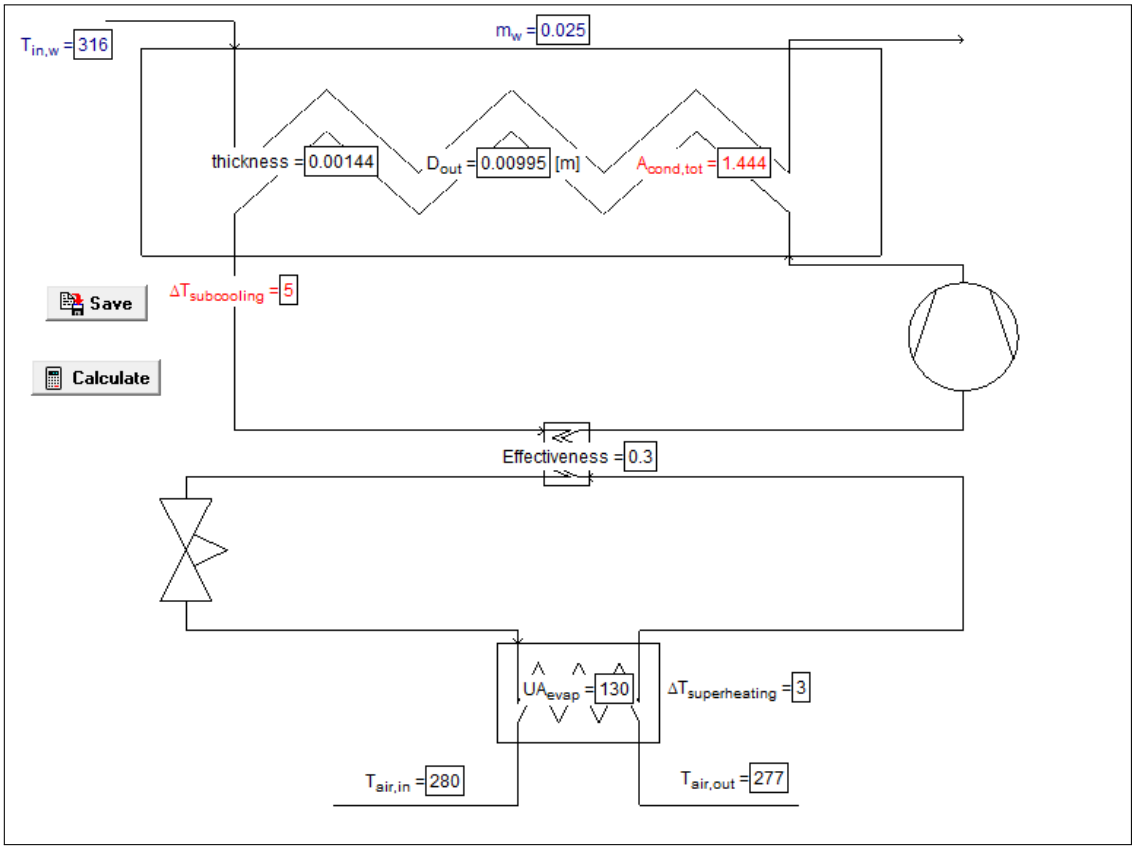

Figure F.1: Diagram window used to run the EES code.

G Dymola code

In this chapter the code implemented in Dymola to simulate the heating phenomena in the tank is presented.

```
model Tank
import SI = Modelica.SIunits;
import cons = Modelica.Constants;

  replaceable package Water = HeatPump_all.Fluids.Water constrainedby
    Modelica.Media.Interfaces.PartialTwoPhaseMedium
      annotation(choicesAllMatching = true);

Water.ThermodynamicState WaterIn;
Water.ThermodynamicState WaterOut;

  HeatPump_all.Port portA
                       ;
  HeatPump_all.Port portB
                       ;

parameter Integer n;

SI.Temperature[n] T;
SI.Mass[n] M;

parameter SI.Volume V "Volume of tank";
parameter SI.Length D "Diameter of tank";
parameter SI.Length b "Thickness of tank shell";
parameter SI.ThermalConductivity k_steel "Thermal conductivity steel, 16";
parameter SI.ThermalConductivity k_water "Thermal conductivity Water, 0.58";
SI.ThermalConductivity Dk;

parameter SI.Temperature T_initial "Initial water temperature";
parameter SI.Temperature T_a "Ambient temperature";
```

```
SI.Temperature T_out;
parameter Real U;
parameter SI.SpecificHeatCapacity cp_water "Specific heat capacity water,
  4200";
parameter SI.SpecificHeatCapacity cp_steel "Specific heat capacity steel, 420";
parameter SI.Density d_steel "Density steel, 7775";
parameter SI.Density d_water "Density Water, 1000";
parameter Real y "Mass fraction of each node which is circulated";

SI.Heat[n] Q_cond;
SI.Heat[n] Q;
SI.Heat[n] Qmix1;
SI.Heat[n] Qmix2;
SI.Heat[n] Qmix3;
SI.Heat[n] Qmix4;
SI.Heat Q_total;
SI.Heat Q_c;

SI.Heat Q_cond_total;
SI.Heat Q_balance;

SI.Length[n] x;
SI.Length L;
SI.Area A_s;
SI.Area A_c;
SI.Efficiency COP;
SI.Efficiency COP_tot;

parameter SI.Pressure p "Water pressure";
SI.SpecificEnthalpy h_out( start=Water.specificEnthalpy_pT(p=p, T=T_initial));

SI.MassFlowRate m_flow_up;
SI.MassFlowRate m_flow_down;

SI.Temperature T_in(start=273+40);

SI.Temperature T_avg_w;
SI.Work W_comp;
SI.Temperature T_avg;
Integer z;

initial equation

  for i in 1:n loop
    T[i]=T_initial;
  end for;
```

```
if T_initial>=47+273 then
  z=1;
else
  z=2;
end if;

equation

  T_in=Water.temperature(WaterIn);
  h_out=Water.specificEnthalpy(WaterOut);

  L=V/(cons.pi*(D/2)^2*n);
  A_s=cons.pi*D*L;
  A_c=cons.pi*(D/2)^2;
  Dk=k_steel*(cons.pi*D*b)/A_c;

if portA.m_flow>0 then
m_flow_up=0;
m_flow_down=portA.m_flow;
  WaterIn=Water.setState_ph(p=p, h=portA.h);
  WaterOut=Water.setState_pT(p=p, T=T[n]);
  portB.h=h_out;
else
m_flow_up=portB.m_flow;
m_flow_down=0;
WaterIn=Water.setState_ph(p=p, h=portB.h);
WaterOut=Water.setState_pT(p=p, T=T[1]);
portA.h=h_out;
end if;

T_avg=sum(T)/n;
Q_total=sum(Q);
Q_cond_total=sum(Q_cond);
Q_balance=Q_total-Q_cond_total;

  for i in 1:n loop
    M[i]=L*A_c*d_water;
  end for;
x[1]=L;
x[n]=L*n;
Q_cond[1]=0;
Q_cond[n]=0;
(Qmix2[n])=0;
(Qmix1[n])=0;
(Qmix3[1])=0;
(Qmix4[1])=0;
```

```
  if T[2]>T[1] then
  (Qmix2[1]) = y*M[2]*cp_water*(T[2]);
  (Qmix1[1])= y*M[1]*cp_water*(T[1]);
  else
  (Qmix2[1])=0;
  (Qmix1[1])=0;
  end if;

M[1]*cp_water*der(T[1])=(k_water+Dk)*A_c/L*(T[2]-T[1])+U*A_s*(T_a-T[1])
-m_flow_down*cp_water*T[1]+m_flow_up*cp_water*T[1+1]+m_flow_down*cp_water*T_in
-m_flow_up*cp_water*T[1]+(Qmix2[1])-(Qmix1[1]);
der(Q[1])=M[1]*cp_water*der(T[1]);
  for i in 2:n-1 loop

x[i]=L*i;

  if T[i+1]>T[i] then
  (Qmix2[i]) = y*M[i+1]*cp_water*(T[i+1]);
  (Qmix1[i])= y*M[i]*cp_water*(T[i]);
  else
  (Qmix2[i])=0;
  (Qmix1[i])=0;
  end if;

  if T[i-1]>T[i] then
  (Qmix3[i])=0;
  (Qmix4[i])=0;
    else
  (Qmix3[i]) = y*M[i-1]*cp_water*(T[i-1]);
  (Qmix4[i])= y*M[i]*cp_water*(T[i]);
  end if;

if x[i]>=1.26 and x[i]<1.33 and z==2 and T[i]<55+273 then

  der(Q_cond[i])=0.1489*T[18]+4.9027;                    //Case1


elseif x[i]>=1.05 and x[i]<1.26 and z==2 and T[i]<55+273 then

    der(Q_cond[i])=(-8.1028*T[16]+3605.2)/3;             //Case1

elseif x[i]>0.98 and x[i]<1.05 and z==2 and T[i]<55+273 then

    der(Q_cond[i])=(3.9343*T[14]-997.78);                //Case1

else
  der(Q_cond[i])=0;
```

```
end if;

M[i]*cp_water*der(T[i])=(k_water+Dk)*A_c/L*(T[i+1]-T[i])
+(k_water+Dk)*A_c/L*(T[i-1]-T[i])+U*A_s*(T_a-T[i])
+m_flow_down*cp_water*T[i-1]-m_flow_up*cp_water*T[i]+m_flow_up*cp_water*T[i+1]
-m_flow_down*cp_water*T[i]+der(Q_cond[i])+(Qmix2[i])
-(Qmix1[i])-(Qmix4[i])+(Qmix3[i]);
der(Q[i])=M[i]*cp_water*der(T[i]);
end for;

  if T[n-1]>T[n] then
  (Qmix3[n])=0;
  (Qmix4[n])=0;
    else
  (Qmix3[n]) = y*M[n-1]*cp_water*(T[n-1]);
  (Qmix4[n])= y*M[n]*cp_water*(T[n]);
  end if;

M[n]*cp_water*der(T[n])=(k_water+Dk)*A_c/L*(T[n-1]-T[n])+U*A_s*(T_a-T[n])
+m_flow_down*cp_water*T[n-1]-m_flow_down*cp_water*T[n]+m_flow_up*cp_water*T_in-
m_flow_up*cp_water*T[n]+(Qmix3[n])-(Qmix4[n]);
der(Q[n])=M[n]*cp_water*der(T[n]);
T_out=Water.temperature(WaterOut);
portA.m_flow+portB.m_flow=0;

portA.p=p;
portB.p=p;

if z==2 then

  der(W_comp) =4.6511*T_avg_w - 1129.7; //Case1

  COP=der(Q_c)/der(W_comp);
else
  der(W_comp)=0;
  COP=0;
end if;

der(Q_c)=der(sum(Q_cond));
COP_tot=Q_c/(W_comp+0.001);

T_avg_w=(T[14]+T[18])/2;
algorithm
      when T[16]<=47+273 and z==1 then
      z:=2;
      elsewhen T[16]>= 52+273 and z==2 then
      z:=1;
```

```
    end when;

end Tank;
```

Acknowledgements

The accomplishment of this thesis and of this full master was an exciting experience, enriched by the support of loved persons and the possibility to meet and cooperate with different people. These few words aim to thank all these people. It was really difficult to choose the right words to express my gratitude, but I hope they can be representative for my excitement.

First of all I thank Erasmus Damgaard Rothuizen, my co-supervisor, for the assistance provided throughout the all duration of the project. He was always available to meet me and in his office I found decisive advices and very productive dialogues. Secondly, my gratitude goes to Wiebke Brix Markussen, my supervisor, for the passion for the refrigeration field she transmitted me. Her help was important to launch the project. Thirdly, I am grateful to Davide Del Col, my supervisor at the Università degli Studi di Padova, for his trust and interest for the project.

Kasper Korsholm Østergaard deserves another sincere thank because of his supervision during the days spent at Metro Therm A/S. He has been a really patient and helpful guide, always willing to share his deep experience and knowledge with me. I am grateful also to all his colleagues for making exciting my time in the company.

Vorrei poi ringraziare mio papà Bruno, del quale ho sempre sentito il supporto durante questi anni nonostante la sua assenza fisica. Spero possa essere orgoglioso di me. Un grazie enorme anche a mia mamma Emilia e mia sorella Elisa. La prima non mi ha mai fatto mancare nulla, ha sempre creduto in me, mi ha insegnato importanti valori assieme al papà e mi ha dato tutto il suo amore. La seconda è a mio parere una persona incredibile e fantastica: mi ha sempre trasmesso forza e dispensato sorrisi grazie alla sua vitalità innata. Ha sempre saputo tutto di me e abbiamo condiviso tutto. Un grazie di cuore anche a tutti gli altri familiari per i momenti spesi insieme. Una menzione particolare merita la nonna Lidia che, insieme al nonno Giovanni, mi ha sempre fatto trovare in Pugnello un porto sicuro e colmo di affetto.

Un paragrafo a sè stante merita la mia fidanzata Giulia. Ha accettato la relazione a distanza ed è stata paziente nell'aspettare il mio ritorno. Sono stati due anni intensi, fatti di tante risate

e momenti indimenticabili trascorsi insieme, tanti arrivi per poi essere costretti ai saluti a causa di ripartenze sempre troppo precoci. Tutto questo insieme fa parte di quel sentimento chiamato amore che proviamo l'uno per l'altro. Grazie!

I want to thank also all the amazing people that I met during my Danish "journey". I had great moments with you. The bad part of these experiences comes in the moments in which you are required to say "bye bye" to all these people. Hopefully, this "bye bye" is a synonymous of "see you soon". Last but not least, I am grateful to all my friends in Italy, especially the "Amici del Bombardino", for waiting me home to share some talks and many funny moments together.

Avrai, avrai, avrai il tuo tempo per andar lontano,
camminerai dimenticando, ti fermerai sognando...
Avrai, avrai, avrai la stessa mia triste speranza
e sentirai di non avere amato mai abbastanza

— Claudio Baglioni